Winu Pit Lake Model

June 2024

Prepared for: **Rio Tinto Winu Pty Ltd**
Level 25, 123 Albert Street
Brisbane QLD 4000

Prepared by: **HydroGeoLogica, Inc.**
12600 W. Colfax Avenue
Lakewood, CO 80215

www.hydrogeologica.com
Now Part of:

www.LREWater.com

TABLE OF CONTENTS

LIST OF FIGURES

LIST OF TABLES

LIST OF APPENDICES

1 Introduction

Rio Tinto Winu Pty Limited (Rio Tinto) is evaluating the development of mineralized deposits for a proposed copper-gold mine within the Winu Project area (Winu or Project). Winu is located approximately 320 kilometers (km) east of Port Hedland in the Yeneena Basin of the Paterson Province in northwest Western Australia (Figure 1-1).

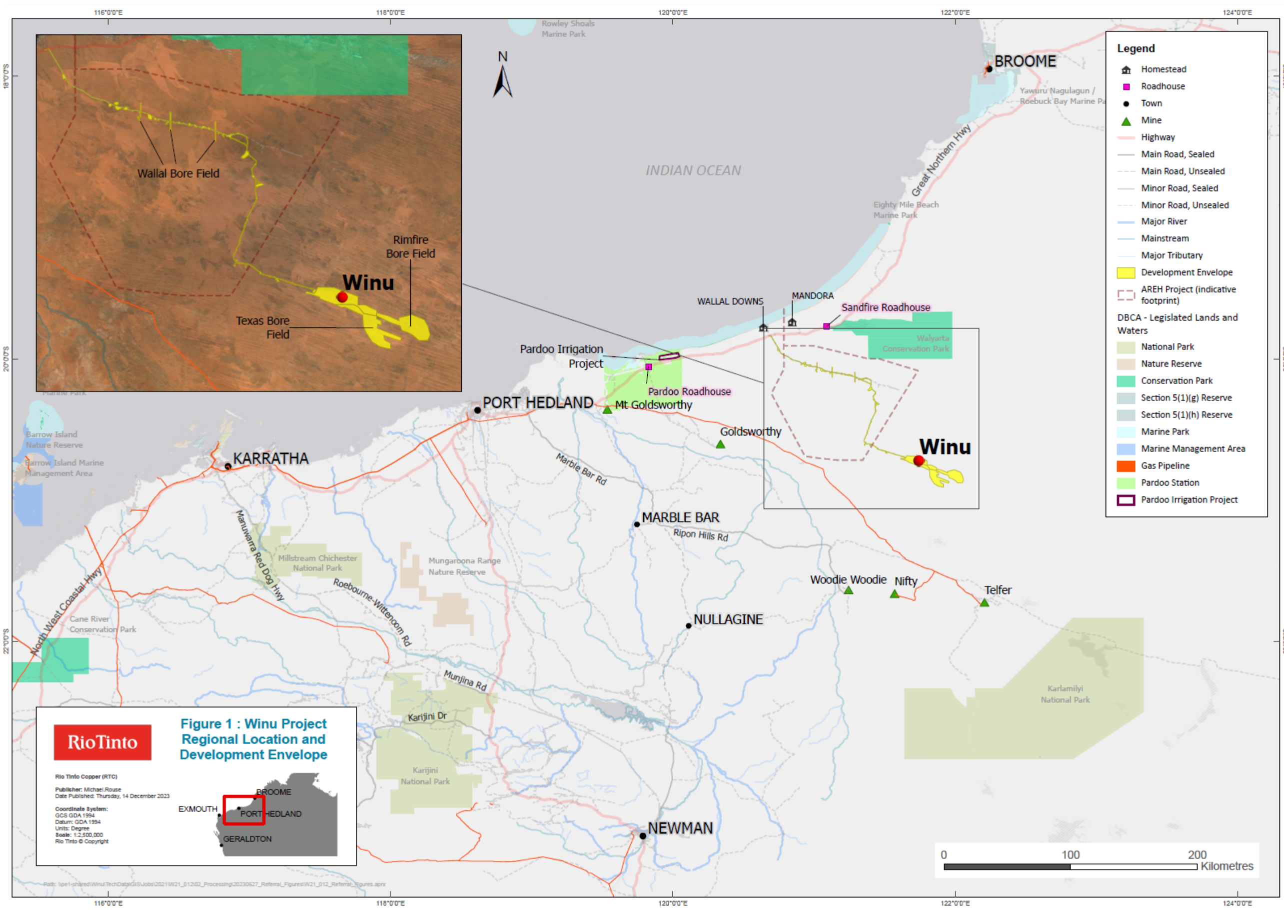

Figure 1-1 Site location (provided by Rio Tinto)

This report documents closure pit late filling and geochemical modeling for the proposed Winu Project. This evaluation will inform permitting activities as well as optimization of facility designs and closure studies.

2 Project and Site Conditions Summary

Figure 2-1 shows the proposed Project layout from the 2024 Winu Operations Closure Plan. Conventional open pit mining methods (cut, drill and blast, load, and haul) will be implemented at Winu. Mining will be conducted above and below the water table and will generate approximately 280 million tonnes (Mt) of ore and 490 Mt of waste rock over a 41-year mine life (26 years of open pit mining operations; Rio Tinto, 2023, 2024d). The resulting open pit will be 485 meters (m) deep and create approximately 170 hectares (Ha) of disturbance (Rio Tinto, 2024d). A combined waste rock landform (WRL) and tailings storage facility (TSF) with multiple cells (including a high-sulfur tailings cell) will be constructed in close proximity to the open pit.

Other mine facilities will include the ore processing facilities, ore, and topsoil stockpiles, and associated mine infrastructure. Ore concentrate will be transported from the site by truck (by a third party) via the access road and Great Northern Highway to a local port for export. At closure, pit dewatering will cease, the TSF and top of the WRL will be capped and the remaining mine facilities will be decommissioned.

The climate is considered arid with relatively low rainfall and high evaporation. Pan evaporation is approximately ten times higher than precipitation (site climate characteristics are described in detail in Section 6.1.1). During the summer and early autumn months (December to March), average daily temperatures at Winu exceed 30°C. During winter months (June to August), average temperatures are typically around 20°C. The seasonal maximum temperatures generally range from 29°C – 41°C, with minimum temperatures ranging from 11°C – 26°C.

Rainfall in the area is mainly associated with tropical cyclone systems which develop from January through March. Rainfall also occurs during May and June as a result of cold fronts moving across the south of Western Australia, and occasionally extending into the site area. Storms are infrequent and of short duration, but they are intense and often result in flash flooding. Typical annual rainfall is between 360 mm and 410mm. Pan evaporation ranges from approximately 3,300mm to 3,900mm.

The topography at the site is characterized by extensive west northwest trending sand dunes with poorly defined surface water drainage routes. Internal drainage systems between dunes are common and form soakaways across the region leading to the development of ephemeral, perched water tables.

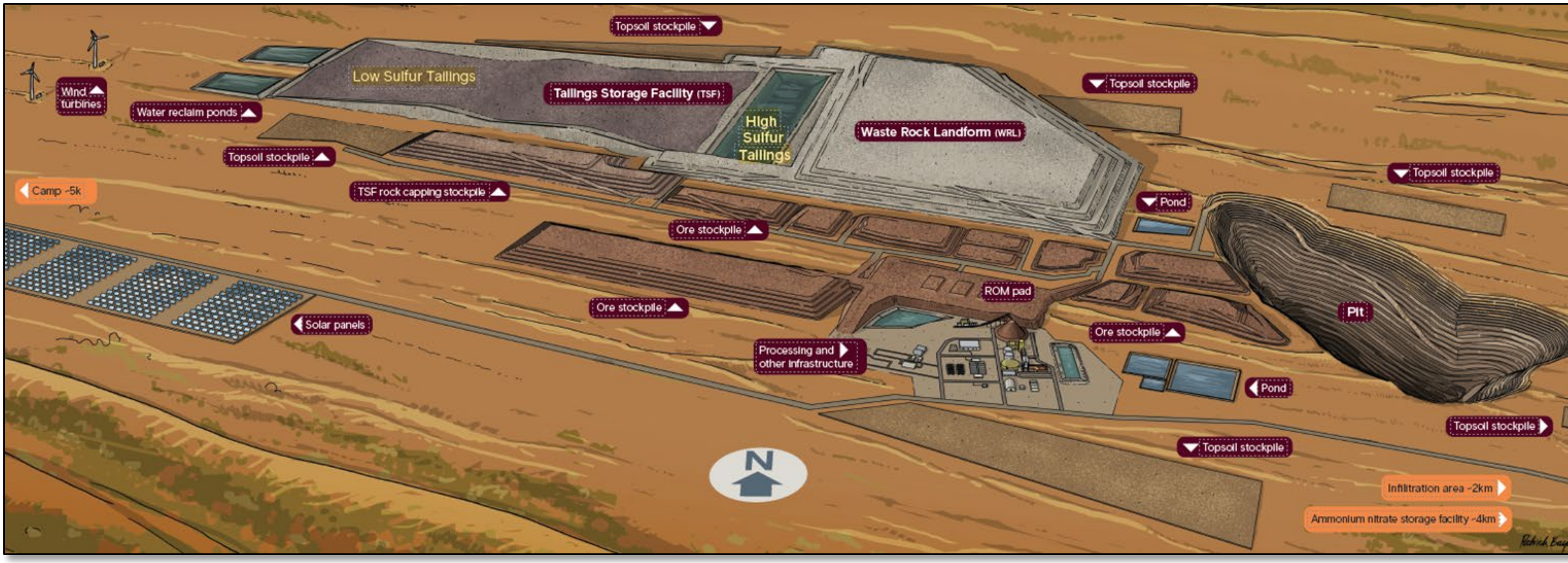

Figure 2-1 Conceptual mine layout (Rio Tinto, 2024d)

3 Approach

A conceptual model of flows associated with the post-closure Winu pit lake was developed based on preliminary modeling performed for the facility by Golder Associates (Golder), (2021) and Advisian (2022). Analytical/numerical (numerical[1]) pit lake modeling was performed using the dynamic systems modeling platform GoldSim (www.goldsim.com; Goldsim Technology Group, 2021) along with the geochemical modeling code PHREEQC developed by the United States Geological Survey (USGS) (Parkhurst and Appelo, 2013) coupled using a customized dynamic link library (DLL) code.

GoldSim modeling of pit lake recovery during the post-closure period was developed based on existing climate and hydrogeological studies and modeling for the site, together with ultimate pit shell designs and geologic block modeling developed by Rio Tinto. Rio Tinto performed extensive geochemical testing on waste and tailings materials that will be generated during mining (Rio Tinto 2021, 2022, 2024b, 2024c; SRK 2023, 2024). The results of this testing informed the development of geochemical source terms used as input to the pit lake geochemistry modeling.

The GoldSim model was used to estimate and track the various water inflows to, and outflows from, the pit lake to predict the pit lake filling and the steady-state pit lake elevation. A Base Case model was developed using the current mine plan (Rio Tinto, 2024d); central-tendency values for input parameters and selected alternative scenarios/sensitivity analyses with alternative values for uncertain, and potentially variable, model input parameters. Each of the water balance scenarios was coupled with a Base Case geochemical model, and alternative geochemical models using various geochemical source terms and chemical release timing as indicated by observed the variability in geochemical characterization data that were used to support model input values.

Based on results from the numerical pit lake water quality model, screening level calculations were performed to assess potential for density-drive outflow from the pit lake to the surrounding groundwater system and the likelihood for the development of permanent, density-induced stratification of the pit lake.

The post-closure simulation period was set to 300 years (starting at the beginning of 2054 through 2353). This period was selected in consultation with Rio Tinto and provides adequate time for the pit lake level to stabilize and for water chemistry trends to develop.

[1] The combined Goldsim/PHREEQC model contains both analytical and numerical modeling algorithms. For this evaluation the term "numerical" was used generally to differentiate the GoldSim/PHREEQC model from the conceptual model.

4 Pit Lake Conceptual Model

4.1 Hydrologic Components

Figure 4-1 shows a schematic diagram of the Winu pit lake conceptual model. The conceptual model flow components and processes that are represented in the GoldSim pit lake model are:

- Direct rainfall onto the pit lake (based on climate data described in Section 6.1.1)
- Evaporation from the pit lake (based on climate data described in Section 6.1.1)
- Pit wall runoff (described in Section 6.1.3)
- Groundwater inflows (described in Section 6.1.5)
- Seepage from closed TSF (described in Section 6.1.6). The actual seepage mechanisms have not been simulated as part of this exercise. Assumptions regarding these mechanisms are described in Section 6.1.6.
- Potential inflow of WRL seepage via groundwater (described in Section 6.1.7);
- Pit lake mixing (described in Section 6.1.11)
- Flushing of the damaged rock zone and talus piles associated with the pit walls (described in Section 6.1.11)

The primary component of pit lake filling will be groundwater. As indicated by the Mine Closure Plan (Rio Tinto, 2024d), abandonment bunds will be constructed approximately 180 to 200 m from the pit rim and according to Safety Bund Walls Around Abandoned Open Pit Mined Guideline (DIR, 1997). However, these bunds are not expected to be constructed to be fit-for-purpose for water flow diversion as recommended by DRDMW (2022a, b). Based on the high evaporation rates at the site, minimal topographic relief, and lack of evidence of surficial ephemeral runoff drainages, for the purposes of these modeling efforts, it was assumed that the proposed abandonment bunds will divert potential catchment run-in away from the pit. Within the bund, precipitation and runoff is expected to report to the pit lake (surface runoff is further discussed in Section 6.1.3).

Pit lake outflow is limited to evaporation from the pit lake surface (based on climate data described in Section 6.1.1). Groundwater flow modeling (Advisian, 2022) indicates that the final pit lake elevation is likely to be significantly lower than the pre-mining groundwater elevation so, in the case of the Winu pit lake, it is anticipated that groundwater outflow will be zero at all times. Because the ultimate pit lake elevation is likely to be significantly below the pre-mining groundwater elevation, the pit lake will likely form a strong hydraulic sink at all times. As such, no groundwater outflow from the pit is expected. Because of the strong hydraulic gradient into the pit, no density driven groundwater outflows are expected at any point in the future despite ongoing evapoconcentration of the pit lake. No surface water outflows from the pit lake are anticipated. It would be necessary for the pit lake elevation to exceed the pre-mining groundwater level and reach the lowest point on the pit rim in order for this to occur. No reasonable storm events for the area would generate adequate water for this to occur.

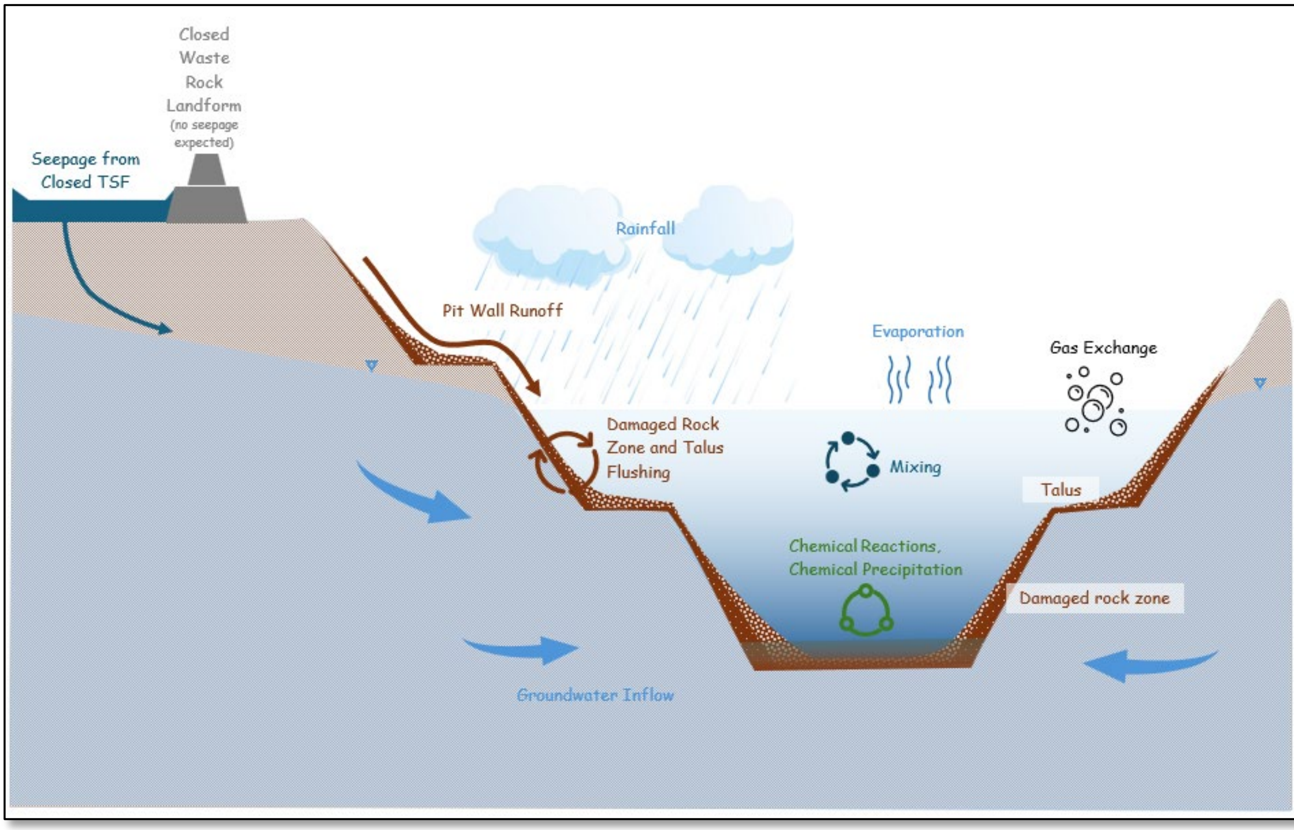

Figure 4-1 Winu pit lake conceptual model

4.2 Geochemical Components

Each pit lake inflow and outflow has an associated water chemistry. These source term water chemistries, together with associated geochemical processes are described in Section 6.2.

Geochemical mechanisms associated with pit lake development are included in the conceptual model (Figure 4-1). These mechanisms provide the basis for geochemical assumptions in the numerical modeling. Relevant geochemical mechanisms that may affect the pit lake chemistry include:

- Direct rainfall onto the pit lake (described in Section 6.2.1);
- Inflow of TSF seepage via groundwater (described in Section 6.1.6);
- Potential inflow of WRL seepage via groundwater (described in Section 6.1.7);
- Inflow of groundwater (described in Section 6.2.4);
- Water-rock interaction and reactions associated with pit wall runoff (described in Section 6.2.2);
- Flushing of chemical mass into the pit lake as the water level rises and inundates the damaged rock zone in the pit walls and talus accumulated on the pit wall benches (this does not provide additional water, however it does bring chemical mass to the pit lake based on the rock type being flushed; described in Section 6.2.2);

- Gas (O2 and CO2) exchange between the pit lake and the atmosphere (described in Section 5.2); and,
- Geochemical reactions resulting in precipitation of solids, and associated solids sedimentation (described in Section 5.1). These reactions assume complete mixing of the pit lake and equilibration with oxygen and carbon dioxide concentrations defined in Figure 5-1. Whilst some temporary stratification may develop seasonally, no long-term stratification is expected based on the small local temperature range and lack of anticipated chemical gradients in the pit lake.

Because the primary component of pit lake filling is groundwater, groundwater chemistry is expected to dominate the chemistry of the pit lake during filling, while long-term pit lake chemistry is expected to be strongly affected by evapoconcentration. Evaporation removes only pure water from the pit lake, so no chemical mass is removed during pit filling.

5 Numerical Modeling Approach

Changes in pit lake water chemistry during the post closure period were simulated using PHREEQC. PHREEQC (from pH-REdox-EQuilibrium in C), is a free, publicly available hydrogeochemical modeling software (Parkhurst and Appelo, 2013). PHREEQC simulates geochemical reactions that occur in pit lakes, such as mixing, mineral precipitation, sorption of trace inorganic species to ferrihydrite surfaces, equilibration with atmospheric gas concentrations and temperature conditions and gas phases, and evapoconcentration of dissolved constituents.

Hydrologic (and associated mass balance chemistry) components of pit lake modeling are simulated in GoldSim. GoldSim is a dynamic-systems modeling platform which provides a way to represent time-varying engineered and natural processes, some of which may also involve complex feedback loops.

GoldSim allows customized programing to link simulations to external software. Hydrologic and geochemical components of the pit lake modeling were connected via a customized dynamic link library (DLL) developed in C++. This approach allows PHREEQC calculations to be performed for each GoldSim model timestep. The DLL passes data from GoldSim to PHREEQC for geochemical reaction modeling and then passes the modeling results back to GoldSim each timestep throughout the simulated time period. This approach allows frequent evaluation of the saturation indices of selected minerals and ultimately more rigorous calculation of pit lake water chemistry over time. This calculation flow is illustrated in Figure 5-1.

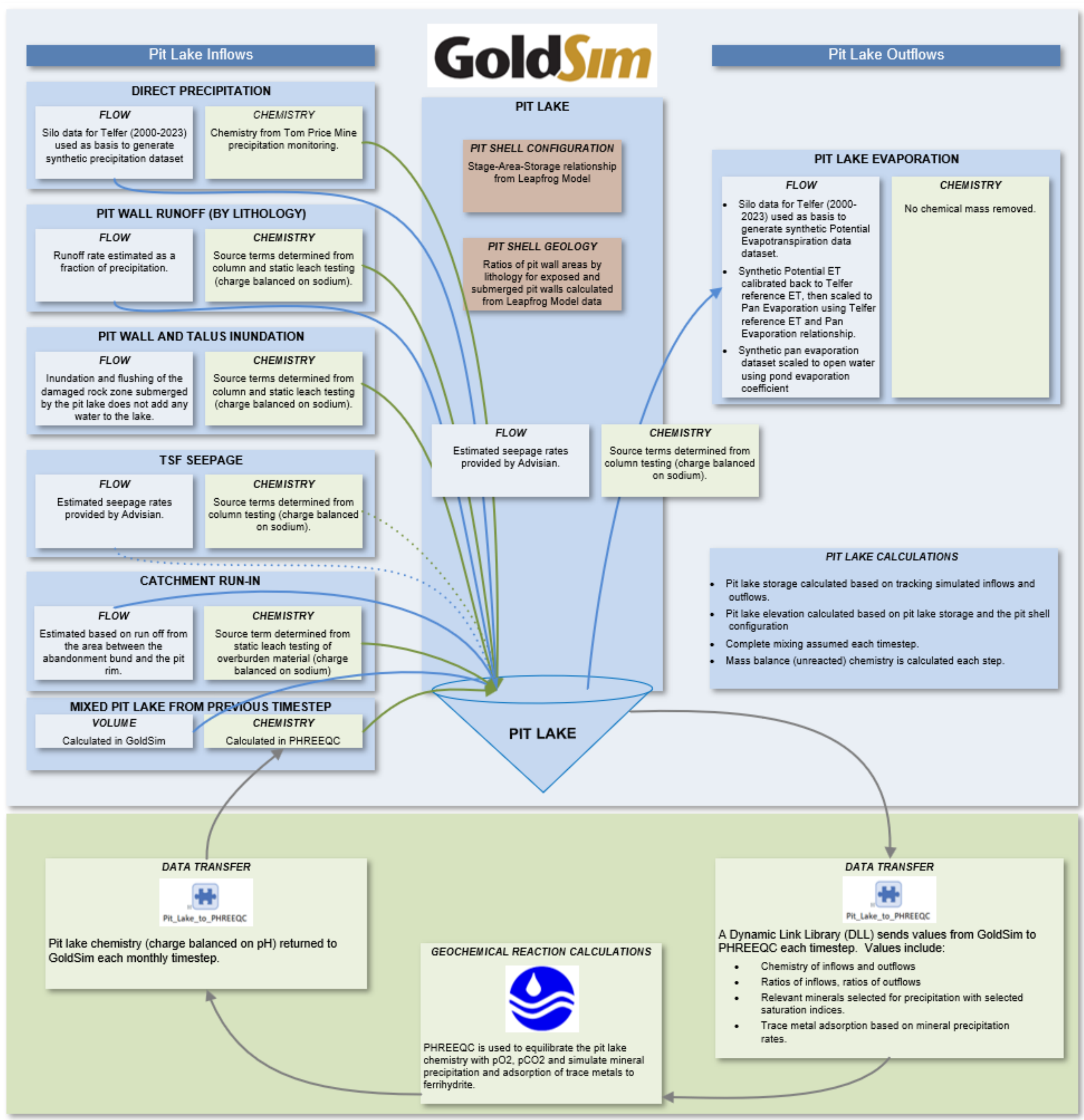

Figure 5-1 GoldSim/PHREEQC calculation flow diagram

5.1 PHREEQC Calculations

In the geochemical model, solution mixing is simulated based on their relative flow rates as predicted by the GoldSim model (as mixing ratios). If non-evaporative outflows from the pits are predicted by the water balance, both water and chemical mass associated with these outflows are mathematically removed from the pit lake prior to performing geochemical mixing calculations for each next timestep. Following mixing calculations, evaporation is simulated through removal of pure water (with no chemical mass), in an amount determined by the water balance. Following evaporation, the geochemical model accounts for aqueous reactions, reduction-oxidation (redox) reactions, mineral precipitation, mineral dissolution, sorption onto mineral surfaces, and gas exchange. The geochemical model basis and the geochemical reactions and controls used for the Winu model are summarized in Table 5-1.

Table 5-1 Geochemical conditions and controls for modeling

Model Component	Selection	Notes
Code	PHREEQC 3.7.3	Version release January 2021; Parkhurst and Appelo (2013).
Database	gs2phreeqc 031122.dat	Provided by Rio Tinto. Rio Tinto-Modified version of *minteq.v4* database. The basis of this Rio Tinto-modified database relies on the *minteq* database (prepared for the US EPA) which is considered appropriate for low temperature, environmental applications such as environmental mine water chemistry predictions.
Temperature	25°C	Near average annual average temperature for the Project site.
Oxidation-reduction (redox) conditions	A fixed P_{O2} of 10^{-35}	The selected P_{O2} value allows Eh values to evolve, based on the current pH of the pit lake at any given timestep. Semi-oxidizing waters are assumed, considering some contact with the atmosphere, and the fact that the majority of the lake water originates from groundwater (Garrels and Christ, 1965). Complete mixing of the entire pit lake volume is assumed for the modeling, although it is recognized that some temporary seasonal stratification may develop.
Partial pressure of carbon dioxide (P_{CO2})	Fixed at 10^{-3}	The selected P_{CO2} is slightly higher than that of atmospheric CO_2, assuming a well-mixed lake in contact with the atmosphere. (This is consistent with 18 existing pit lakes evaluated by Eary (1999) in climatologically similar locations).
Sorption	Sorption allows metals to sorb to precipitated ferrihydrite in each timestep using sorption thermodynamic data parameters in the geochemical database, and surface areas and sorption site densities from Dzombak and Morel (1990).	
Mineral precipitation and dissolution	Ferrihydrite, gypsum, calcite, alunite, gibbsite, amorphous aluminum-hydroxide, barite, malachite, fluorite, potassium-jarosite, sodium-jarosite, amorphous copper carbonate	Mineral precipitation and dissolution are allowed in the model for these minerals selected, though actual mineral precipitation and dissolution amount is determined by the saturation index in the model. The mineral list was selected based on HGL/LRE's experience and judgement, site conditions, Eary (1999), and Nordstrom and Alpers (1999).

5.2 Pit Wall Inundation Solute Release Mechanisms

During each timestep of the pit lake filling, the water level of the pit rises and inundates a section of the pit wall. As each section of pit wall is inundated (including damaged rock zone and talus), labile salts and minerals which have accumulated from exposure to the atmosphere (i.e., wetting/drying cycles), will be dissolved, contributing solute mass to the pit lake. These salts and minerals are assumed to be a) weathering products following atmospheric exposure of the pit walls over time, and/or b) naturally-present, soluble minerals or weathering products not previously flushed from the pit walls materials during runoff events. The chemical mass loading from pit wall inundation is calculated based on the following:

- The surface area of each lithologic unit being inundated during a timestep;
- A damaged rock zone thickness where inundation and mobilization will occur;
- Calculated volumes of talus accumulated on benches;
- An assumed porosity for the damaged rock zone and talus;
- The number of pore volumes required to flush the damaged rock zone and talus of solutes; and,
- The chemical source term for the relevant lithologic unit (Section 6.2).

The thickness and porosity of the damaged rock zone and talus can be highly variable, depending on factors such as rock type and blasting practices. The areas of each lithologic unit in each interval of the pit wall are calculated from the pit shell and geologic model information provided by Rio Tinto. It may take several pore volumes to flush the damaged rock zone and talus depending on the amount of weathering products and soluble minerals present. The flushing of pore volumes introduces solute mass into the pit lake. Adding or subtracting pore volumes to the model also accounts for differences in the water/rock ratio used in kinetic testing. A Base Case value of 10 pore volumes was used in the modeling based on long-term solute release rates from unsaturated free-draining column and short-term multiple extraction procedure (MEP) leaching results. Because of the uncertainty associated with this value, scenarios with flushing of 1 and 50 pore volumes are also simulated as sensitivities (Table 7-2).

6 Input Data

6.1 Pit Lake Flow Components

6.1.1 Climate

This section describes available climate data sources, data quality and how the data were used to develop synthetic climate data sets for Base Case and alternative climate scenarios.

6.1.1.1 Climate Data Sources

Historical rainfall and evaporation records for Winu are available from the enhanced climate database Scientific Information for Land Owners (SILO) hosted by the Science and Technology Division (Queensland Department of Environment and Science, 2018). SILO rainfall datasets can be developed for all Australian locations and are based on interpolated data derived from records at approximately

8,000 weather stations across Australia. Previous studies used datasets interpolated by SILO for Winu. HGL/LRE considered the potential skewing of this dataset with data from nearby costal weather stations associated with a wetter climatic regime than Winu. The interpolated SILO data for monthly and annual rainfall and pan evaporation estimates at Winu were compared with data from the nearest, publicly available station at 13030 Telfer Aero Station (Bureau of Meteorology (BoM)) ('Telfer station'). The datasets were found to be similar, as shown in Figure 6-1, however interpolated rainfall tends to be slightly higher, and evaporation tends to be slightly lower for the SILO interpolated Winu data. For this study the Telfer station data were selected as more closely representing the climatic conditions at Winu.

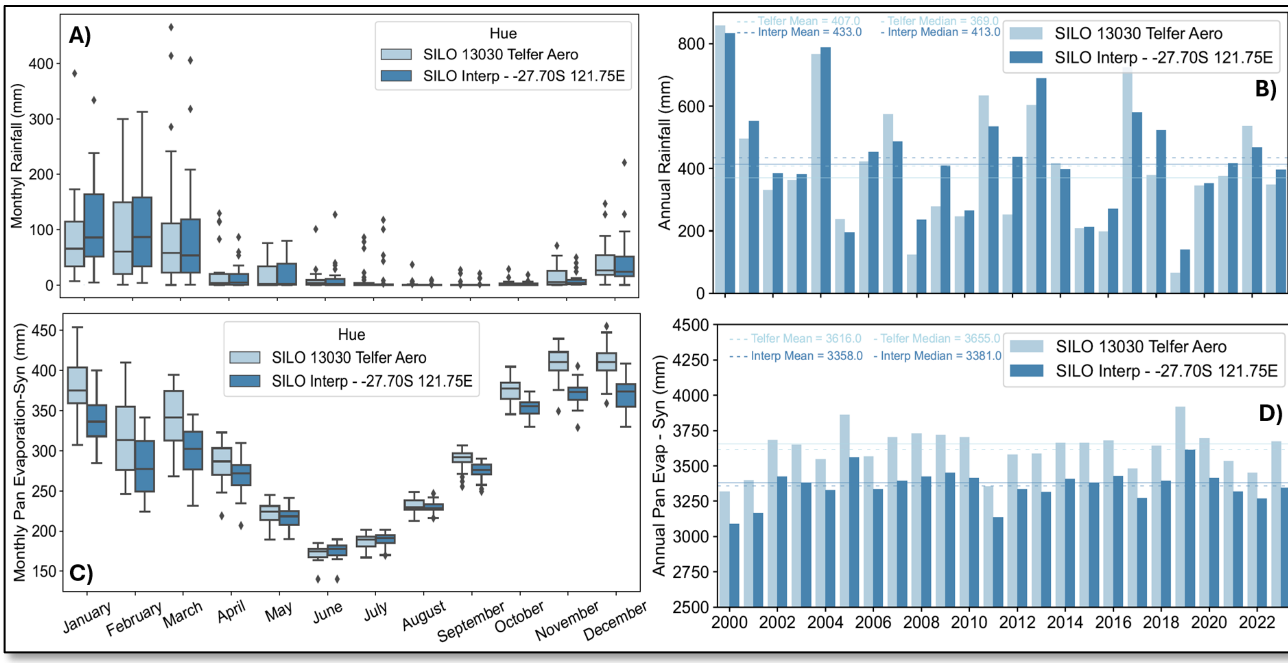

Figure 6-1 Comparison of SILO data interpolated for Winu, to SILO 13030 Telfer Aero Station 2000-2023 data for A) monthly rainfall, B) annual rainfall, C) monthly pan evaporation, and D) annual pan evaporation

6.1.1.2 Representative Rainfall Data

Due to recent changes in climate, a limited period of historical daily data (2000-2023) was assumed to be reasonably representative of current climate conditions at Winu. Historical rainfall records from 2000 to 2023 for the Telfer station (Figure 6-2) were used for statistical analysis and synthetic data generation. The figure illustrates that the median annual rainfall for the station is 369 mm. The mean annual rainfall is 407 mm. The minimum annual rainfall for the selected period is 65 mm and occurred in 2019. The maximum annual rainfall is 857 mm and occurred in 2000.

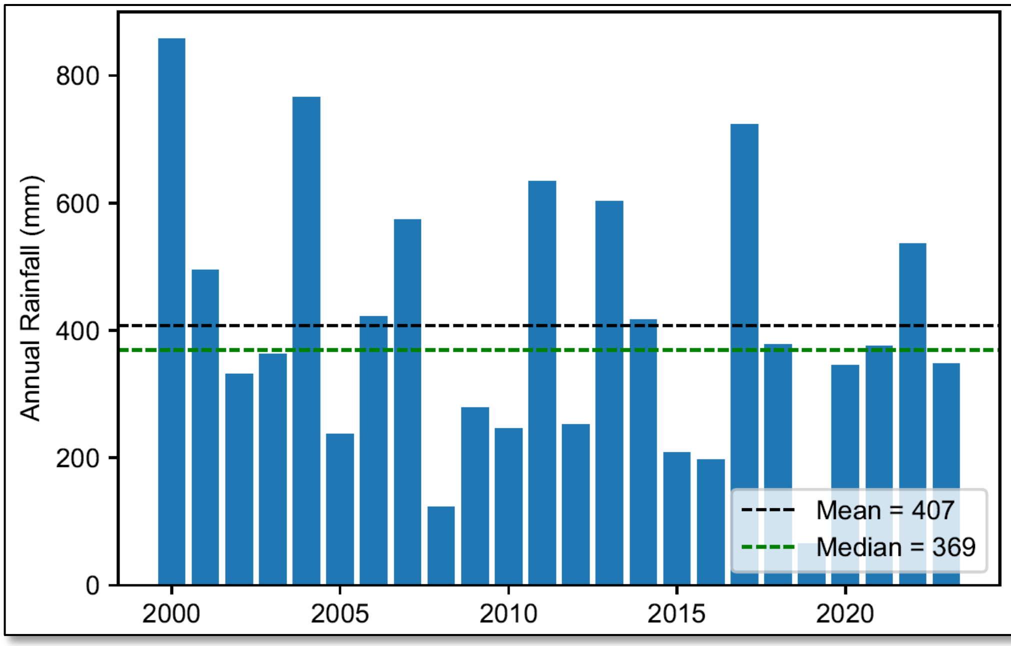

Figure 6-2 Annual rainfall data for SILO 13030 Telfer Aero Station 2000-2023

Monthly distributions of daily rainfall for the historical period are presented in Figure 6-3. Typically, January, February, and March are the wettest months of the year and July, August, September, and October are the driest months.

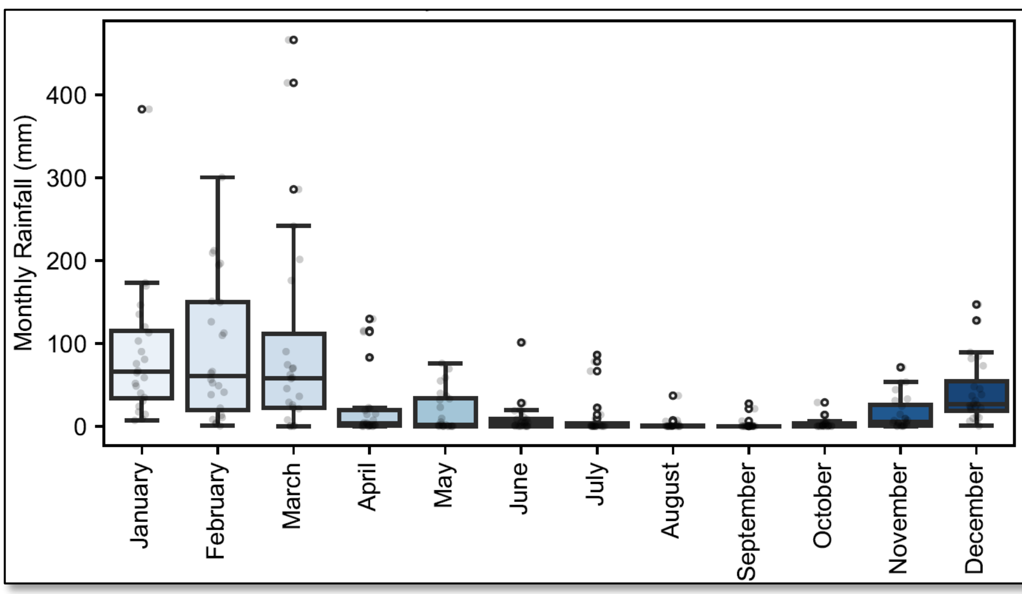

Figure 6-3 Box-whisker plot of monthly rainfall - SILO 13030 Telfer Aero Station 2000-2023

6.1.1.3 Representative Evaporation Data

Historical pan evaporation records from 2000 to 2023 for the Telfer station were used in this analysis (Figure 6-4). The median annual pan evaporation for the station is 3,655 mm for the period of record selected. The mean of the selected annual pan evaporation records is 3,616 mm. The minimum annual pan evaporation of 3,317 mm was recorded in 2000, temporally consistent with the maximum annual rainfall year. The maximum annual pan evaporation of 3,916 mm was recorded in 2019, temporally consistent with the minimum annual rainfall year.

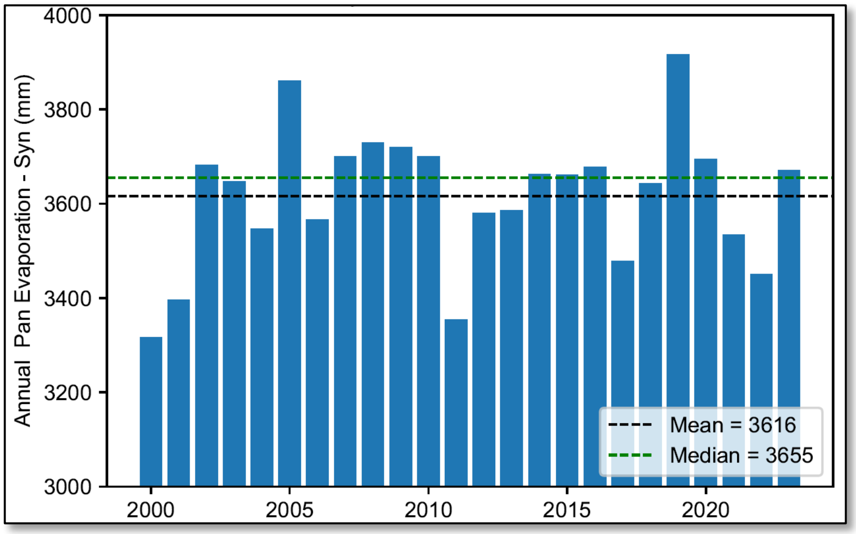

Figure 6-4 Box-whisker plot of monthly annual pan evaporation estimates - SILO 13030 Telfer Aero Station 2000-2023

Monthly distributions of pan evaporation based on daily records are illustrated in Figure 6-5. The highest evaporation rates are typically recorded in the summer months (November, December, and January), with evaporation declining in the cooler winter months (May, June, July, and August).

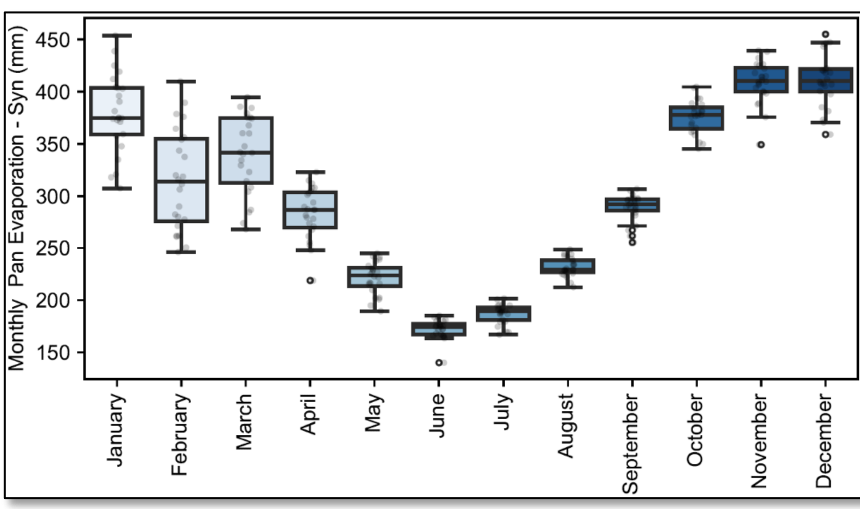

Figure 6-5 Monthly pan evaporation data and statistics for SILO 13030 Telfer Aero Station 2000-2023

6.1.1.4 **Winu Weather Station Data Review**

Climate data are being collected at a weather station recently installed by Rio Tinto near the Winu project, on Copperhead Road (AWS2_CHR, coordinates: 7719324m N, 336341m E). Values have been recorded at approximately one-minute intervals from 2019 through present. Data from 2019 through 2023 were reviewed for this analysis and were compared to publicly available data from the Telfer station for this period.

The datasets were compared at daily, monthly, and annual time scales. Daily rainfall data was reviewed most closely to understand its temporal coverage and quality. Ideally, site-specific climate data would be used to develop long-term synthetic rainfall projections for modeling, however, based significant temporal data gaps in the Winu dataset, combined with the lack of observed climate responses at Winu to major local rainfall events observed at the Telfer station, and the limited temporal extent of the Winu dataset, this was not selected for direct use in this study. Figure 6-6 illustrates the gaps in the Winu weather station data (orange shading). Blue shaded regions indicate periods with some instances of significant rainfall events observed at the Telfer station that are not reflected in the Winu station data. The lack of response at the Winu station calls into question the working order of the rainfall gauge during these time periods, therefore climate data collected from the Copperhead Road (AWS2_CHR) weather station were not used in the climate modeling.

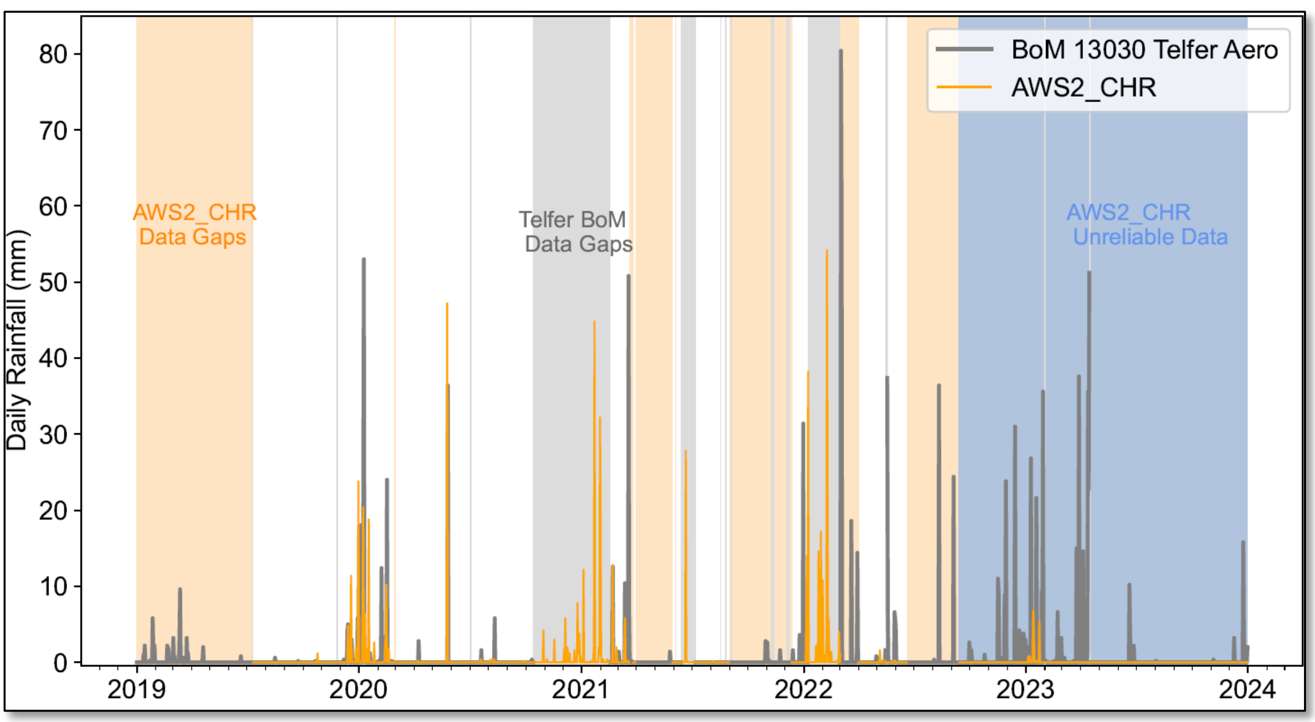

Figure 6-6 Comparison of daily rainfall data: Winu weather station (AWS2_CHR) and BoM 13030 Telfer Aero Station

6.1.1.5 Development of Synthetic Climate Projections for GoldSim Modeling

A workflow was developed to generate representative synthetic rainfall and evaporation datasets for Winu and to extrapolate them into the future for use in the pit lake modeling. The synthetic data were generated based on the statistics of a historical 'training' dataset. The historical training dataset consisted of the Telfer station daily data from 2000-2023 (Section 6.1.1.1). The workflow is described below and illustrated in the workflow diagram provided in Figure 6-7.

Step 1: Source Data

The training dataset was selected: Telfer station from 2000 through 2023. Daily records of rainfall, minimum temperature, maximum temperature, and solar radiation were analyzed.

Step 2: Generation

Generation of the synthetic data was performed using WGEN, a statistics-based weather generation simulator originally developed by the United States Department of Agriculture – Agriculture Research Service, (Richardson et al., 1984). WGEN is a model that generates daily weather variables based on statistics associated with input data. A GoldSim based version of WGEN was used to generate synthetic data for Winu. Daily rainfall, minimum and maximum temperature, and solar radiation from the Telfer station dataset for the period 2000-2023 were used to generate statistics for the historical period. These statistics were then used to generate 100 alternative, statistically consistent, climate realizations (synthetic datasets) for the pit lake model analysis period (2000 to 2360). During this step potential evapotranspiration (PET) was estimated from temperature and solar radiation data using the Samani-Hargreaves approximation (Snyder and Eching, 2002). WGEN does not simulate pan evaporation rates directly.

Step 3: Selection

A root-mean squared error (RMSE) approach was used to identify the closest synthetic dataset to the historical training dataset from the 100 realizations. The RMSE approach included comparison of metrics such as mean, standard deviation, and maximum values for daily rainfall.

Step 4: Calibration

Once the best-matching realization was identified, the WGEN based PET estimates were compared to the observed pan evaporation data from the Telfer station to develop a relationship between synthetic PET and pan evaporation. This relationship was then used to scale the synthetic PET values to create synthetic pan evaporation data.

Step 5: Verification

Verification of synthetic datasets was performed through statistical comparisons of daily, monthly, and annual values in the training and synthetic datasets. Specifically, statistical comparison of the synthetic 2000-2360 datasets to those from the historical training dataset from the Telfer station (2000-2023) was performed together with time series comparisons for the training period.

Step 6: Climate Change

Climate change scenarios developed for Rio Tinto by CLIMSystems were provided to HGL/LRE (Rio Tinto, 2024a) were represented the pit lake modeling. Temporally varying scaling factors for monthly Rainfall and PET were provided for each climate scenario and these were then applied to the Base Case synthetic climate data to create alternative model inputs for modeling pit lake climate scenarios.

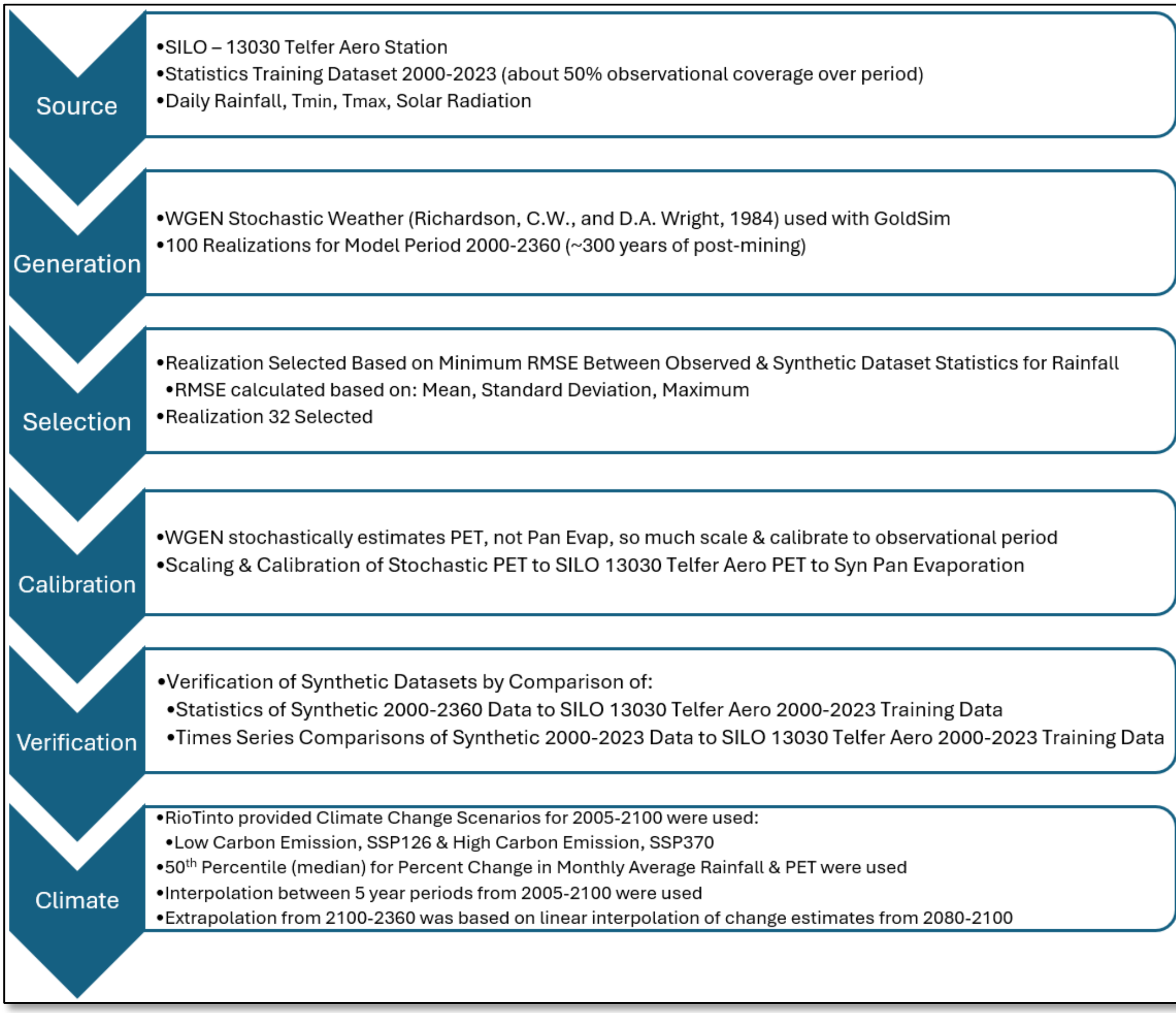

Figure 6-7 Workflow summary for climate data projection

6.1.1.5.1 Synthetic Rainfall Dataset

Synthetic rainfall data for all 100 WGEN realizations is illustrated on Figure 6-8. Data for the selected realization (Base Case) is highlighted with a black line and the median realization with an orange line. The top figure (**A**) illustrates Base Case synthetic annual rainfall in mm from 2000-2360 and the bottom figure (**B**) illustrates the same data at a monthly timescale in mm from 2100-2110 to provide a finer view of temporal variability.

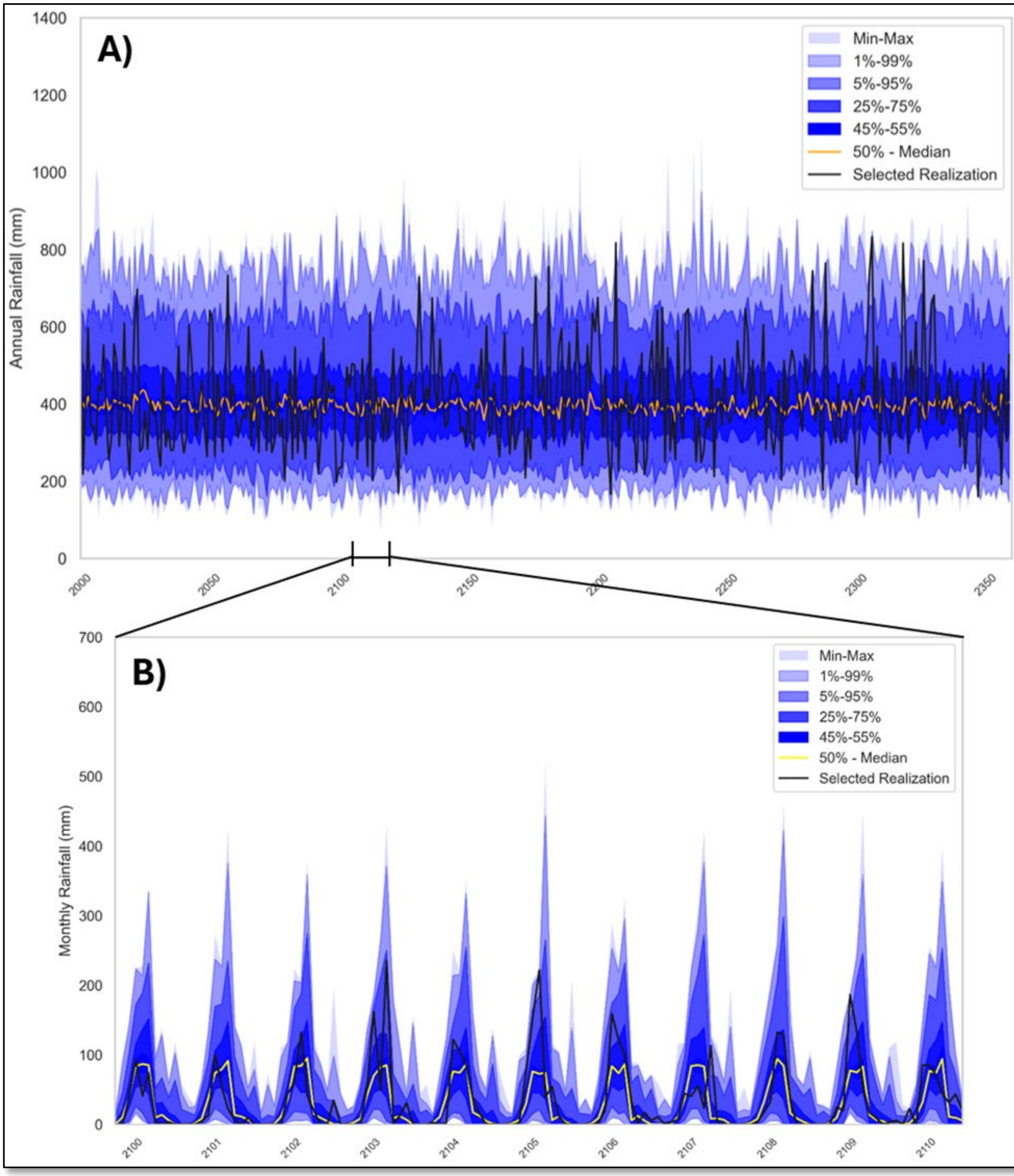

Figure 6-8 All synthetic rainfall realizations with selected realization highlighted in black. A) annual rainfall from 2000-2360 B) monthly rainfall from 2100-2110

The synthetic rainfall values for the selected realization were compared with the historical training dataset for verification (Figure 6-9). The selected synthetic dataset is shown in blue, and the historical training dataset is shown in black. The top figure (A) compares the datasets with respect to monthly averages. The bottom left figure (B) compares daily summary statistics. The bottom right figure (**C**) compares the datasets with respect to annual averages. There is strong agreement between the selected synthetic rainfall dataset and the historical training dataset.

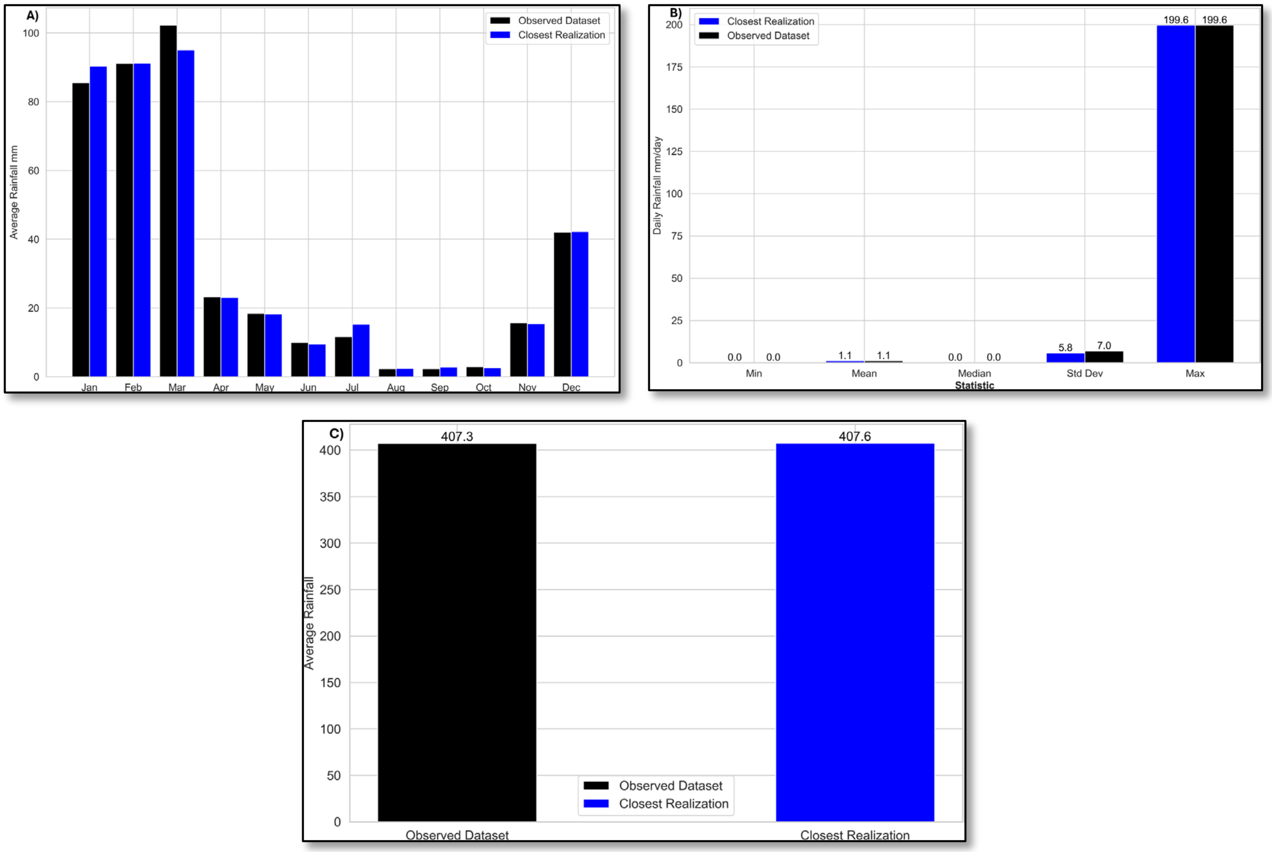

Figure 6-9 Comparison of selected synthetic rainfall dataset 2000-2360 to historical training dataset 2000-2023 A) monthly average rainfall B) daily statistics comparison C) annual average rainfall

6.1.1.5.2 Evaporation Dataset

Synthetic pan evaporation values for all 100 realizations were summarized as shown on Figure 6-10. The selected realization is highlighted with a black line and the median with an orange line. The top figure (**A**) illustrates synthetic annual pan evaporation in mm from 2000-2360 and the bottom figure (**B**) showcases the same data at a monthly timescale for the period 2100-2110 to provide a finer view of temporal variability.

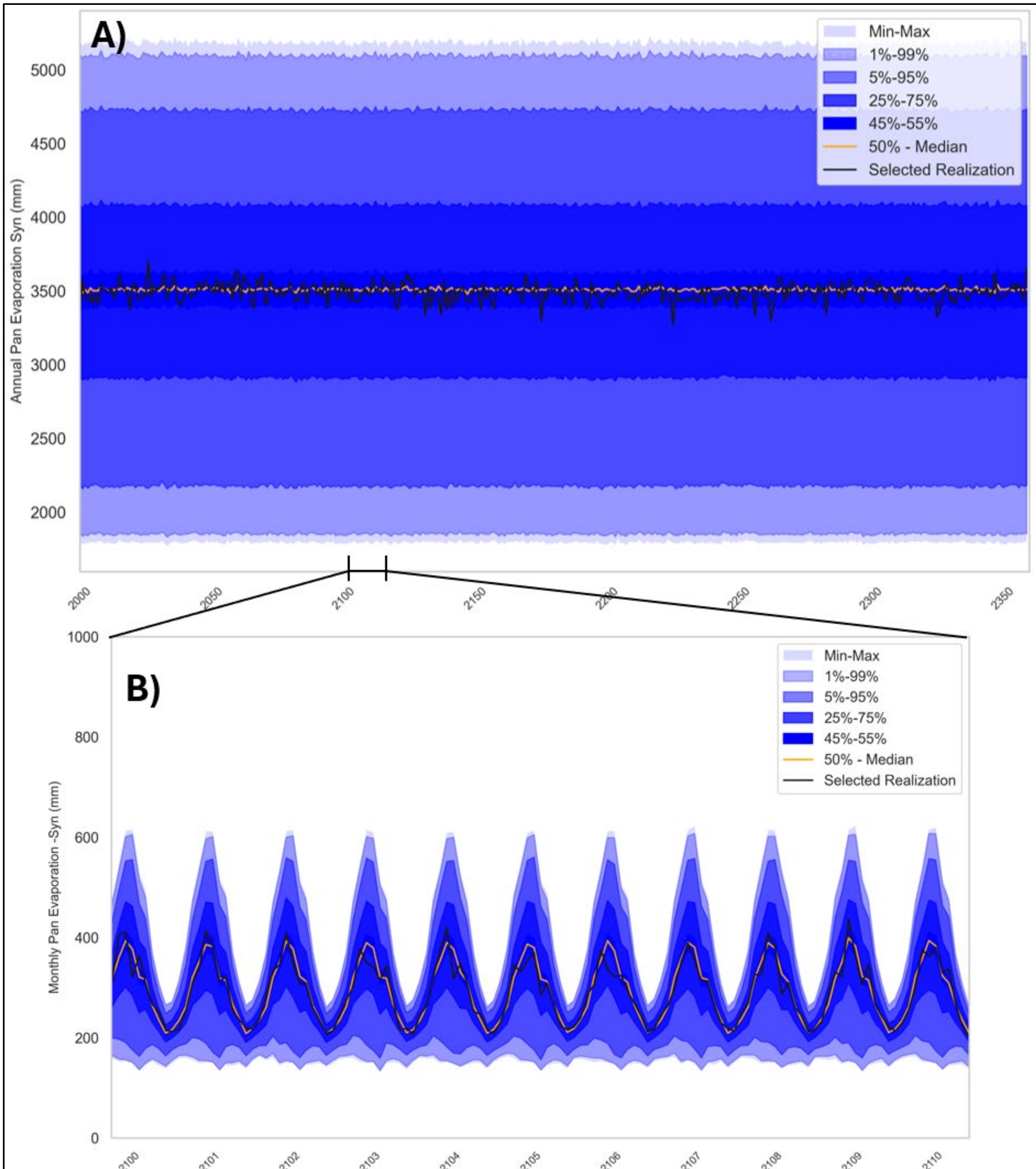

Figure 6-10 Synthetic pan evaporation probability with selected realization highlighted in black. A) annual pan evaporation from 2000-2360 B) monthly pan evaporation from 2100-2110

Comparison of synthetic pan evaporation for the selected realization at different time-horizons with the historical training dataset was performed for verification purposes (Figure 6-11). The selected synthetic dataset is shown in blue, and the historical training dataset is shown in black. The top figure

(**A**) compares the datasets with respect to monthly averages. The bottom left figure (**B**) compares daily summary statistics. The bottom right figure (C) compares the datasets with respect to annual averages. The figure demonstrates that there is reasonable agreement between the selected synthetic evaporation dataset and the historical training dataset.

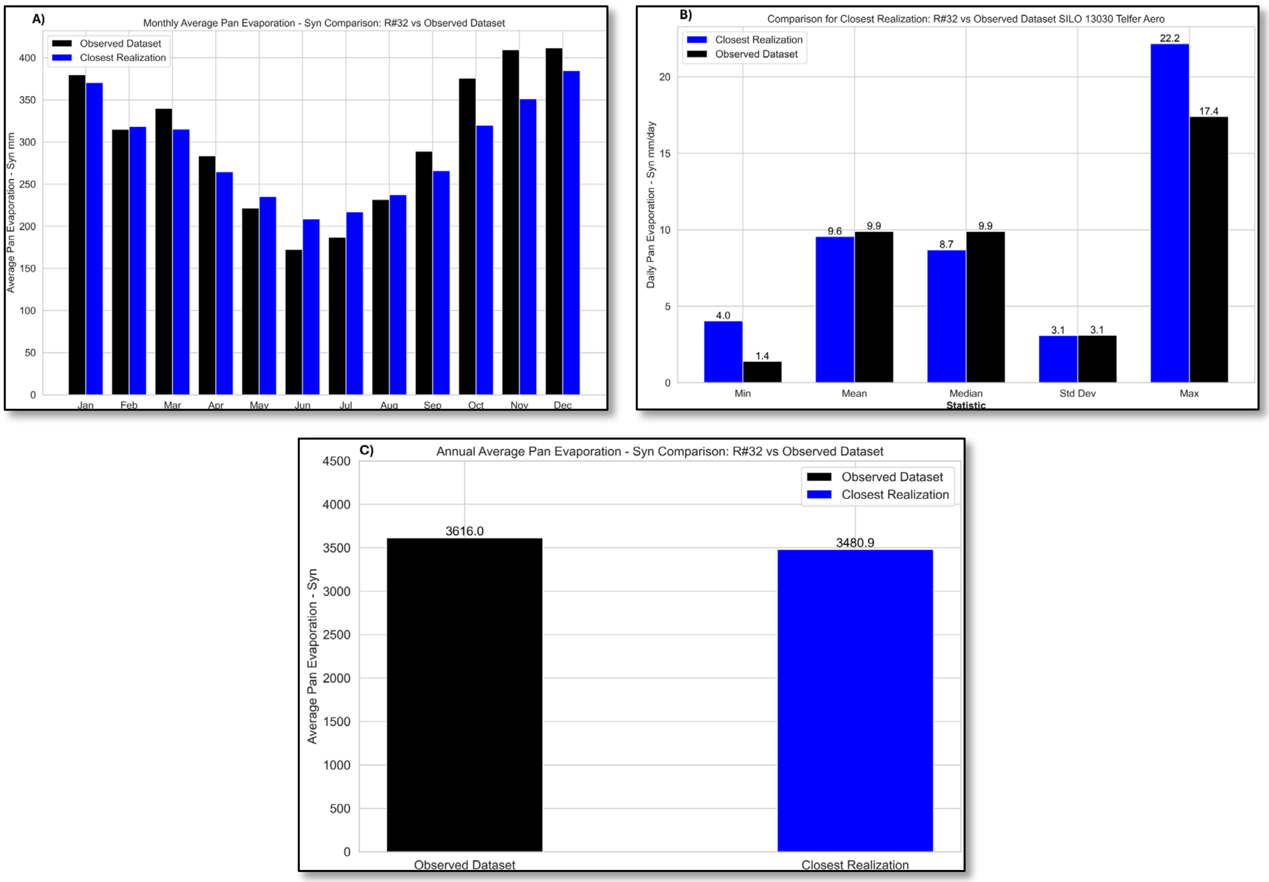

Figure 6-11 Pan Evaporation comparison of selected synthetic dataset 2000-2360 to historical training dataset 2000-2023 A) Monthly average pan evaporation B) Daily statistics comparison C) Annual average pan evaporation

The synthetically generated pan evaporation datasets were scaled to open water evaporation using a constant evaporation coefficient of 0.7, which is a commonly used value in lake studies of similar climate (Yihdego, 2018).

6.1.2 Synthetic Climate Change Datasets for Scenario Simulations

Two climate change scenarios from those developed by CLIMSystems (Rio Tinto, 2024a) were selected by HGL/LRE in conjunction with Rio Tinto for incorporation into the GoldSim model as alternative scenarios:

- Low Carbon Emission (SSP126)
- Moderate to High Carbon Emission (SSP370)

Scaling factors for monthly rainfall and PET varying at five-(5) year increments were provided by Rio Tinto for the period 2005-2100. Mean monthly scaling factors for each parameter representing the 50th percentile (median) were used. Because the pit lake model period extends beyond the climate change analysis period, it was necessary to extrapolate the scaling factors provided through the end of the pit lake analysis period (2360). A linear extrapolation of the scaling factors for the period 2080-2100 was performed. Scaling factors were then applied to the Base Case synthetic climate datasets to generate synthetic datasets for the climate change scenarios. After scaling PET for each climate change scenario, PET was then translated to pan evaporation using the same process described for synthetic data generation. An example of the extrapolation of rainfall scaling factors is shown for January for the two climate change scenarios (Figure 6-12). Extrapolations were performed for both rainfall and pan evaporation, and for each month of the year.

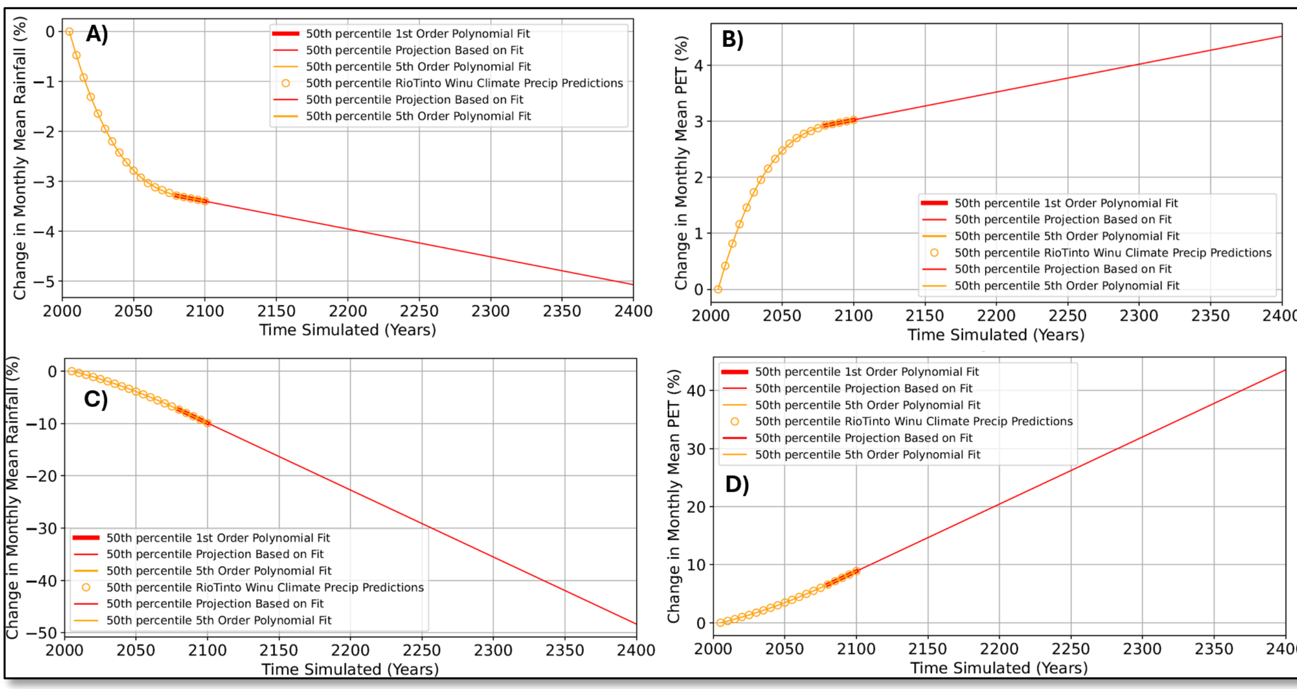

Figure 6-12 Climate change interpolated and extrapolated scaling factors for A) SSP126 January rainfall B) SSP126 January PET C) SSP370 January Rainfall D) SSP370 January PET

Figure 6-13 illustrates the scaled climate change data for annual rainfall and annual pan evaporation rates for the two selected climate change scenarios, SSP126 and SSP370.

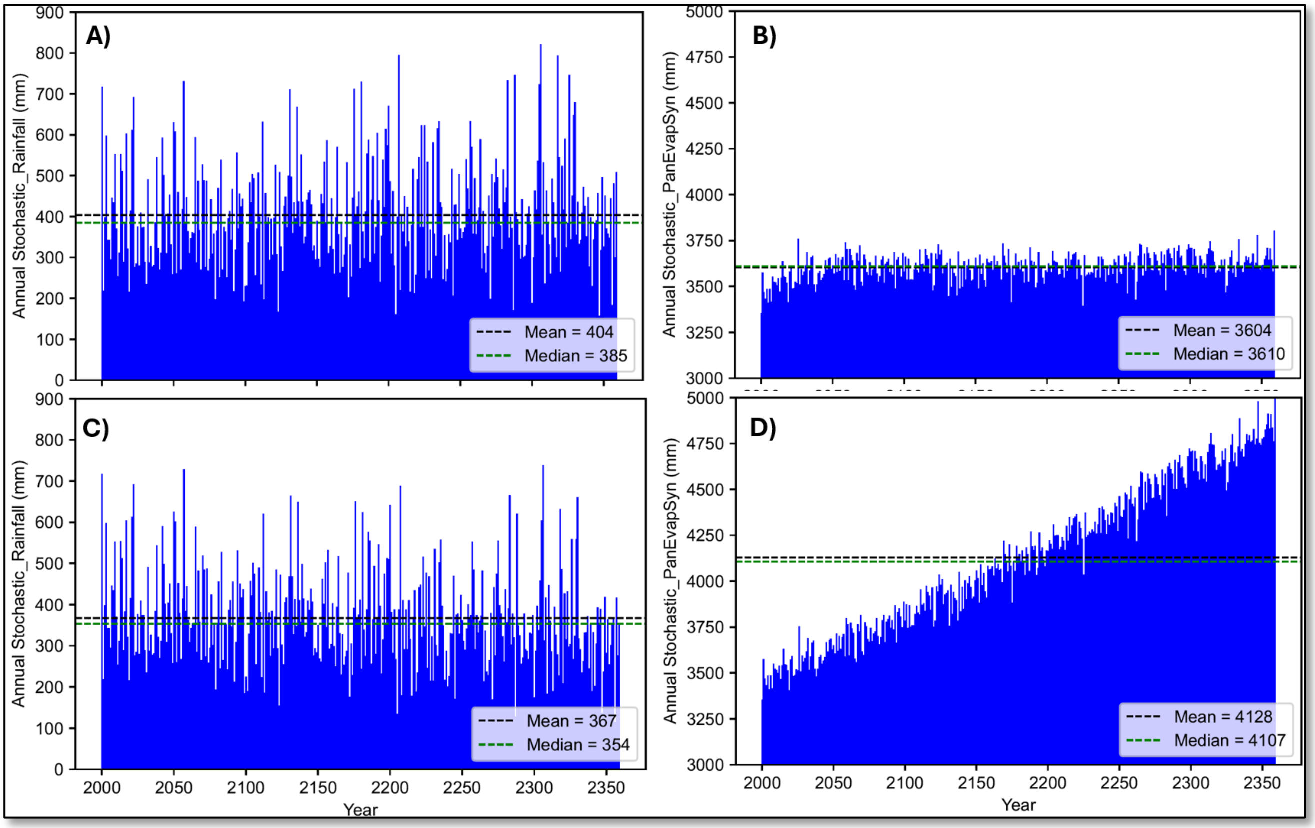

Figure 6-13 Climate Change Data A) Annual Rainfall SSP126 B) Annual Pan Evaporation SSP126 C) Annual Rainfall SSP370 D) Annual Pan Evaporation SSP370

6.1.3 **Pit Wall Runoff**

The majority of precipitation onto the pit walls in arid climates evaporates quickly from the walls and benches. During larger and/or longer-duration events, a fraction of rain falling onto the pit walls will run off into the pit lake and/or infiltrate to nearby groundwater (which also reports to the pit lake). The fraction of rainfall onto the pit wall that ultimately flows into the pit lake tends to be small in arid and semi-arid climates and is sensitive to several factors including rainfall intensity and antecedent moisture conditions (Williams, 2012; McCullough et al., 2013). A dynamic pit wall runoff coefficient was developed from synthetic daily rainfall data according to the criteria shown in Table 6-1. Sensitivity analyses were not conducted on the dynamic pit wall and catchment runoff coefficients. Monthly totals were calculated from the corrected daily values for use in the modeling. Monthly pit wall runoff volumes are calculated in the water balance by multiplying the runoff depth (mm) by the pit footprint area (two-dimensional plan view) minus the pit lake area. The exposed pit wall area declines during pit filling as the volume (and therefore area) of the pit lake increases.

Table 6-1 Dynamic pit wall and catchment runoff coefficients

Daily Rainfall	Previous Day Rainfall	Pit Wall Runoff Coefficient	Catchment Runoff Coefficient
mm/day	mm/day		
<5	-	0	0
<40	<20	0.2	0.05
<40	≥20	0.6	0.15
Else	-	0.6	0.15

The values in Table 6-1 are estimated based on the following criteria:

- Due to the dry climate and high evaporation rates at the site, it was assumed that zero runoff will occur when daily rainfall is less than 5 mm.
- When daily rainfall is between 5 and 40 mm, the runoff coefficient depends on the antecedent moisture content from the previous day. If the previous day's rainfall is less than 20 mm, it is assumed that 20 percent of the rainfall will runoff into the pit lake, and when the previous day's rainfall is greater than or equal to 20 mm, 60 percent of rainfall will runoff to the pit lake. [2]
- During more intense storm events (≥40 mm per day), it is expected that 60 percent of rainfall will runoff into the pit, regardless of previous-day rainfall.

The logic for the dynamic pit wall runoff coefficient is presented in Table 6-1 and is comparable to values presented by McCullough et al. (2013) for a Western Australia semi-arid climate pit lake.

6.1.4 Runoff from Surrounding Areas

An abandonment bund will be constructed at closure approximately 180 to 200 m from the pit rim to mitigate the potential risk from zones of instability impacts and limit fauna and unauthorized human access to the pit void (Rio Tinto, 2024d). However, this bund is not expected to be constructed to be fit-for-purpose for water flow diversion as recommended by DRDMW (2022a, b). For the purposes of these modeling efforts, it was assumed that the proposed abandonment bund will divert potential catchment runoff away from the pit. This assumption is based on the high evaporation rates at the site, minimal topographic relief, and absence of nearby surficial ephemeral runoff drainages. Surface runoff from the WRL and TSF is not expected to report to the pit lake due to diversion of surface water flow by the abandonment bund.

The catchment area between the pit edge and abandonment bund is approximately 1,089,000 m^2 (Figure 6-14). The majority of precipitation onto the catchment area will evaporate and only a low percentage is expected to report to the pit lake due to the low relief and high evaporation rates at site. The same approach of employing dynamic runoff coefficients was applied to precipitation within

[2] These coefficients are considered conservative as the talus on the benches will likely serve as a water store, limiting runoff to the lake.

the catchment area. The logic for the dynamic catchment runoff coefficient is presented Table 6-1. It was assumed that 5 percent of precipitation falling within the catchment area will report to the pit lake. As with the pit wall runoff, it was assumed that zero runoff will occur when daily rainfall is less than 5 mm. When daily rainfall is between 5 and 40 mm, the runoff coefficient depends on the antecedent moisture content from the previous day. If the previous day's rainfall is less than 20 mm, it is assumed that 5 percent of the rainfall will runoff into the pit lake, and when the previous day rainfall is greater than or equal to 20 mm, 15 percent of rainfall will runoff to the pit lake. During more intense storm events (≥40 mm per day), it is expected that 15 percent of rainfall will runoff into the pit, regardless of previous-day rainfall.

The catchment runoff coefficients applied for the modeling assume less runoff compared to pit wall runoff due to several factors including the very low relief inside the abandonment bund perimeter, the apparent segmentation by existing northwest-southeast trending surficial dune lineations, and lack of apparent ephemeral drainage from aerial imagery. Catchment runoff estimates associated with the Winu pit lake model are based on lower runoff coefficients than have been applied at other Western Australia pit lakes; specifically, the Collie pit lake located in southwestern Western Australia where the climate is wetter, and more temperate than Winu. For the Collie district, a catchment runoff coefficient of 25 percent of precipitation was used (Lund, 2018, 2020).

6.1.5 **Groundwater Inflow**

The ultimate pit will extend from a rim elevation of approximately 245 meters Australian Height Datum (m AHD) to an elevation of approximately -190 m AHD, creating an open pit roughly 435 m deep at closure. The elevation of the pre-mining groundwater table is approximately 190 to 200 m AHD (Figure 6-15) in the area adjacent to the pit, and the ultimate pit floor elevation is roughly 390 m below this elevation.

Groundwater inflow rates during post-closure were simulated in the three-dimensional MODFLOW (Modular Finite-Difference Flow Model; Langevin et. al., 2017) groundwater flow model developed by Advisian as part of the 2022 Hydrology and Hydrogeology Study (Advisian, 2022). Groundwater inflow rates predicted by the Advisian model do not account for infiltration pond or surplus water management as an input. Base case modeling indicates that the water would be expected to mound above the silcrete and not report to the pit. Groundwater inflow rates to the pit are highest during initial filling, because of high hydraulic gradient between the pit lake and the surrounding groundwater. The hydraulic gradient toward the pit declines as the pit lake water level rises (Figure 6-16) but a gradient towards the pit, and ongoing associated groundwater inflow is expected at all times post-closure.

The Advisian groundwater flow model does not predict groundwater outflow from the pit as the pit lake is predicted to act as a hydraulic sink.

Figure 6-14 Abandonment bund location at closure

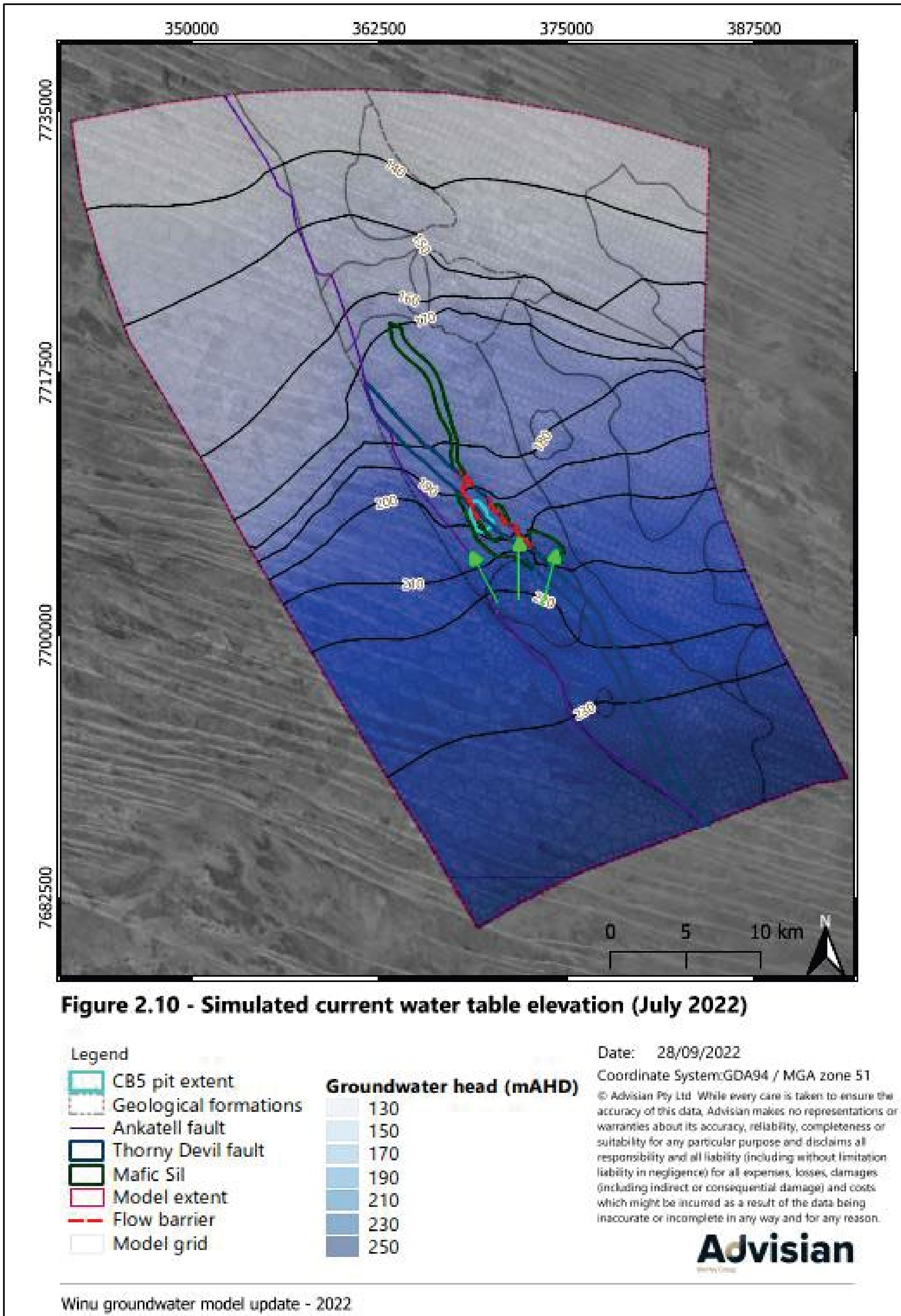

Figure 6-15 Simulated current water table elevation (From Winu Dewatering Strategy and Groundwater Supply Update, Advisian, 2022)

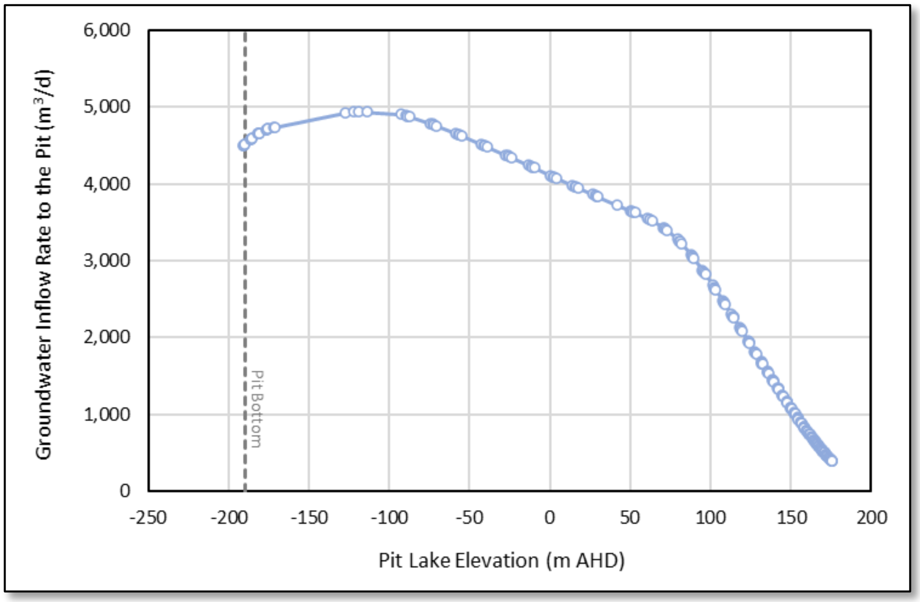

Figure 6-16 Groundwater inflow rates by pit lake level (from Advisian, 2022).

6.1.6 Seepage From Tailings Storage Facility

Water, Waste and Land Australia Pty Ltd (WWL) (2023), performed flow modeling to predict potential seepage rates into the foundation of the TSF towards the end of operations and continuing into post closure. Seepage from the TSF is expected to occur in the future due to progressive degradation of the system underlying the entire TSF. TSF design reviews (WWL, 2024) indicate that an LLDPE liner w will be in use for the high sulfur tailings cells and a bituminous geomembrane will be in use for the low sulfur tailings cells (WWL, 2024). WWL (2023) modeling predicted upper and lower bound seepage rates from the TSF extending 250 years into post closure (Figure 6-17). (Modeling results were extrapolated using linear regression for an additional 50 years (to the end of the modeling period, 300 years post closure) based on the preceding 50 years to create a dataset matching the pit lake modeling period). Seepage rates predicted by WWL (2023) are understood to represent the entire TSF including the two high sulfur cells (HST1 and HST2) and two low sulfur cells (LST1 and LST2).

The seepage rate used in the Base Case scenario was calculated as the average of the upper and lower bound results generated by WWL (2023). For the purposes of the pit lake modeling, it was assumed that the seepage rates and timing presented represents solution migration through the geomembrane liner and vertically through the vadose zone below the TSF to the water table. Upon reaching the water table, TSF seepage is expected to flow towards the pit in under saturated conditions. For the current modeling, zero travel time for TSF seepage migration in saturated bedrock was assumed. In order to understand the effects of the TSF seepage on the water balance and pit lake water quality, an alternative scenario was also simulated with zero TSF seepage arriving at the pit lake during the simulation period. This scenario represents what might be a potentially extended travel time for the TSF seepage through the vadose zone. There may be associated dispersion of TSF seepage in the vadose zone which may further delay, or even preclude, seepage arrival rate at the pit lake.

The Advisian (2022) groundwater flow model does not include TSF seepage (G. Jacobs, pers. communication, 1 Apr 2024). This may lead to a difference in pit lake filling predictions between the two models.

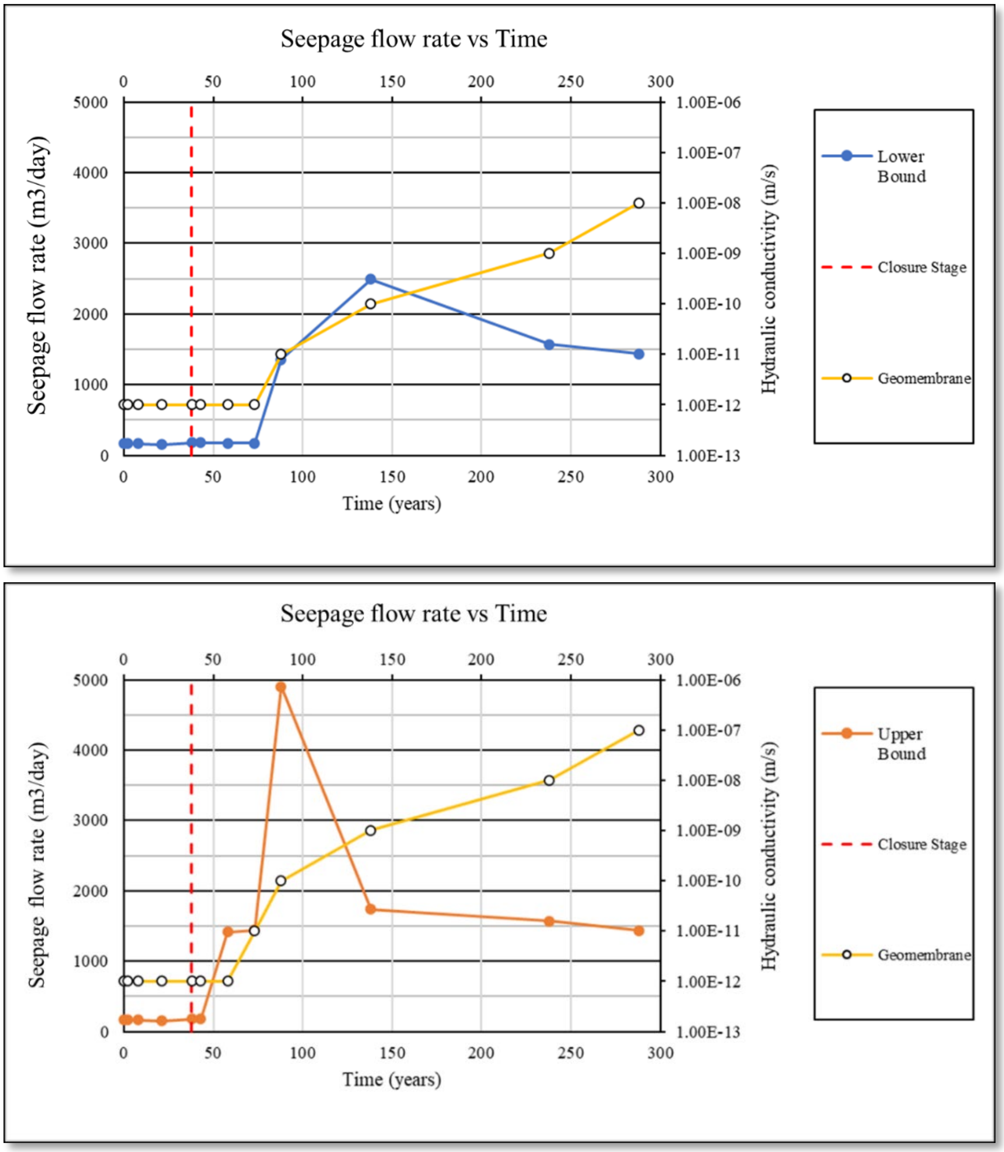

Figure 6-17 Predicted TSF seepage rates (figure by WWL 2023)

6.1.7 Waste Rock Landform Seepage Potential

The pit lake water balance modeling incorporated consideration of the waste rock landform (WRL) that will be constructed and used to store waste rock for the operation (Rio Tinto, 2024e). The WRL will be located between the open pit and the TSF. If seepage out of the base of the WRL occurs, and exceeds the uptake capacity of the vadose zone, the seepage would mix with local groundwater in the post-closure pit lake cone of depression and report with groundwater to the pit. HGL/LRE developed a screening level evaluation of infiltration into, and seepage through, the WRL during the operational period prior to construction of a final cover. The closure plan AMD strategy and management plan (Rio Tinto 2024d and 2024e) specify a maximum WRL height of 80 meters (m) with individual lifts being less than 10 m in height (Figure 6-18).

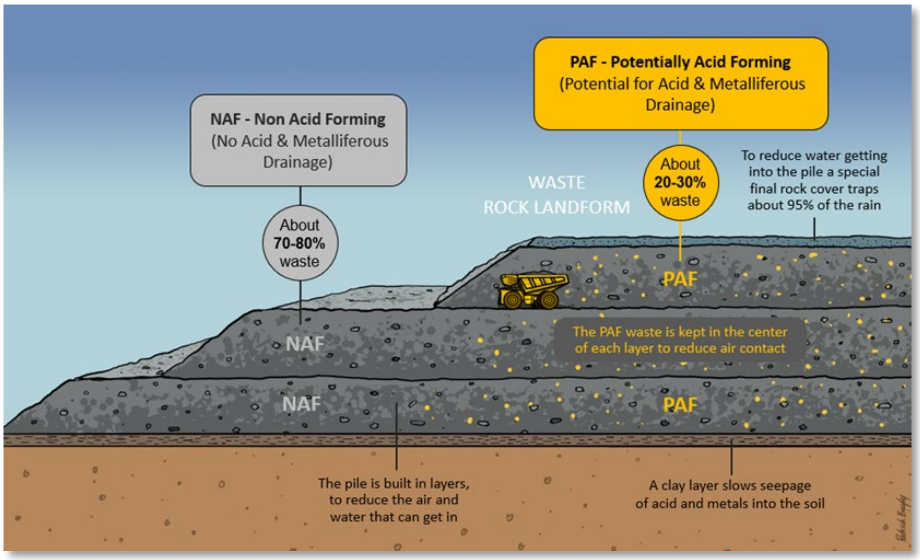

Figure 6-18 WRL Conceptual-Level Design at Closure

PAF: Potentially Acid Forming NAF: Non Acid-Forming

Based on the climate at Winu, deep percolation of rainfall into the WRL is expected to be limited, with much of the rainfall becoming shallow, temporary, pore water storage in the waste rock followed by subsequent evaporation. Modeling was performed to provide some quantification of possible percolation into the landform and available moisture uptake capacity of the materials and to understand the possibility of seepage out of the bottom of the WRL, into the underlying vadose zone and down to the water table during operations. The WRL generalized seepage conceptual model is illustrated in Figure 6-19.

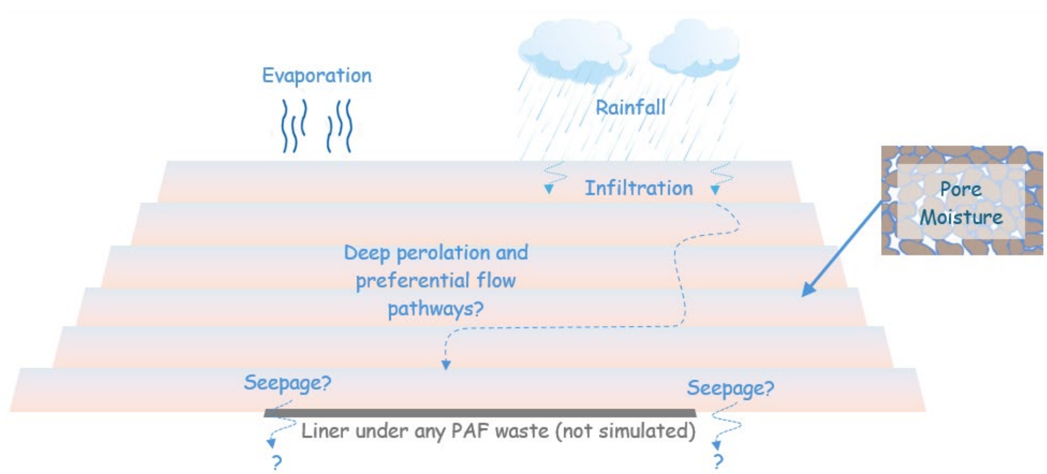

Figure 6-19 General WRL Conceptual Model during Operations

Two modeling stages were implemented in this study. Numerical modeling was developed to predict infiltration into the WRL and was performed using the infiltration modeling code Hydrus-1D. The simulated infiltration rate was then used as an input to a one-dimensional analytical model representing the WRL and the underlying, undisturbed, vadose zone. One-dimensional modeling represents a vertical line through a central area of the WRL where newly placed waste rock will have a thin layer of truck-traffic-compacted material at the surface as a result of vehicular placement of the waste rock. The side slopes of the facility will not be compacted by truck traffic. These areas will have a smaller average thickness which may result in somewhat more infiltration around the perimeter of the WRL. However, no PAF material is expected in the side slopes of the WRL as indicated in Figure 6-18.

The analytical modeling used a water balance approach and calculated the uptake of moisture from infiltration within each waste rock lift to predict the amount of any excess water that might be available for seepage to the underlying lift and then, cumulatively, from the base of the WRL. The analytical model was also designed to account for the moisture uptake capacity of the vadose zone in the event of any seepage out of the base of the WRL being predicted.

The range of predicted infiltration rates into the WRL based on Hydrus-1D modeling is illustrated in Figure 6-20 (in units of percent of annual precipitation). The range of infiltration rates reflects the uncertainty in model input parameters.

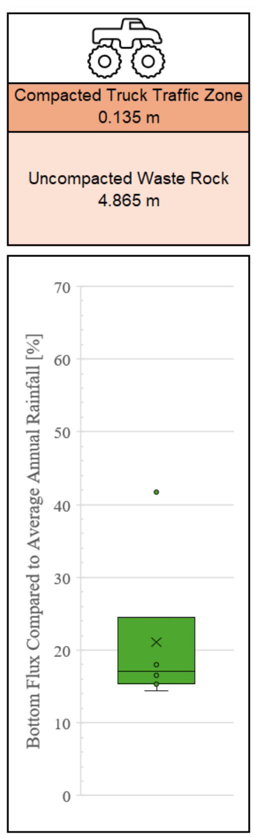

Figure 6-20 Hydrus-1D steady-state percolation rates

Parameters affecting the moisture uptake capacity of the materials include the initial moisture content of the material, the material's field capacity, and the likely fraction of preferential flow through the material. Four sensitivity analyses were performed (in addition to the base estimate) by varying selected parameter values within reasonable ranges. Figure 6-21 illustrates the analytical modeling input data and predicted one-dimensional seepage rates. The qualitative representation of infiltration depth in Figure 6-21 shows the schematic wetting front for each of the simulations and indicates that moisture is not expected to infiltrate through the entire WRL thickness during operations (blue shading only extends part way through the orange WRL lifts). This is also indicated by green shading in the tables above. Although some moisture uptake capacity in the WRL is consumed, there is still adequate capacity to prevent seepage from occurring. Consequently, no water is expected to infiltrate down to the vadose zone and therefore no water is expected to reach the water table during operations.

WRL Specifications	Units	Values
Total Height	m	80
Mine Life	years	26
Rate of Rise	m/yr	3.1
Mean Annual Rainfall	mm	387
Runoff Ratio for Rainfall (Overland Flow)	%	0

Shading Key
Seepage
No Seepage
Sensitivity Value
Unsaturated

WRL	Units	0.135 m Truck Traffic Zone Only				
		Estimate	Sens. 1	Sens. 2	Sens. 3	Sens. 4
Annual Rise Height	m	3.1	3.1	3.1	3.1	3.1
Percent Infiltration (Input from Hydrus Model)	fraction of precipitation	0.21	0.21	0.21	0.14	0.42
Initial Moisture Content	% water by weight	0.03	0.03	0.03	0.03	0.03
Field Capacity	% water by weight	0.18	0.18	0.18	0.18	0.18
Percent Preferential Flow	Fractional reduction in moisture uptake capacity	0.5	0.3	0.7	0.5	0.5
Deep Infiltration	mm	82	82	82	56	162
Uptake Capacity	mm	231	323	138	231	231
Seepage	mm	0	0	0	0	0
Percent Uptake Capacity Consumed	%	35	25	59	24	70

Vadose Zone	Units	0.135 m Truck Traffic Zone Only				
Thickness	m	50	50	50	50	50
Annual Seepage from WRL	mm	0	0	0	0	0
Total LOM Seepage from WRL	mm	0	0	0	0	0
Initial Moisture Capacity	% water by weight	0.03	0.03	0.03	0.03	0.03
Field Capacity	% water by weight	0.080	0.080	0.080	0.080	0.080
Percent Preferential Flow	Fractional reduction in moisture uptake capacity	0.5	0.5	0.5	0.5	0.5
Uptake Capacity	mm	1250	1250	1250	1250	1250
Seepage to Water Table	mm	0	0	0	0	0
Percent Uptake Capacity Consumed	%	0	0	0	0	0

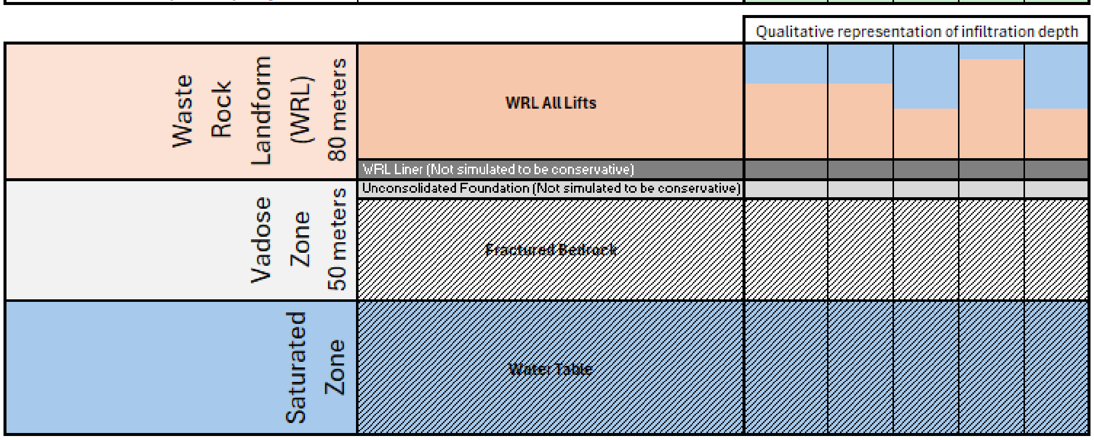

Figure 6-21 Analytical WRL Percolation Modeling

At closure, a cover will be placed on the surface of the WRL, reducing infiltration of rainfall from approximately 21% of precipitation (based on Hydrus-1D modeling of operations) to approximately 3 to 6% of precipitation (Okane, 2020). As a result, the progression of a wetting front through the WRL is expected to be negligible after closure. In addition, the modeling conservatively disregarded the seepage reduction benefits of the WRL liner and the compaction of the unconsolidated WRL foundation. It was assumed for the purposes of pit lake modeling that the likelihood of any WRL seepage occurring, reaching the water table and migrating towards the pit lake during the 300-year pit lake simulation period was negligible.

6.1.8 Ultimate Pit Shell

Relationships for elevation with volume and surface area required for the model were generated using the *Winu_Pit_CB_6_20230614* pit shell provided by Rio Tinto. Updated three-dimensional geologic models of geology and geometallurgical classification were also provided by Rio Tinto and were used to generate volumes and surface areas of lithology by elevation.

6.1.9 Elevation-Area-Volume Relationship

Lake volume and pit wall surface area relationships to elevation of the pit were extracted from the *Winu_Pit_CB_6_20230614* pit shell. The total volume of the pit is approximately 311 million cubic meters (Mm^3), with a total pit wall exposure of approximately 3.1 million meters squared (Mm^2). The pit wall surface area (perpendicular to the pit walls) and two-dimensional plan view surface area were calculated from the pit shell model and used to inform the volume of damaged rock zone and the plan view catchment area for pit wall runoff, respectively.

6.1.10 Pit Shell Geology

Pit wall exposures of lithologies by elevation were extracted from the pit shell and lithologic and geometallurgy three-dimensional geologic models. Lumping of lithology and geometallurgy classes from the geologic models was performed in collaboration with Rio Tinto and resulted in 14 collated lithologies being represented in the pit lake model. The geologic and geometallurgical models provide by Rio Tinto were intersected with the pit design in the three-dimensional geologic modeling software Leapfrog (Bentley, 2024) to calculate the perpendicular surface areas each lithology in the pit wall at closure. Total perpendicular surface areas by lithology are summarized in Table 6-2.

The three major rock types exposed in the ultimate pit wall (cover, mafic, and metasediments) were split into geometallurgical classifications based on mineralization style and sulfide content (i.e., sulfide, oxide, mixed, and leached cap). Cover materials, exclusively located above approximately 100 m AHD on the exposed pit walls, include six separate lithologies (Quaternary Sand, Permian Regolith, Permian Sandstone, Oxidized Mudstone, Reduced Mudstone, and Diamictite) which can collectively be referred to as Cover materials due to similar lithologic and geochemical characteristics between the six units.

Figure 6-22 displays the pit wall exposure (m²) of each lithology by each bench and Figure 6-23 displays the distribution of lithology exposure on the pit walls.

Table 6-2 Total Pit Wall Exposure by Lithology

Lithology	Total Surface Area	
	m²	Percent
QA Sand	149,814	4.9
Permian Regolith	191,048	6.2
Permian Sandstone	285,562	9.3
Oxidized Mudstone	161,552	5.3
Reduced Mudstone	98,562	3.2
Diamictite	15,518	0.51
Mafic - Leached Cap	5,426	0.18
Mafic - CuOx	383	0.012
Pre-mineral Mafic	41,228	1.3
Metasediments - Leached Cap	305,880	10
Metasediments - CuOx	3,532	0.12
Metasediments - Oxide/Sulfide Mixed	3,489	0.11
Metasediments - Secondary Sulfides	29,673	1.0
Metasediments - Primary Sulfides (Hypogene)	1,778,056	58
Total	**3,069,723**	**100**

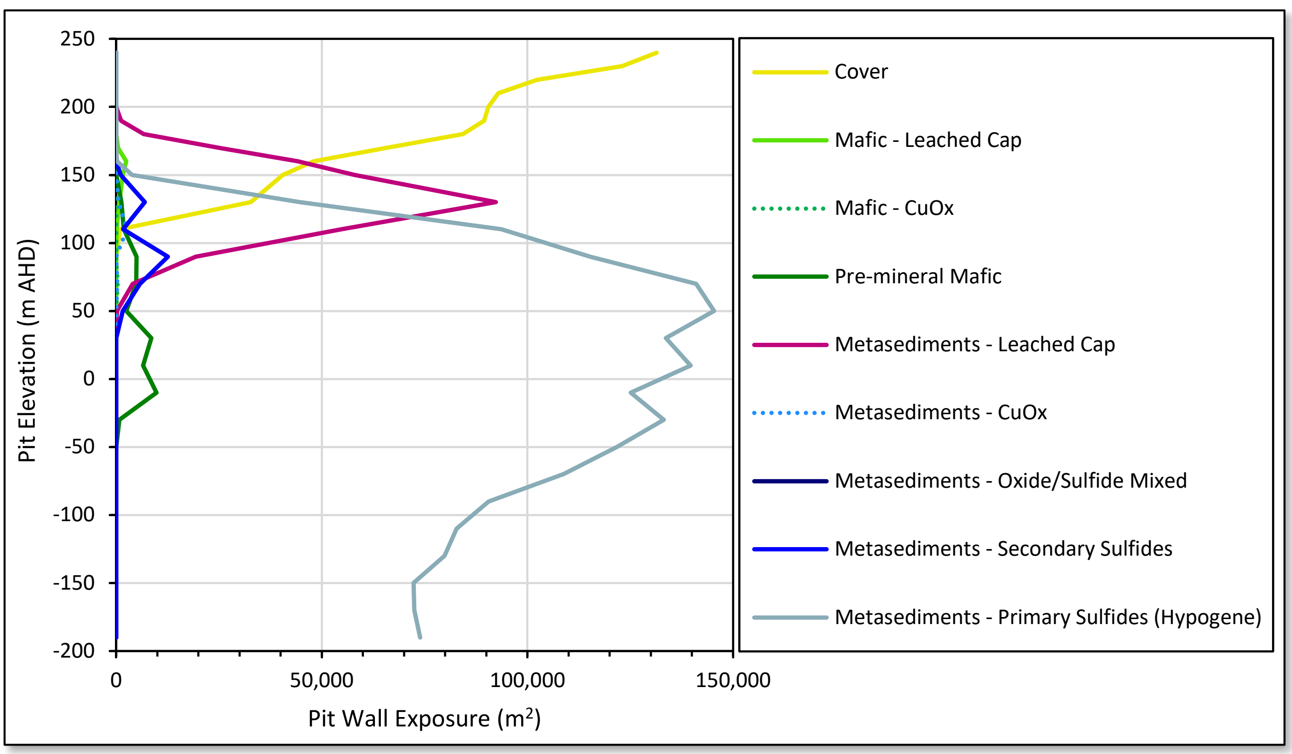

Figure 6-22 Pit wall exposure by bench elevation for major lithologic units

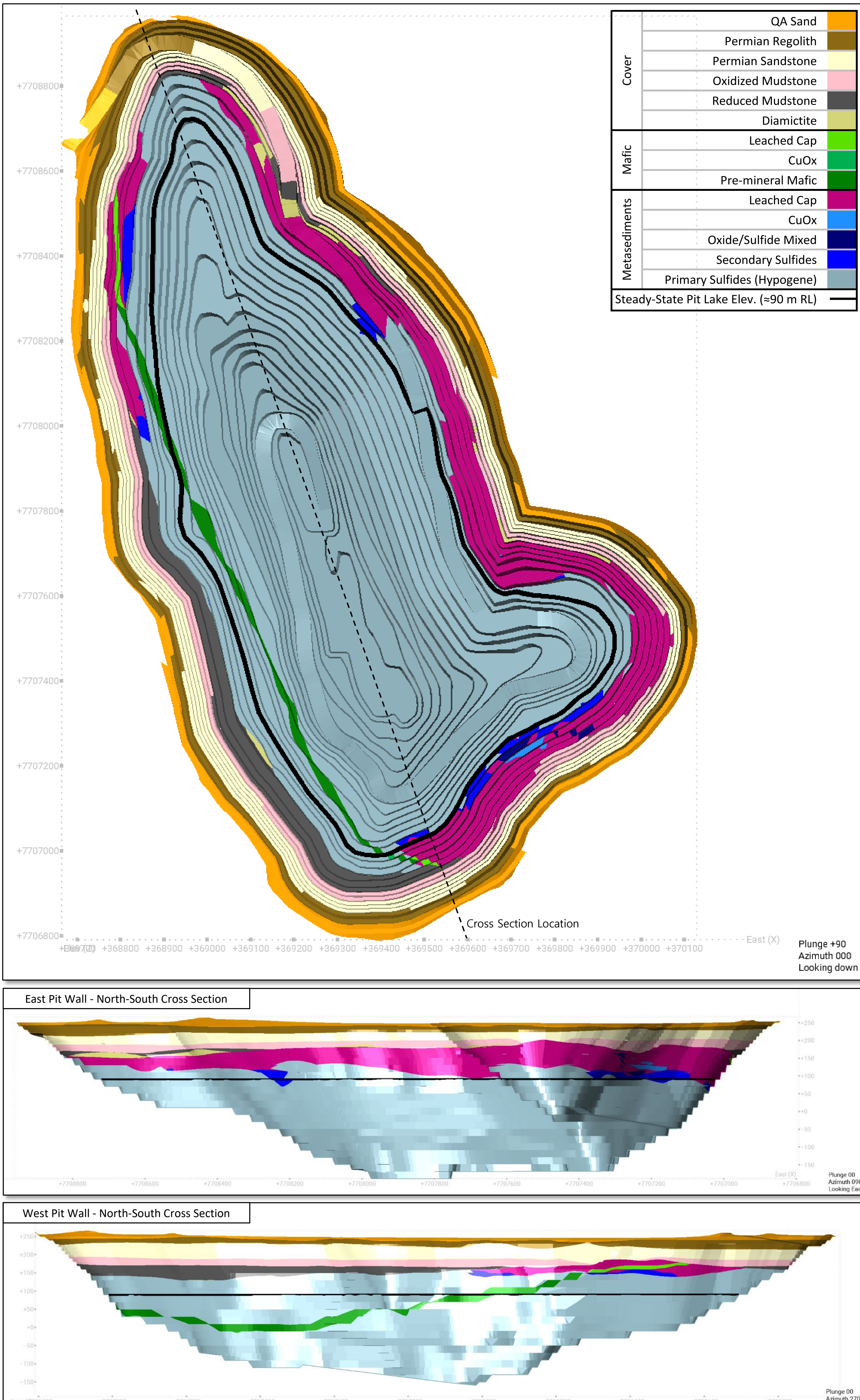

Figure 6-23 Lithology exposures on pit walls

6.1.11 **Talus and Damaged Rock Zone**

Talus is expected to accumulate on pit benches during mining. All talus is assumed to have formed before closure for modeling purposes. Talus is assumed to accumulate at the angle of repose of 36° and fill to the width of the bench. Pit construction employs 10m bench heights above 150 m AHD within cover and overburden rock types and 20 m bench heights below 150 m AHD in weathered and fresh mafic and metasediment rock types. The geometry of the talus "layer" was calculated for the 10 m and 20 m benches using the average Bench Face Angle (BFA) and Catchbench width (CB) provided by Rio Tinto (R. Green, pers communication March 5, 2024). The cross-sectional area of talus was calculated to be 34.1 m^2 and 32.3 m^2 for the 10 m and 20 m bench geometries respectively (Figure 6-24). The talus volume accumulated on each bench was calculated as the cross-sectional area multiplied by the bench length. A lithology was assigned to the talus based on the neighboring exposed pit wall lithology determined from the geologic model. It was assumed that the total volume of the talus (3.5 Mm^3) would not affect the original ultimate pit volume-elevation relationship (it forms <1.1% of total pit volume). Talus was assigned a rock density of 2.69 tonne/m^3 and a porosity of 30%.

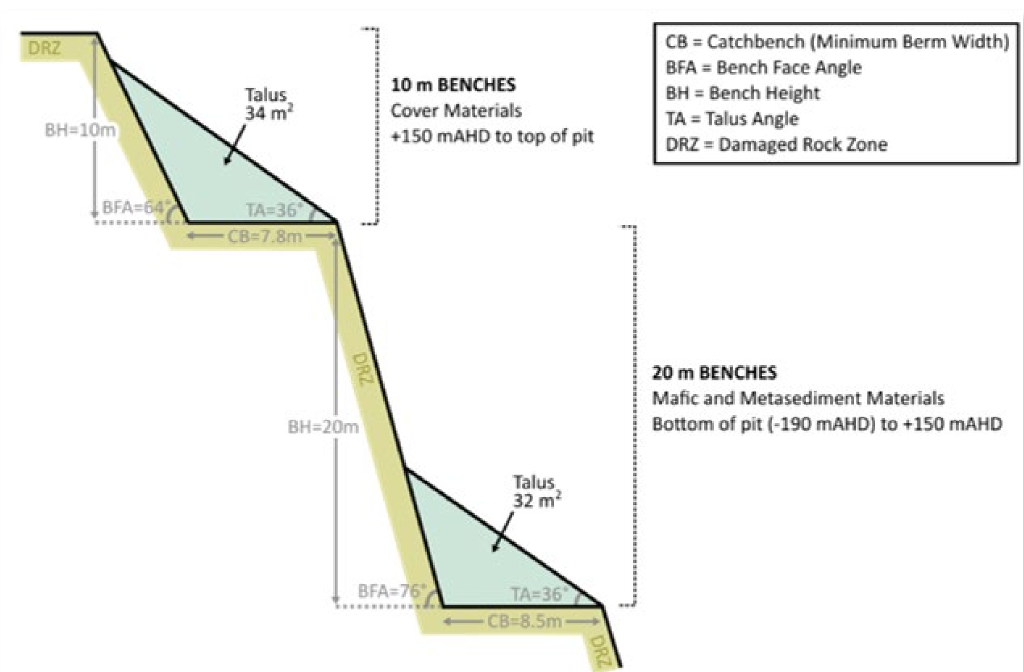

Figure 6-24 Schematic diagram of talus formation on benches

It was assumed that the presence and thickness of talus would not affect oxygen ingress or solute loading from the underlying or concealed damaged rock zone. The Base Case damage rock zone was assigned a uniform 1 m thickness across the pit including along catch benches and faces (Figure 6-24), and a porosity of 8% to represent the average porosity through the 1 m thick damaged rock zone.

6.2 Geochemical Source Terms

A chemistry was assigned to each pit inflow/chemical mass loading source. These chemistries were mixed in PHREEQC, along with the pit lake solution chemistry from the previous timestep, to calculate a pit lake chemistry for the current timestep. Input chemistries are associated with:

- Rainfall;
- Pit wall runoff;
- Catchment runoff;
- Chemical mass loading from inundation of the pit wall damaged rock zone and bench talus;
- Groundwater inflow; and
- Seepage from the TSF.

Chemistries associated with these sources are described later in this section. Chemical mass loading associated with inundation of the pit wall is caused by the rising pit lake inundating the pit walls and mobilizing solutes and weathering products from the pore spaces. This geochemical input is purely a chemical mass source associated with the rising pit lake level. There is no additional water associated with this mass, unlike the other pit inflows which bring both water and chemical mass into the pit lake.

6.2.1 Rainfall

Rain falling directly on the pit lake surface is expected to have low concentrations of dissolved constituents and to be in equilibrium with atmospheric gases. The chemistry of rainfall used in the model is based on data collected from the Tom Price Iron Ore mine in the Pilbara of Western Australia and is presented in Table 6-3 (Golder, 2021). The rainfall chemistry was charge-balanced on sodium prior to input to the water quality modeling.

Table 6-3 Rainfall Chemistry

Parameter	Units	Tom Price Iron Ore Mine Precipitation Chemistry
Temperature	°C	25
pe	-	11
pH	s.u.	6.4
Total Alkalinity	mg/L as $CaCO_3$	5.7
Chloride	mg/L	1.0
Sulfate	mg/L	1.0
Calcium	mg/L	0.6
Iron	mg/L	0.016
Sodium	mg/L	2.5
Potassium	mg/L	0.2
Magnesium	mg/L	0.2
Silicon	mg/L	0.23
Strontium	mg/L	0.030

6.2.2 Catchment Runoff

The Quaternary sand lithologic unit (QA Sand) represents nearly the entire surface exposure within the abandonment bund. Monitoring data from seasonal or annual surface runoff was not available, therefore, the source term was derived from MEP results from a single QA Sand sample. The source term for catchment runoff is presented in Table 6-4. For most parameters, MEP results were below the limit of detection, and are displayed in Table 6-4. In order to provide a more conservative estimate of runoff water quality, the concentration of the limit of detection was used (rather than one-half the limit). The resulting source term was charge balanced based on sodium concentration.

Table 6-4 Catchment runoff source term

Parameter	Unit	Catchment Runoff Source Term
Temperature	°C	25
pH	s.u.	6.41
Total Alkalinity	mg/L as $CaCO_3$	2.8
Ca	mg/L	-
Na	mg/L	1.2
K	mg/L	1
Mg	mg/L	-
SO4	mg/L	1
Cl	mg/L	2.0
F	mg/L	0.1
Nitrate	mg/L as N	0.060
Nitrite	mg/L as N	0.010
Ammonia	mg/L as N	0.010
P	mg/L	0.01
Al	mg/L	0.01
Sb	mg/L	0.001
As	mg/L	0.001
Ba	mg/L	0.0056
B	mg/L	0.05
Cd	mg/L	0.0001
Co	mg/L	0.001
Cr	mg/L	0.001
Cu	mg/L	0.001
Fe	mg/L	0.05
Pb	mg/L	0.001
Mn	mg/L	0.001
Mo	mg/L	0.001
Hg	mg/L	0.0001
Ni	mg/L	0.001
Se	mg/L	0.01
Si	mg/L	10.6
Sr	mg/L	-
Ag	mg/L	0.001
U	mg/L	0.001
V	mg/L	0.01
Zn	mg/L	0.0054

- not measured. Ca and Mg replaced with 0.5 mg/L.

Value below limit of detection. Limit of detection shown.

6.2.3 Pit Wall Source Terms

Fourteen lithologies were modelled on the pit walls post-closure (Table 6-2). The mineralization and oxidation state of the pit wall materials determines the chemistry of associated runoff and inundation. The chemistries used in the pit lake model to represent pit wall runoff and inundation are based on the results of historical and ongoing geochemical characterization programs performed for the project.

Static and kinetic geochemical testing databases for Winu waste and ore materials were provided by Rio Tinto (Rio Tinto 2021, 2024b, c) for derivation of geochemical source terms and evaluation of potential lag times (for the primary sulfides) associated with the generation of acidic leachate from potentially acid-forming (PAF) materials exposed on the pit walls and in bench talus. Source terms developed from MEP and column testing were applied to both pit wall runoff (unsaturated) and inundated (saturated) mass loading associated with lithologies exposed on the pit wall and talus.

MEP testing was conducted exclusively on low-sulfur cover/overburden lithologies and leached cap samples. The testing was conducted to evaluate whether geochemical mass release from low-sulfur overburden materials is expected to occur either as short-term flushing or as a sustained mass release from waste samples (Rio Tinto, 2024b). The MEP leaching procedure involves iterative leaching and agitation of each sample with deionized water at a liquid to solid ratio of 2:1 for 12 hours (Rio Tinto, 2024a). These iterative leach cycles were conducted on each overburden sample either five or ten times. Filtered leachate was collected and analyzed after each leaching cycle.

The results from testing 22 of these samples were used for derivation of geochemical source terms. Leachate chemistry from the final five leach cycles was averaged for this purpose. The final five leaches are considered to represent long-term leaching conditions and solute release from exposed pit wall materials. MEP testing results were only used to derive source terms for materials overwhelmingly determined to be non acid-forming (NAF).

Free draining (unsaturated) column testing was conducted on 22 samples of sulfide-bearing ore and waste materials. The operation of the columns adhered to the AMIRA free draining column testing procedure (AMIRA, 2002). Currently, three columns remain active with at least 170 weeks of testing, with all other columns having operated for between 32 and 180 weeks. The free-draining column tests were performed to assess mass release, oxidation rates, and acidification lag times associated with sulfide-bearing waste and ore materials under conditions reflective of wetting and drying cycles with unlimited exposure to atmospheric oxygen conditions. One to two kilograms of sample material was loaded into a Buchner funnel as <4mm chips. Flushing operates on a weekly wetting cycle at a liquid to solid ratio of 0.1:1 (100 milliliters (mL) of deionized water applied per kilogram of sample mass per week), together with a flushing cycle occurring every four weeks in which a 0.4:1 liquid to solid (400 mL deionized water per kilogram of sample) is applied and collected for leachate analysis. Heat lamps are applied to the columns to promote drying between weekly wetting applications.

The columns often exhibit a high total dissolved solids (TDS) "first flush," in which readily available salts and secondary minerals on sample surfaces are dissolved by solution in the initial weekly cycles of testing. The "first flush" is typically followed by an "equilibrium phase," where the leaching mechanisms tend to be diffusion controlled or surface area controlled, resulting in "steady-state" concentrations of leached metals and metalloids. Based on a review of columns testing results, the final four months of data associated with wall rock displayed "steady-state" behavior. For rock types with available column testing data, wall rock source terms were developed by calculating the average solution chemistries from the final four months of column testing.

Representative water chemistry source terms for each lithologic unit were developed from free-draining column and MEP results. Due to limited data availability for some of the 14 lithologic units, it was necessary to use some a geochemical source terms for multiple lithological units, resulting in seven unique geochemical source terms for pit wall materials.

Table 6-5 indicates the selected geochemical source term for each lithologic unit together with its acid and metalliferous drainage (AMD) classification, summary testing and pit wall exposure statistics. The area of pit wall exposure was determined by intersecting the geologic model and pit shell provided by Rio Tinto in the Leapfrog modeling software (Section 6.1.10). PAF and NAF percentages were determined from waste and ore tonnages provided by Rio Tinto (*NAF and PAF tonnages Jan 24.xlsx*). The pit wall source term chemistries are presented in Appendix A.

Table 6-5 Summary of geochemical testing statistics, geochemical source term assignments and pit wall exposure statistics

Lithology	Area of Pit Wall Surface		AMD Classification		Selected Source Term	No. of Kinetic Columns	No. of MEP Samples
	m^2	Percent	% PAF	% NAF			
QA Sand	149,814	4.9%	0%	100%	Cover	0	10
Permian Regolith	191,048	6.2%					
Permian Sandstone	285,562	9.3%					
Oxidized Mudstone	161,552	5.3%					
Reduced Mudstone	98,562	3.2%					
Diamictite	15,518	0.51%					
Mafic - Leached Cap	5,426	0.18%	5%	95%	Leached Cap	0	4
Metasediments - Leached Cap	305,880	10%					
Pre-mineral Mafic	41,228	1.3%	95%	5%	Mafic Primary Sulfide	4 *	0
Mafic - CuOx	383	0.012%	9%	91%	Cu-Oxide	0	8
Metasediments - CuOx	3,532	0.12%					
Metasediments - Oxide/Sulfide Mixed	3,489	0.11%					
Metasediments - Secondary Sulfides	29,673	1.0%	62%	38%	Metasediment Secondary Sulfide	3	0
Metasediments - Primary Sulfides	1,778,056	58%	84%	16%	Metasediment Primary Sulfide	14 **	0

* Source term derived from 2 NAF columns of Pre-Mineral Mafic and 2 PAF columns of Mafic Secondary Sulfide
** Source term derived from 11 columns of Metasediment Primary Sulfide and 3 columns of Metasediment Secondary Sulfide

6.2.3.1 Cover/Overburden

Cover materials comprise six waste overburden lithologic units (Quaternary Sand, Permian Regolith, Permian Sandstone, Oxidized Mudstone, Reduced Mudstone, and Diamictite) that represent 29% (902,000 m^2) of the total pit wall exposure. Derivation of the geochemical source term for the cover materials was based on results from 10 MEP samples. One geochemical source term was generated for all cover materials by weighting the MEP concentrations according to their relative pit wall exposures. There are no available MEP data for Permian Regolith and Diamictite samples. According to the AMD Management Plan (Rio Tinto, 2024e), 100% of cover materials are classified as NAF. Additionally, nearly all cover material exposed on the pit walls is present at elevations above approximately 100 m AHD and is expected to remain above the long-term pit lake elevation. It is therefore only necessary to use this source term for runoff from exposed cover material in the pit walls, and not for inundation calculations.

6.2.3.2 Mafic Primary Sulfide

The source term for the pre-mineral mafic lithology was derived from two column tests. This lithology is overwhelmingly classified as PAF (95% according to the AMD Management Plan (Rio Tinto, 2024e)), although only represents approximately 1.3% of the ultimate pit wall area. Column testing of PAF pre-mineral mafic samples (10689917 and W81 LM) indicates a lag time to the generation of acidic conditions on the order of 15 to 20 years (HGL, 2021a). Column testing did not generate acidic leachate within the testing timeframe and circum-neutral column results and were used to derive the source term prior to acidification.

Results from two Mafic Secondary Sulfide columns which generated acidic leachate were used to derive a source term for this lithology post-acidification (Appendix A).

6.2.3.3 Mafic Secondary Sulfide

Mafic Secondary Sulfide material is either not expected to intersect the pit wall or represent only a small fraction and therefore is not represented in the model.

6.2.3.4 Leached Cap (Metasediment and Mafic)

The leached cap (mafic and metasediment) material is expected to represent approximately 10% of the ultimate pit wall area. This material is overwhelmingly classified as NAF (95%) according to the AMD Management Plan (Rio Tinto 2024e); therefore, it is not expected that this material will generate acidic leachate. The geochemical source term for Leached Cap material was derived from results from four MEP samples (one PAF ore sample and three NAF waste samples that were appropriately weighted based on the NAF/PAF proportions according to the AMD Management Plan (Rio Tinto 2024e)).

6.2.3.5 Cu-Oxide (Metasediment and Mafic)

The Cu-Oxide source term is applied to several lithologies including Metasediment Cu-Oxide, Metasediment Mixed Oxide/Secondary Sulfide, and Mafic Cu-Oxide. Together, these lithologies represent 0.24% of total pit wall exposure, and are overwhelmingly classified as NAF (91%) due to low sulfur content. Source terms for all Cu-Oxide materials were derived from eight MEP samples (four waste samples and four ore composites, weighted respective of NAF/PAF proportion).

6.2.3.6 Metasediment Secondary Sulfide

Metasediment Secondary Sulfide material will be exposed on only a small proportion of the ultimate pit wall (0.97%). This lithologic unit is largely classified as PAF (62%) according to the AMD Management Plan (Rio Tinto 2024e). The source term for Metasediment Secondary Sulfide material was derived from three column tests on Metasediment Secondary Sulfide materials, including two PAF samples (10689913 and 10689924) and one sample classified as uncertain with respect to acid formation potential (W93 SS).

Column testing results indicate the potential for the PAF material to immediately generate acidic leachate, therefore no lag time was considered. After one year of column testing, the two columns classified as PAF were generating acidic leachate (pH < 4.5 s.u.), and the pH of the column classified as uncertain was between 4.5 and 5.0 (s.u.). Depletion calculations for these three columns indicate ANP is expected to be depleted within 2 to 8 years of testing.

6.2.3.7 **Metasediment Primary Sulfide**

The Metasediment Primary Sulfide (Hypogene Metasediments) represent the largest lithologic unit exposed on the pit walls (58%), the majority of which (84%) is classified as PAF according to the AMD Management Plan (Rio Tinto 2024e). The AMD Management Plan (Rio Tinto 2024e) indicates that approximately 60% of Metasediment Primary Sulfide is expected to be classified as PAF based on drilling database results, however, tonnages provided by the mine plan (including delineation by lithology and PAF/NAF classification) indicate that 84% of Metasediment Primary Sulfide waste will be PAF. As a conservative approach in the derivation of geochemical source terms, it was assumed that 84% is PAF.

In total, 11 columns of this material have been, or are currently being, tested including 5 NAF or uncertain samples (10689914, 10689919, 10689923, 10689911, and 10689918) and 6 PAF samples (10689926, 10689910, 10689915, 10689925, W331 PAR, and W332 PSS), none of which have generated acidic leachate to date. Depletion calculations for the column testing program were originally completed approximately one year into the program (HGL, 2021a). As part of this pit lake modeling, depletion timeframes were recalculated with the most recent column results. Original and updated depletion calculations agree with Metasediment Primary Sulfide column results, indicating the materials may exhibit lag times to acidification on the order of 15 to 50 years of testing under laboratory conditions. Source terms for the PAF materials pre-acidification were derived from the 11 Metasediment Primary Sulfide columns which produced circum-neutral leachate, whereas source terms for the PAF material post-acidification were instead derived from acidic column results from Metasediment Secondary Sulfide materials. Pre- and post-acidification source terms are calculated using the same method, averaging the leachate concentrations from the final 4 months of column data (Section 6.2.2).

6.2.4 **Groundwater Inflows**

6.2.4.1 **Natural Groundwater**

Groundwater inflow chemistry is based on evaluation of groundwater samples collected from 52 bores within 5 km of the proposed pit. Water chemistry associated with some bores was disqualified based on potential contamination from drilling mud (pH ≥ 10 s.u.) or incomplete analytical results. Data from the remaining 90 samples from 22 bores was evaluated. The source term was derived as the median concentration of the 90 samples. The resulting source term was charge balanced in PHREEQC based on sodium (Table 6-6).

Table 6-6 Summary of groundwater chemistry statistics

Parameter	Unit	25th Percentile	Average	Median [Best Estimate]	75th Percentile
Temperature	°C	25	25	25	25
pH	s.u.	7.4	7.5	7.61	7.93
Total Alkalinity	mg/L as $CaCO_3$	74	154	98	208
Ca	mg/L	12	24	17	34
Na	mg/L	77	163	119	236
K	mg/L	6	8	8	10
Mg	mg/L	6	11	8	14
SO4	mg/L	15	49	35	68
Cl	mg/L	61	180	140	218
F	mg/L	0.3	0.5	0.4	0.5
Nitrate	mg/L as N	0.043	3.33	3.05	5.605
Nitrite	mg/L as N	0.005	0.043	0.005	0.005
Ammonia	mg/L as N	0.005	0.16	0.02	0.098
P	mg/L	0.03	0.129	0.07	0.14
Al	mg/L	0.005	0.021	0.005	0.02
Sb	mg/L	0.0001	0.0001	0.0001	0.0001
As	mg/L	0.0005	0.0015	0.0005	0.002
Ba	mg/L	-	-	-	-
B	mg/L	-	-	-	-
Cd	mg/L	0.00005	0.000051	0.00005	0.00005
Co	mg/L	-	-	-	-
Cr	mg/L	0.0005	0.0009	0.0005	0.001
Cu	mg/L	0.0005	0.0032	0.0005	0.0017
Fe	mg/L	0.025	0.115	0.025	0.025
Pb	mg/L	0.0005	0.0005	0.0005	0.0005
Mn	mg/L	0.001	0.1395	0.012	0.1665
Mo	mg/L	0.0005	0.0064	0.002	0.008
Hg	mg/L	0.00002	0.00002	0.00002	0.00002
Ni	mg/L	0.0005	0.00152	0.0005	0.002
Se	mg/L	0.005	0.005	0.005	0.005
Si	mg/L	14	19.1	18.3	27.5
Sr	mg/L	0.336	0.326	0.336	0.336
Ag	mg/L	0.000005	0.000009	0.000005	0.000005
U	mg/L	0.000025	0.00005	0.000025	0.000025
V	mg/L	-	-	-	-
Zn	mg/L	0.0025	0.0074	0.0025	0.008

- analyte not measured

Value below limit of detection. One-half the limit of detection shown.

Figure 6-25 displays a Piper diagram showing data from all reliable groundwater analyses. Groundwater across the site shows relatively little variation in major ion chemistry and metal concentrations, supporting the use of a single geochemical source term for all groundwater inflow to the pit regardless of lithological source.

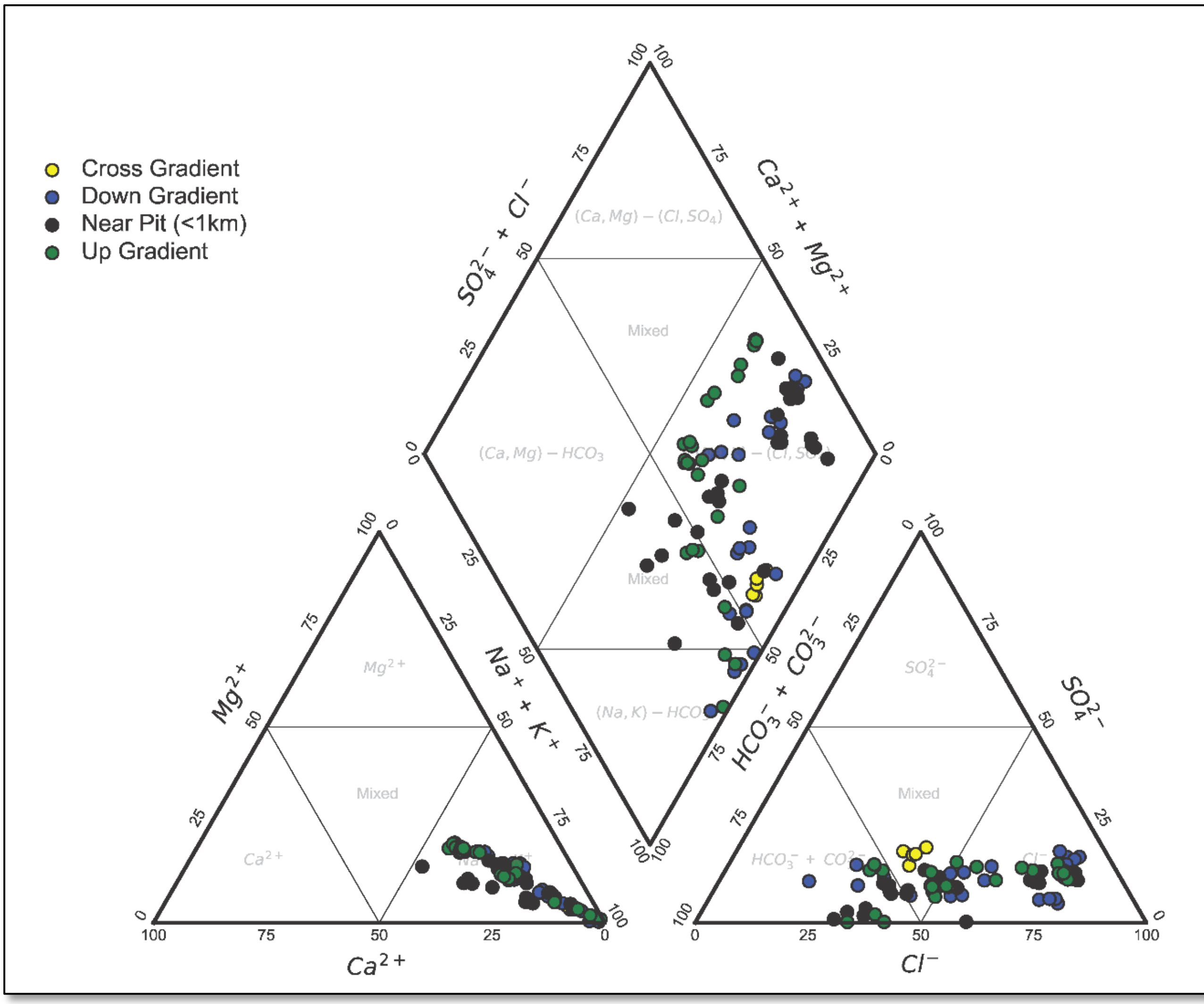

Figure 6-25 Piper diagram of representative groundwater samples

6.2.4.2 **Seepage From Tailings Facility**

It is assumed that TSF seepage estimates developed by WWL (2023) encompass seepage from the entire tailings storage facility, including both low sulfur cells and both high sulfur cells. Therefore, seepage rates and geochemical source terms for seepage generated from high sulfur tailings and low sulfur tailings were not able to be developed separately. Additionally, available kinetic column testing results from tailings materials exclusively analyzed low sulfur tailings, including 8 low sulfur samples, no high sulfur samples, and 1 filtrate sample of tailings supernatant fluid from low sulfur tailings (HGL, 2021b; Rio Tinto, 2022; SRK, 2023, 2024). Columns and filtrate samples used for development of the TSF seepage source term are listed below:

- Whole Tailings: 2019 Rougher + cleaner tailings blend (Whole) JAN MC DP1471 RT & DP1554-1560 CT + 3 kg DWE [Unsaturated Column]
- Low Sulfur: 2019 Rougher tailings blend A19905, DP1741 RO Tail Bucket 4 Wet Cake [Unsaturated Column]
- Low Sulfur: Secondary W-338 SS2 [HCT]
- Low Sulfur: Primary W-339 PSHCu_YR [HCT]
- Low Sulfur: DP1739 cycle 4,5,6 (3kg DWE) [HCT]
- Low Sulfur: DP2728 cycle 4,5,6 (3kg DWE) [HCT]
- Low Sulfur: A19905 DP1947 after CiL Detox [HCT]
- Low Sulfur: A19905 DP1947 after CiL Detox [Saturated Column]
- Low Sulfur: A19905 DP1947 after CiL Detox [Filtrate]

The tailings seepage source term was developed using first-flush leachate chemistry from saturated columns, unsaturated columns, and unsaturated HCT results for the 8 low sulfur tailings samples. The first 3 flushing cycles from each sample were equally mixed in PHREEQC (as well as the Low Sulfur A19905 DP1947 after CiL Detox filtrate sample). The resulting chemistry was charge balanced based on sodium concentration and is presented in

Table 6-7.

The first flush chemistry was selected to represent water quality expected in the tailings supernatant that is expected to represent the majority of the seepage during initial draindown. First flush results from tailings kinetic data were comparable to the Low Sulfur A19905 DP1947 after CiL Detox filtrate sample and exhibited circum-neutral pH conditions between pH 6.5-8.0, measurable alkalinity between 10 and 150 mg/L as $CaCO_3$.

The closure strategy aims to maintain a high degree of saturation (>85%) of the high sulfur tailings in order to minimize oxygen ingress by use of a tension saturated cover system to decouple the shallow evapotranspiration zone from the saturated high sulfur tailings (Okane, 2024; Rio Tinto, 2024d, 2024e). The low sulfur tailings is expected to be covered with an erosion protective cover to limit net infiltration; long term seepage estimates predict the low sulfur tailings will stabilize at 50-60% saturation (WWL, 2023). Additional seepage modeling of the high sulfur and low sulfur cells are necessary to validate the closure strategy and further refine the seepage water quality estimates.

Table 6-7 TSF seepage source term

Parameter	Unit	TSF Seepage Source Term
Temperature	°C	25
pH	s.u.	6.32
Total Alkalinity	mg/L as $CaCO_3$	67
Ca	mg/L	121
Na	mg/L	237
K	mg/L	25
Mg	mg/L	24
SO4	mg/L	752
Cl	mg/L	66
F	mg/L	1.3
Nitrate	mg/L as N	1.55
Nitrite	mg/L as N	0.02
Ammonia	mg/L as N	5.48
P	mg/L	0.023
Al	mg/L	0.06
Sb	mg/L	0.0025
As	mg/L	0.0011
Ba	mg/L	0.0976
B	mg/L	0.455
Cd	mg/L	0.00123
Co	mg/L	0.073
Cr	mg/L	0.001
Cu	mg/L	0.112
Fe	mg/L	1.000
Pb	mg/L	0.0007
Mn	mg/L	0.353
Mo	mg/L	0.0241
Hg	mg/L	0.00199
Ni	mg/L	0.045
Se	mg/L	0.011
Si	mg/L	5.0
Sr	mg/L	0.316
Ag	mg/L	0.0048
U	mg/L	0.0013
V	mg/L	0.005
Zn	mg/L	0.153

7 Model Scenarios

7.1 Water Balance Scenarios

In addition to the Base Case scenario, two alternative scenarios were evaluated to test the sensitivity of the model to long-term climate variability. These scenarios evaluated selected long-term changes in precipitation and evaporation rates that may occur due to climate change (Section 6.1.2). One additional scenario assumed zero seepage reporting from the TSF in order to evaluate the effects of this seepage on the water balance and water quality. This sensitivity also represents a scenario in which seepage travel times from the base of the TSF to the pit lake are long (i.e., decades to centuries). Water balance scenario summaries are described in Table 7-1.

Table 7-1 Water balance modeling scenarios

Scenario	Description
Base Case	- Uses synthetically generated monthly climate data (not scaled) - Pond evaporation coefficient = 70% - Dynamic pit wall runoff coefficient - Advisian predicted groundwater inflow rates
Low Carbon Emissions	Synthetic climate data scaled by SSP126 climate change prediction
Moderate to High Carbon Emissions	Synthetic climate data scaled by SSP350 climate change prediction
No TSF Seepage	Assuming zero seepage from TSF. Uses climate and chemistry Base Case assumptions.

7.2 Chemistry Scenarios

Several geochemical scenarios were evaluated to test reasonable ranges of uncertain input variable values. Conservative assumptions and their implications for several of the sensitivity parameters are discussed below. Chemistry scenarios are summarized in Table 7-2.

Table 7-2 Chemistry modeling scenarios

Scenario	Description
Base Case	- Uses hydraulic parameters from Base Case water balance - Inundation applies 10 pore volumes per time step to account for chemical mass loading - Damaged rock zone depth = 1 m; porosity = 8% - Talus porosity = 30% - 20-year acidification lag time for Mafic Primary Sulfide and Metasediment Primary Sulfide source terms
High Flushing	- Inundation applies 50 pore volumes per time step to account for chemical mass loading - Damaged rock zone depth = 1.8 m
Low Flushing	- Inundation applies 1 pore volume per time step to account for chemical mass loading - Damaged rock zone depth = 0.5 m
Immediate Acidification	- Immediate acidification of damaged rock zone, talus, and pit wall runoff for Mafic Primary Sulfide and Metasediment Primary Sulfide source terms

The TSF seepage source term developed from tailings kinetic testing represents a conservative water quality estimate by selecting first-flush chemistry from kinetic testing in an aim to characterize the expected pore water (supernatant) in the TSF at closure. First flush chemistries from kinetic data often exhibited high solute concentrations compared to late-time leachate results. The source term also does not account for dilution of this pore water chemistry by infiltrating precipitation.

Pit wall runoff and inundation source terms were developed from kinetic column testing adhering to the AMIRA free draining column testing procedure (AMRIA, 2002). Laboratory kinetic testing is generally more beneficial to reactions rates compared to field conditions due to several factors including smaller particle size distribution and increased surface area, artificial temperature controls, and attempts to discourage preferential flow paths in lab columns which are likely to form in field conditions. Therefore, kinetic column testing results from waste rock likely represent these higher reaction rates compared to field conditions.

The pit wall dynamic runoff coefficients applied in all scenarios are considered a conservative estimate (i.e., an overestimation of the proportion of precipitation reporting to the lake) because talus on the benches will likely serve as a water storage mechanism, limiting runoff to the lake.

The Immediate Acidification scenario is used to represent a conservative evaluation of the lag time for Mafic Primary Sulfide and Metasediment Primary Sulfide materials present on the pit walls to generate acidic leachate, compared to a 20-year lag time applied in the Base Case scenario.

The High Flushing scenario is used to represent a conversative evaluation of mass loading from inundated pit wall material in terms of solute release mechanisms. Under this scenario, a thicker damaged rock zone is applied (1.8 m), as well as an assumption that inundated pit wall material (talus and damaged rock zone) will require 50 pore volumes to release the solute mass related to weathering products and soluble minerals built up on mineral surfaces while the pit wall materials were exposure to atmospheric conditions and precipitation during the active mining process.

8 Results

8.1 Base Case Scenario

As part of the development of the groundwater flow model by Advisian (Advisian, 2022), preliminary water balance and filling curves for the Winu pit lake were also developed. Details and filling curve results were provided in a presentation (*Pit Lake Recovery Review 2023.pptx*, November 29, 2023) and in tabulated form (*Winu Pit Lake Recovery Goldsim 2023.xlsx*) without an accompanying. It is understood that the Advisian pit lake filling analysis assumed zero contributions from closure landforms including the WRL and TSF; runoff from the surrounding catchment into the pit was assumed to be zero due to diversion by abandonment bunds along the pit rim; and surface water infiltration through the unsaturated zone was not considered. Four Advisian water balance scenarios were developed by varying the pan-to-open water evaporation coefficient between 0.4, 0.5, 0.6, and 0.7. Results from Advisian's 0.7 coefficient scenario were used for comparison to the water balance results generated by HGL/LRE in this report. It is expected that results developed by HGL/LRE and presented in this report are more detailed than, and therefore supersede, the Advisian water balance results.

8.1.1 **Water Balance Results**

The water balance for the Base Case scenario predicts that a pit lake will form and will fill to a near-steady-state elevation of approximately 90 m AHD (110 Mm^3) after approximately 90 years. Between 100–200 years post-closure, predicted seepage rates from the TSF decrease from a peak flow rate of 3,100 m^3/day to a near-constant rate of 1,300 m^3/day resulting a slight decrease in the pit lake elevation (from 91 to 85 m AHD) by the end of the 300-year modeling period. The predicted filling curve is presented in Figure 8-1, together with associated inflow and outflow components.

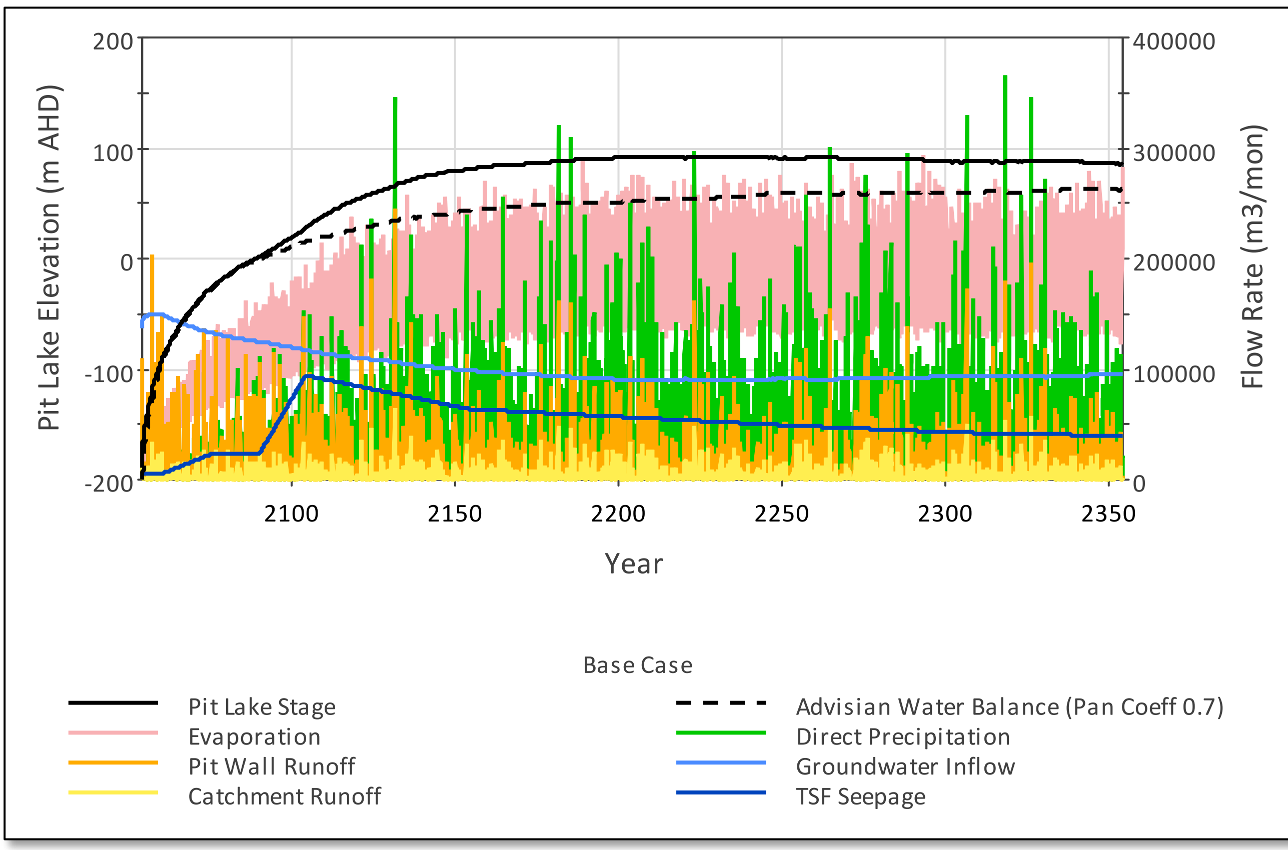

Figure 8-1 Predicted pit lake filling and flow rates (Base Case scenario)

Figure 8-1 includes the preliminary pit lake filling curve for the water balance developed by Advisian (2022) for comparison purposes. The long-term pit lake elevation for the current Base Case model is approximately 20 m higher than the preliminary prediction by Advisian. Both models predict an ultimate pit lake elevation of less than 100 m AHD. The most significant difference between the two models is the addition of TSF seepage as a pit inflow in the current model, as well as updates to the catchment runoff area calculated from the newly delineated abandonment bund. These flows are not included in the Advisian water balance (G. Jacobs, pers. communications, 1 Apr 2024).

Figure 8-2 illustrates the Base Case predicted pit lake filling curve and associated final pit lake area, elevation, and volume in the context of the pit shell. The figure illustrates that the ultimate pit lake elevation is likely to be at least 100 m below the pre-mining groundwater elevation (190–200 m AHD), indicating that the pit lake will likely form a strong hydraulic sink at all times. The ultimate pit lake is predicted to be just under 300 meters deep.

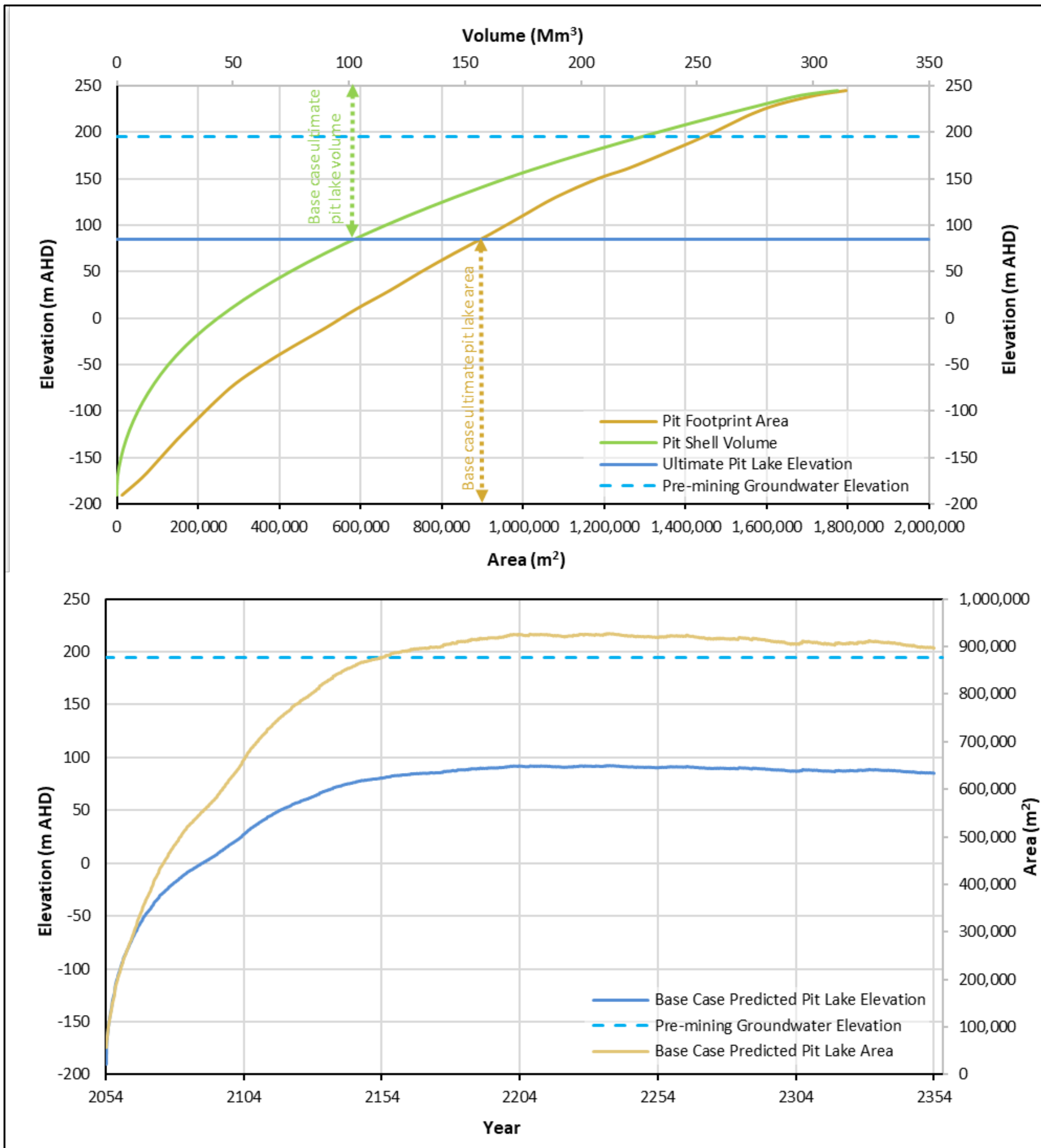

Figure 8-2 Base Case pit lake filling results in pit shell context

At the steady state lake elevation of 85 m AHD, the lithologies exposed on the pit wall are dominated by cover material, comprising approximately 60% of the exposure pit wall surface area. Leached Cap Mafic and Cu-Ox Mafic comprise a negligible proportion of the pit wall exposure, 0.4% and 0%, respectively. Leached Cap Metasediment materials are predicted to be a major exposure on the pit wall, representing approximately 20%, whereas Cu-Ox Metasediment and Mixed Oxide/Sulfide Metasediment are negligible (0.4% combined). PAF lithologies are expected to represent 19% of the exposure pit wall, including Pre-Mineral Mafic (0.5%), Secondary Sulfide Metasediment (1.5%), and Hypogene Metasediment (17%).

8.1.2 Pit Lake Chemistry Results

Pit lake chemistry predictions at 10, 20, 50, 100-, 150-, 200-, and 300-years post-closure for all scenarios are presented in tabular format in Appendix B. Chemistry results are discussed within context of concentration relative to background groundwater quality rather than comparison to Australia/New Zealand water quality guidelines. Mine Closure Plan Guidance documentation for Western Australia (DMIRS, 2020) do not publish province wide pit lake water quality standards. Rather, site-specific water quality standards for pit lakes in Western Australia are instead determined during permitting processes accounting for background groundwater and surface water quality and post-closure land use objectives. A subsequent pit lake ecological risk assessment is planned following this report to be completed by Mine Lake Consulting.

The Winu pit lake is predicted to have a slightly alkaline pH of approximately 7.8 to 8.2 s.u. (Figure 8-3) during filling and throughout the simulated post-closure period (300 years post-closure). The pit lake is predicted to have approximately 110 mg/L as $CaCO_3$ alkalinity during early filling, which is comparable to the median alkalinity of groundwater. After approximately 50 years post-closure, alkalinity concentrations slightly decrease to approximately 85 mg/L as $CaCO_3$, comparable to background groundwater values, for the duration of the modeling period (300 years post-closure; Figure 8-4).

The pit lake is predicted to have a moderate to high concentration of total dissolved solids (TDS) due to evapoconcentration, which is characteristic of a hydraulic sink. The initial pit lake is predicted to have a TDS concentration near 500 mg/L with a gradual increase thereafter, reaching approximately 3,500 mg/L after 300 years for the Base Case scenario (Figure 8-5). Consistent with this evapoconcentration trend, concentrations of sulfate, sodium, chloride, and most metals and metalloids, steadily increase with time due to evapoconcentration (concentration of these parameters are graphically presented in Figure 8-8 through Figure 8-16 for all scenarios). Concentrations of several constituents, such as calcium, iron, and copper, are controlled by precipitation of secondary minerals, including calcite, ferrihydrite, and malachite (and an amorphous copper-carbonate mineral), respectively. Concentrations of these constituents either remain relatively constant through the model period or decrease. Notably, sulfate concentrations slightly increase for the duration of the modeling period but remain less than 1,500 mg/L; as a result, gypsum is not predicted to precipitate within the modeling timeframe (Figure 8-6) for the Base Case scenario.

While predicted metals concentrations are generally low for exposed NAF material and slightly higher for exposed PAF lithologies, corresponding with results from the column and MEP datasets, metals concentrations also increase with time. Metals concentrations generally remain constant for the first 20 years post-closure before increasing upon acidification of the Mafic Primary Sulfide and Metasediment lithologies. Concentrations of some metal(loid)s (e.g., arsenic, chromium, cadmium, copper, lead, vanadium, and zinc) are appreciably attenuated by sorption to ferrihydrite, generally lowering the rate of increase due to evapoconcentration, relative to non-sorbing constituents. Concentrations increase rapidly through approximately 100 years post-closure as the lake level rises and introduced additional mass loading from newly inundated pit wall material. After the steady state lake elevation is achieved, concentrations for nearly all metals slowly increase for the duration of the modeling period due to evapoconcentration. Predicted concentrations of selected metals are displayed in Figure 8-8 through Figure 8-16 for all scenarios.

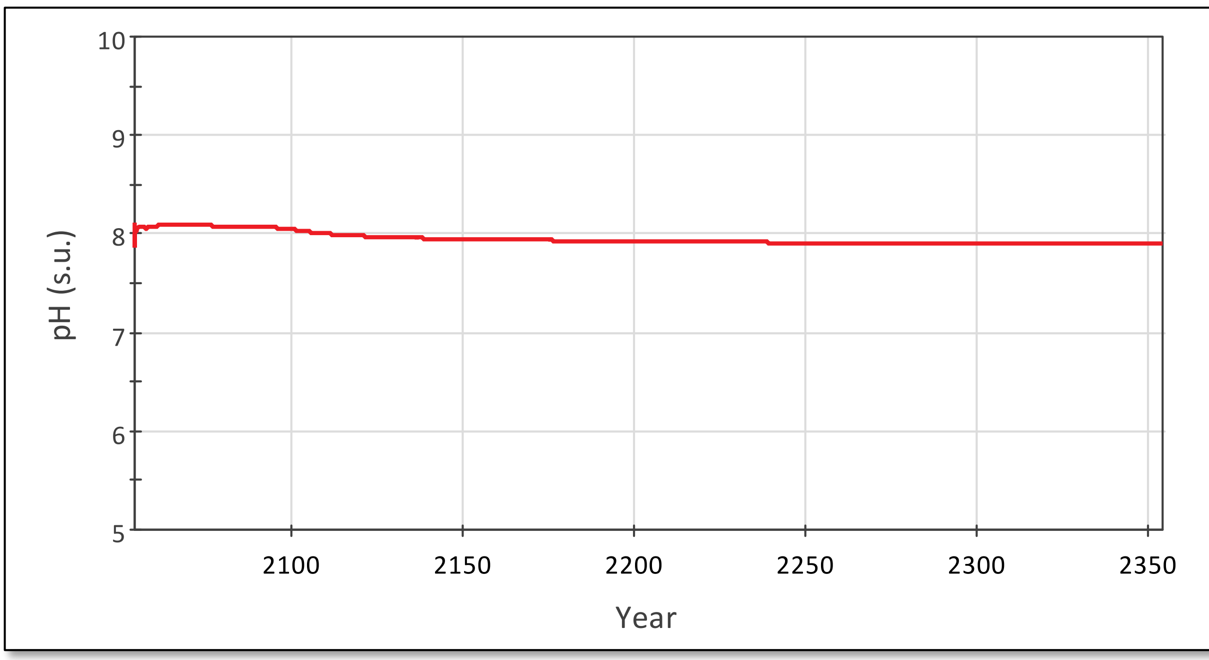

Figure 8-3 Predicted pH of pit lake – Base Case scenario

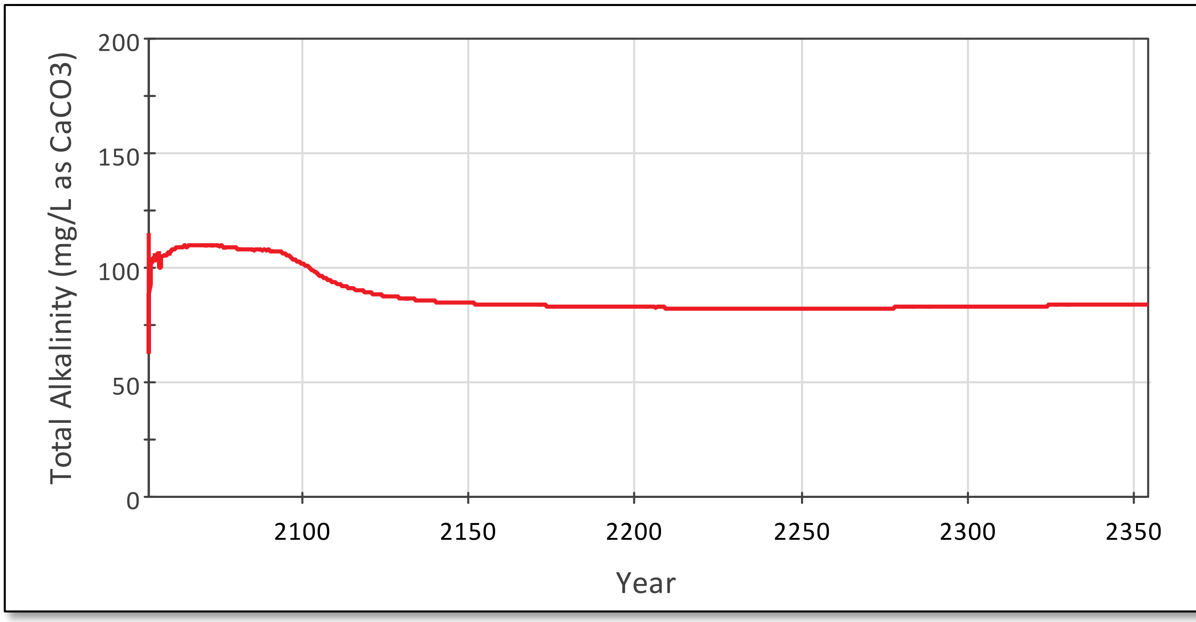

Figure 8-4 Predicted total alkalinity of pit lake – Base Case scenario

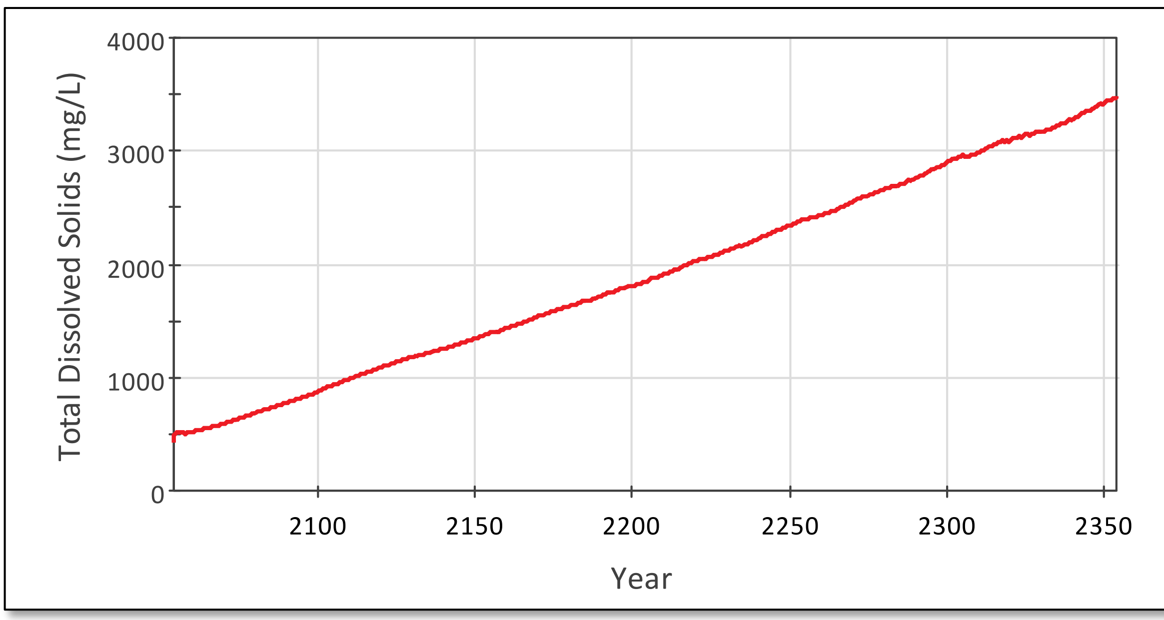

Figure 8-5 Predicted total dissolved solids of pit lake – Base Case scenario

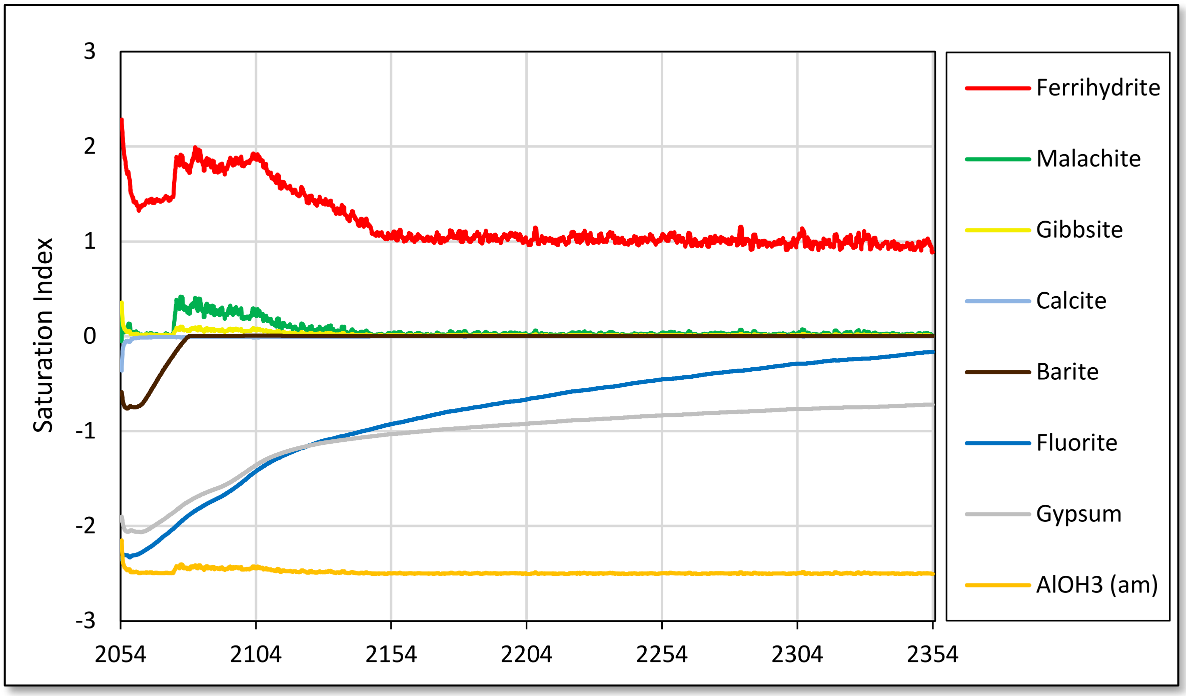

Figure 8-6 Predicted saturation indices for selected minerals phases in pit lake – Base Case scenario

8.2 Sensitivity Analyses/Scenarios

8.2.1 Water Balance Results

The Low Carbon Emissions SSP126 and Moderate-to-High Carbon Emissions SSP370 climate scenarios exhibit lower precipitation and higher evaporation rates resulting in lower pit lake elevations. Filling curves for the Base Case, climate scenarios, and no-TSF-seepage are displayed in Figure 8-7, and pit lake elevations at the end of the modeling period (300 years post closure) are summarized in Table 8-1. The predicted pit lake elevation under the Mod-High Carbon Emissions scenario reaches a maximum elevation of approximately 75 m AHD 90 years post-closure before decreasing to an elevation of 35 m AHD at 300 years post-closure due to increasing evaporation rates and decreasing precipitation.

The scenario assuming no TSF seepage predicts an ultimate pit lake elevation of approximately 50 m AHD at 300 years post-closure, nearly 33 m below the Base Case lake elevation. During the first 50 years post-closure, the filling curves for the Base Case and the scenario predicting no TSF seepage are comparable due to the low inflow rates of TSF seepage during the first 50 years post closure. After approximately 50 years post closure, TSF seepage flow rates are expected to peak for the Base Case scenario, at which point the filling curves diverge resulting in the higher total inflow rate for the Base Case compared to the scenario in which TSF seepage is assumed to be zero.

Table 8-1 Long-term pit lake elevations for all water balance climate scenarios

Scenario	Lake Elevation (m AHD) 300-yrs Post-Closure	Lake Volume (Mm^3) 300-Yrs Post-Closure
Base Case	85	101
Low Carbon Emissions (SSP126)	78	96
Mod-High Carbon Emissions (SSP370)	35	64
No TSF Seepage	50	75

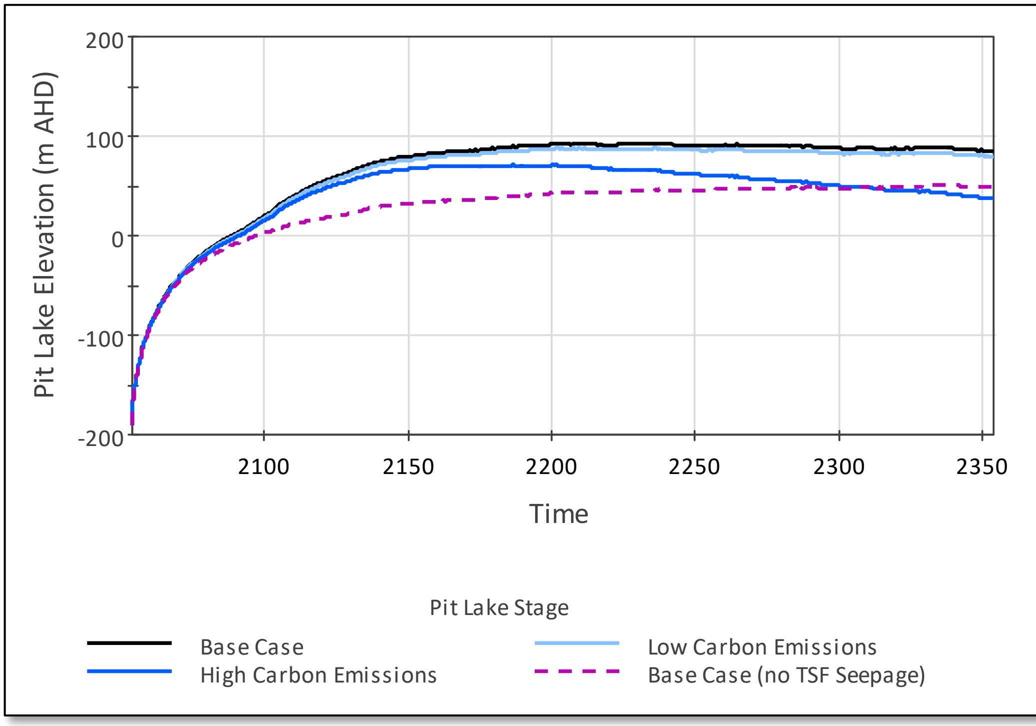

Figure 8-7 Predicted pit lake fillings curves for climate scenarios

8.2.2 Pit Lake Chemistry Results

Predicted pit lake water quality parameters for all scenarios are plotted in timeseries plots in Figure 8-8 through Figure 8-16. All scenarios are predicted to have a circum-neutral pH for the duration of the modeling period comparable to the Base Case scenario. Predicted pH values in the high flushing scenario are slightly lower (approximately 0.2 pH unit) compared to all other scenarios due to the increased flushing of talus and damaged rock zone materials. In the Immediate Acidification scenario, pH values during the first few decades are also slightly lower than the Base Case scenario (approximately 0.1 pH unit). However, under all scenarios the alkalinity supplied by inflowing groundwater is sufficient to neutralize acidity generated from inundation of wall rock and pit wall runoff. Alkalinity concentrations in the pit lake for all scenarios exhibit near-stable trends at approximately 80 to 100 mg/L as $CaCO_3$ during filling and for the duration of modeling (Figure 8-8).

Once the steady state pit lake elevation is achieved and mass release from new talus and damaged rock zone has ceased, minor amounts of acidity loading is only contributed via pit wall runoff. Additionally, the seepage from the TSF reaches the maximum inflow rate to the pit lake approximately 50 years post-closure, at which point calcium loading to the pit lake system increases promoting the precipitation of calcite and consumption of alkalinity, thus attenuating alkalinity concentrations in the pit lake for the duration of the modeling period. Under the scenario in which TSF seepage is assumed to be zero, calcite precipitation rates are lower due to low calcium concentrations resulting in the evapoconcentrative trend observed in alkalinity concentrations and slightly higher pH (by approximately 0.5 pH unit) compared to the Base Case.

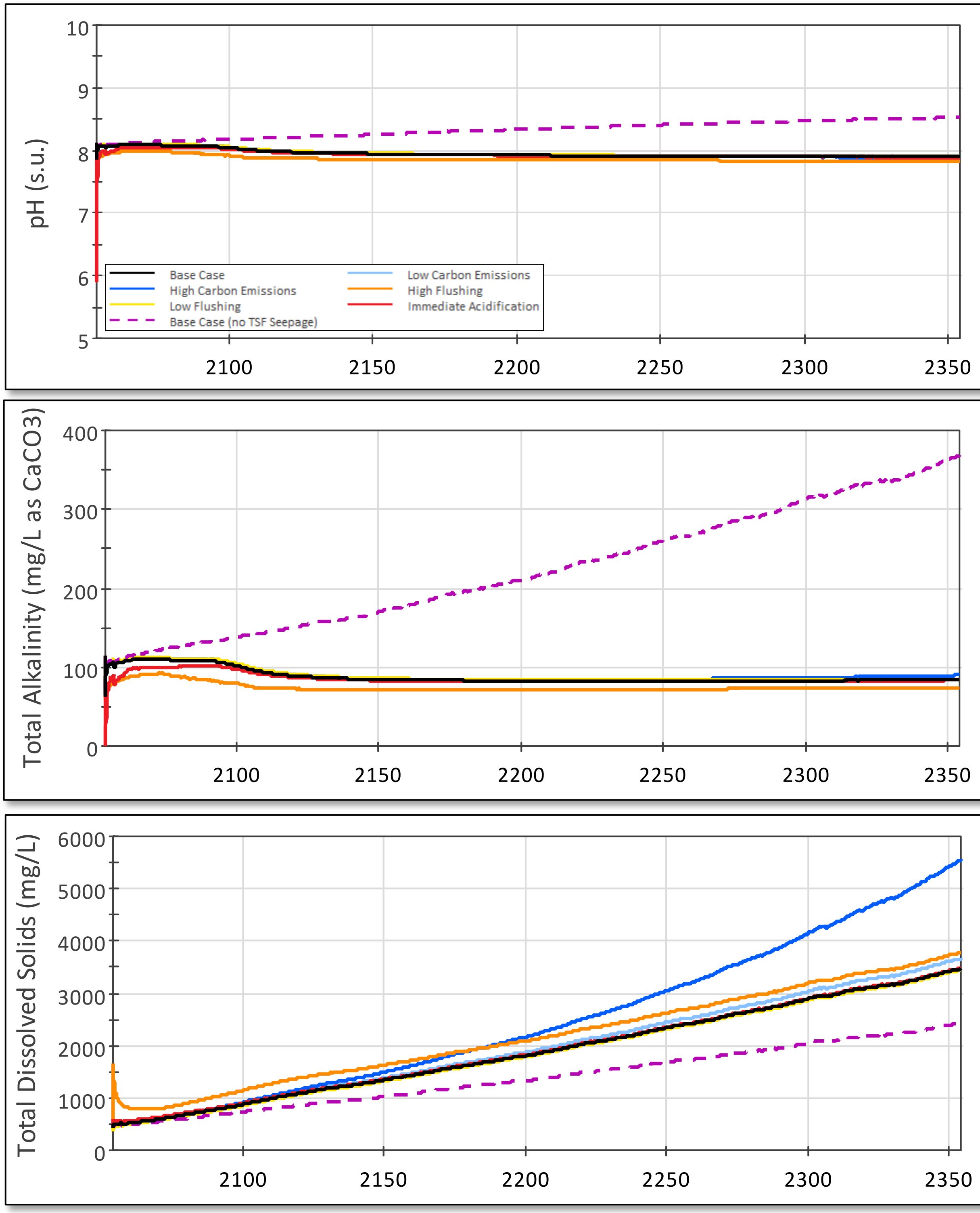

Figure 8-8 Predicted pH, total alkalinity, and TDS of pit lake - all scenarios

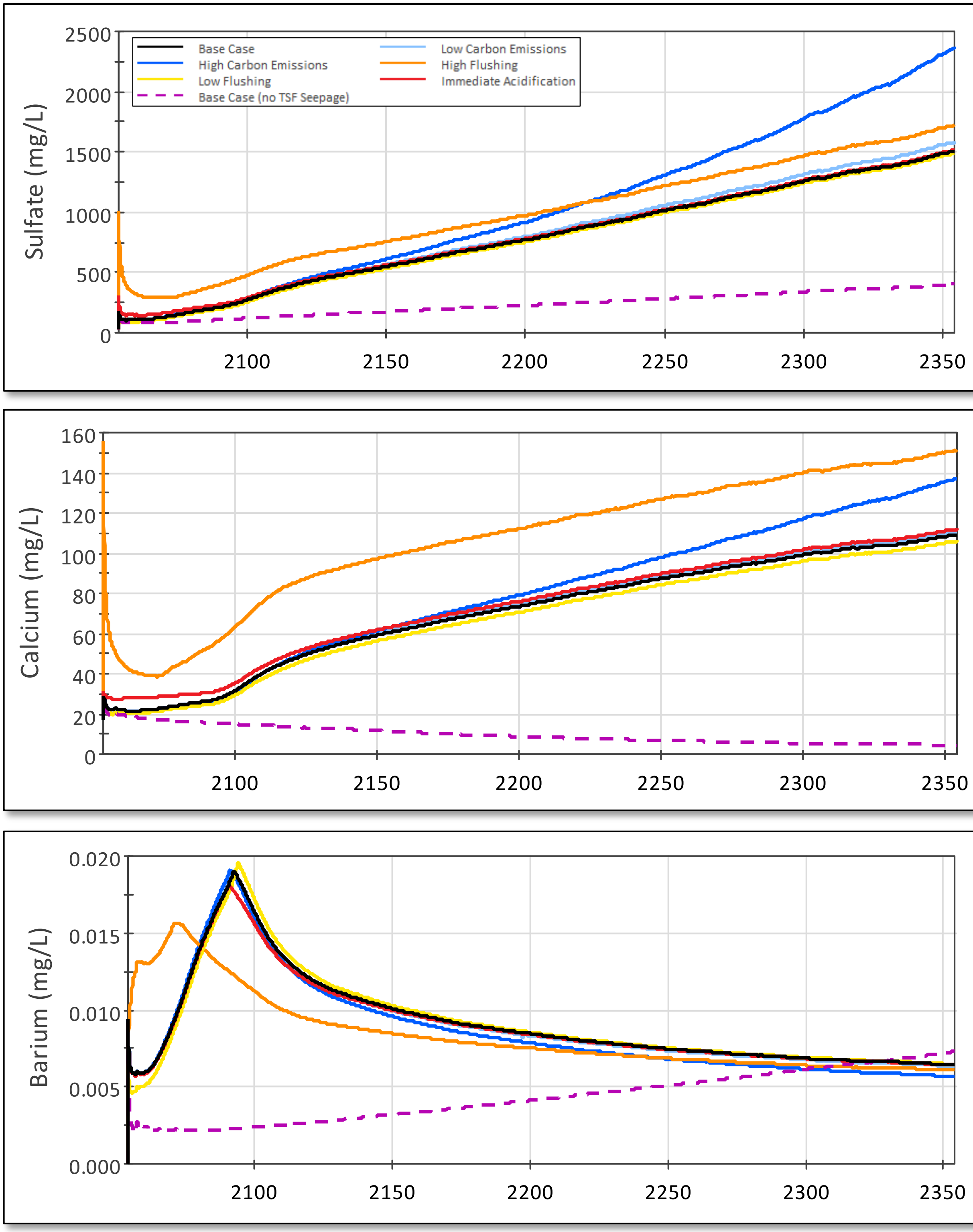

Figure 8-9 Predicted sulfate, calcium, and barium of pit lake - all scenarios

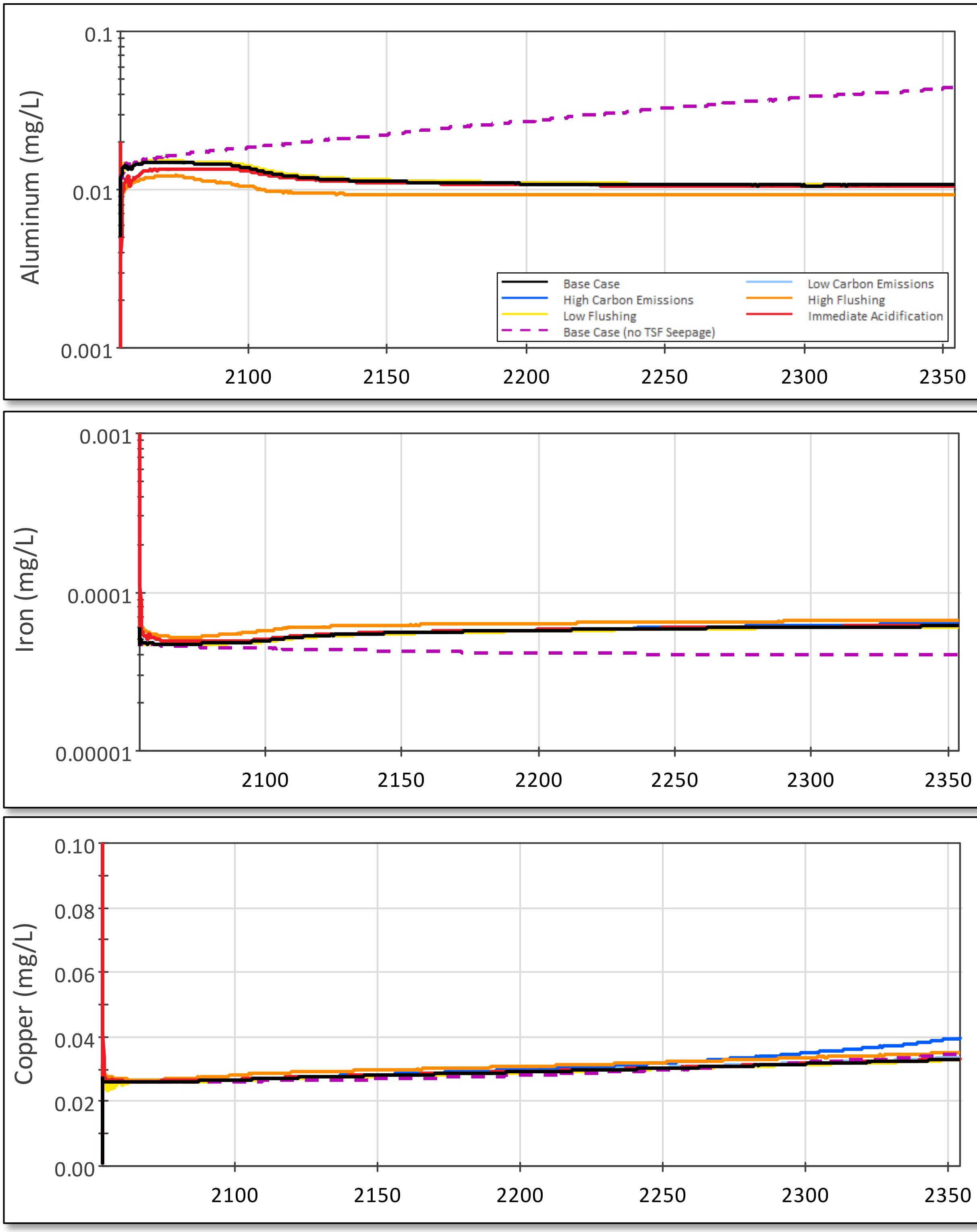

Figure 8-10 Predicted aluminum, iron, and copper concentration in pit lake - all scenarios

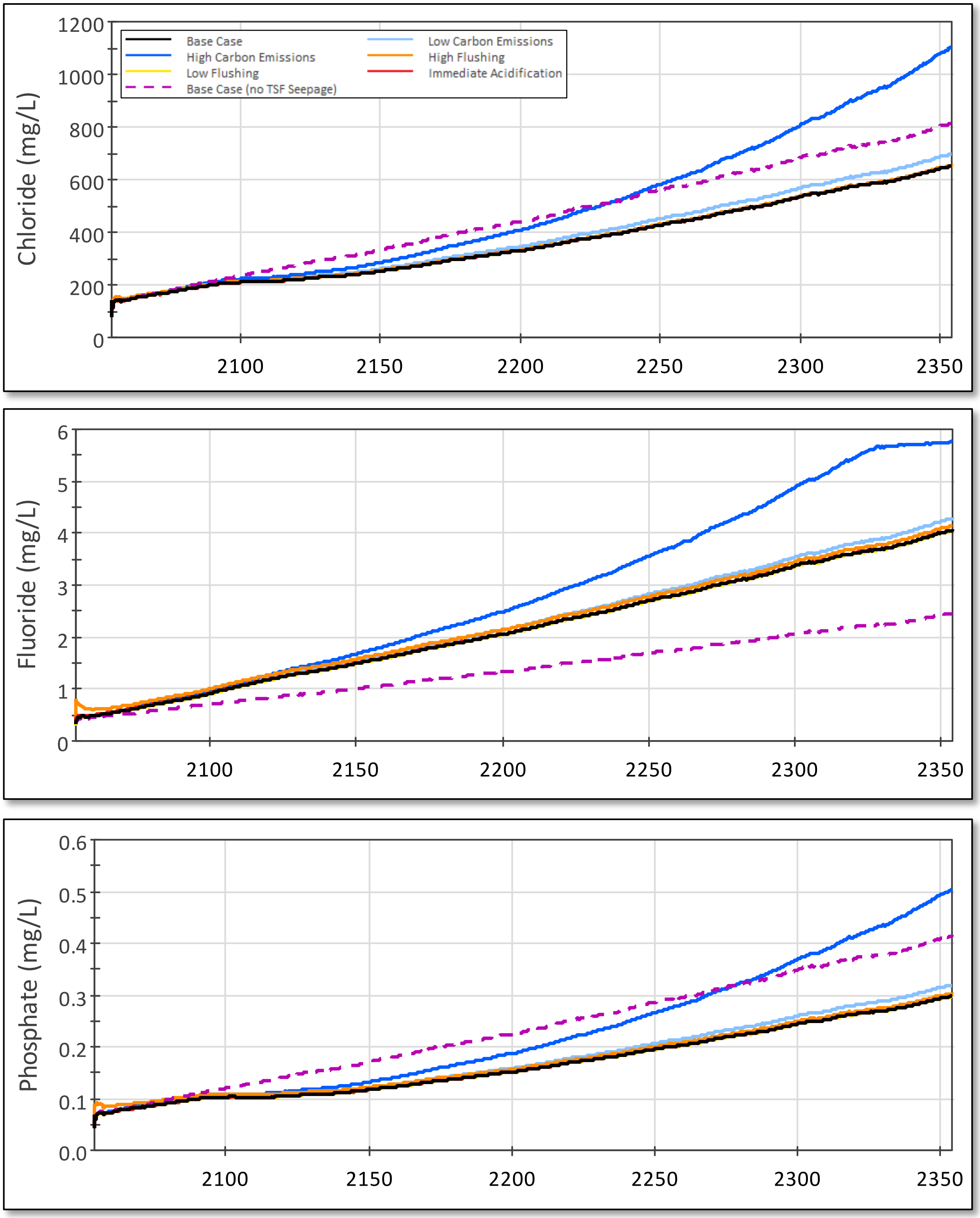

Figure 8-11 Predicted chloride, fluoride, and phosphate concentration in pit lake - all scenarios

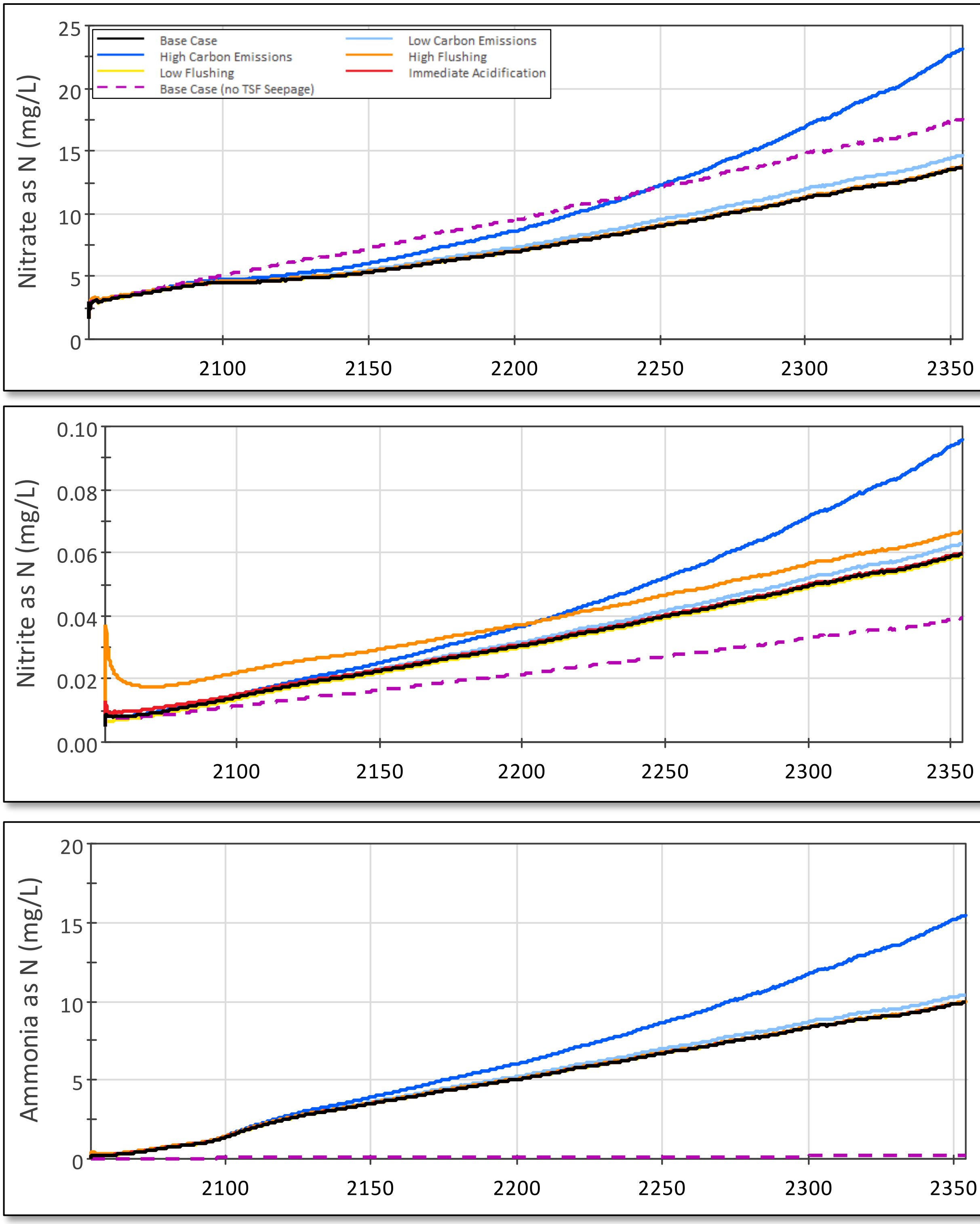

Figure 8-12 Predicted nitrate, nitrite, and ammonia concentration in pit lake - all scenarios

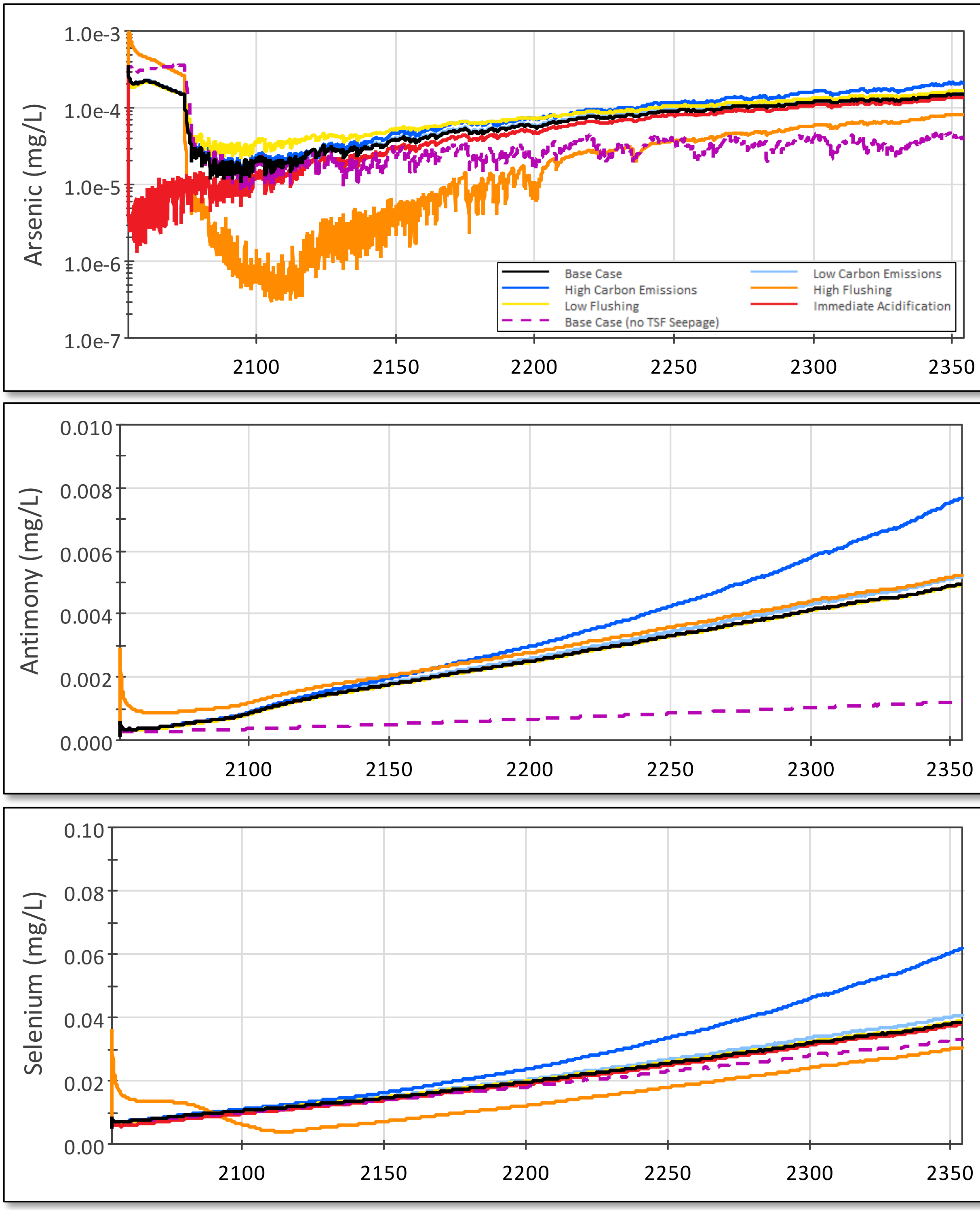

Figure 8-13 Predicted arsenic, antimony, and selenium concentration in pit lake - all scenarios

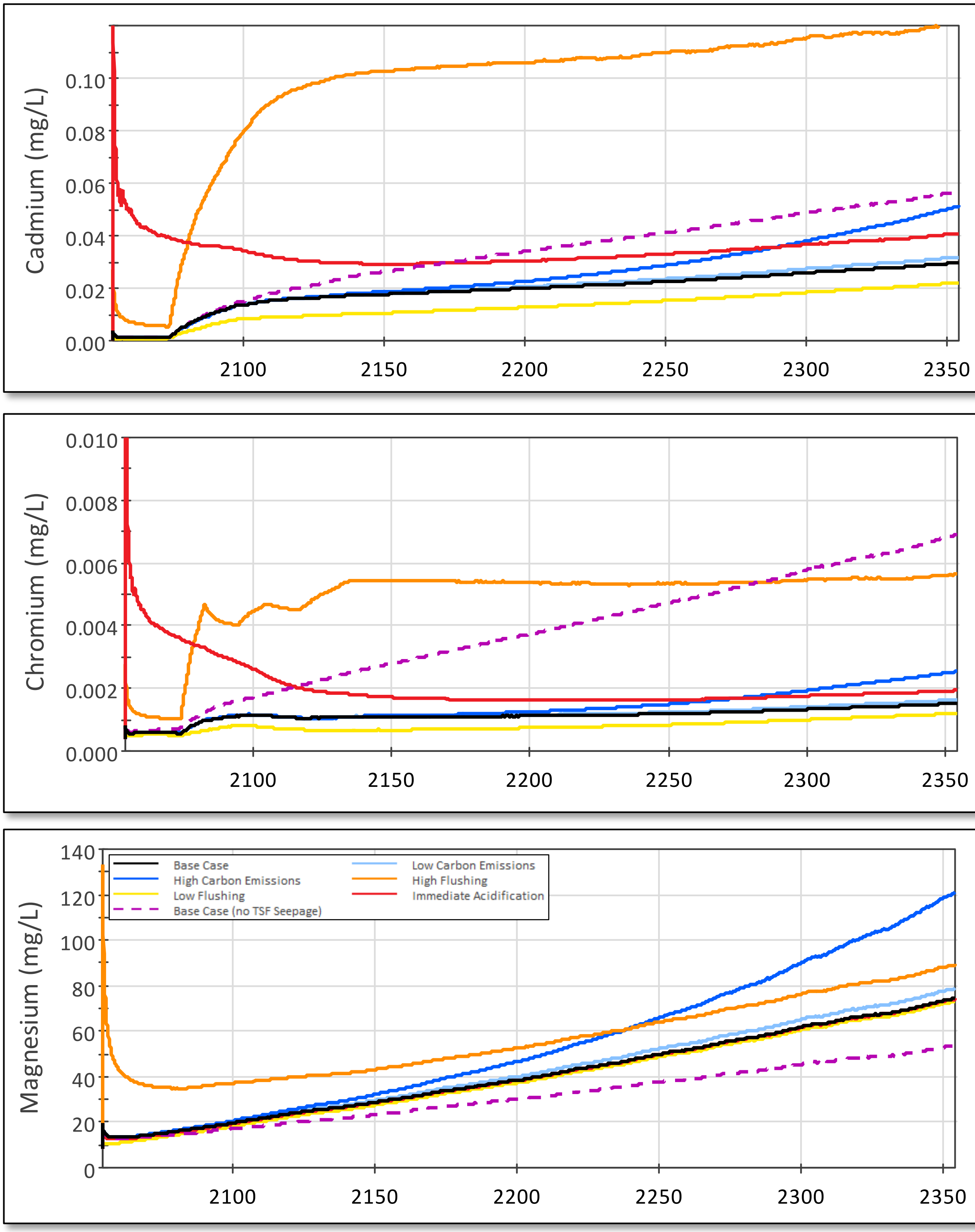

Figure 8-14 Predicted cadmium, chromium, and magnesium concentration in pit lake - all scenarios

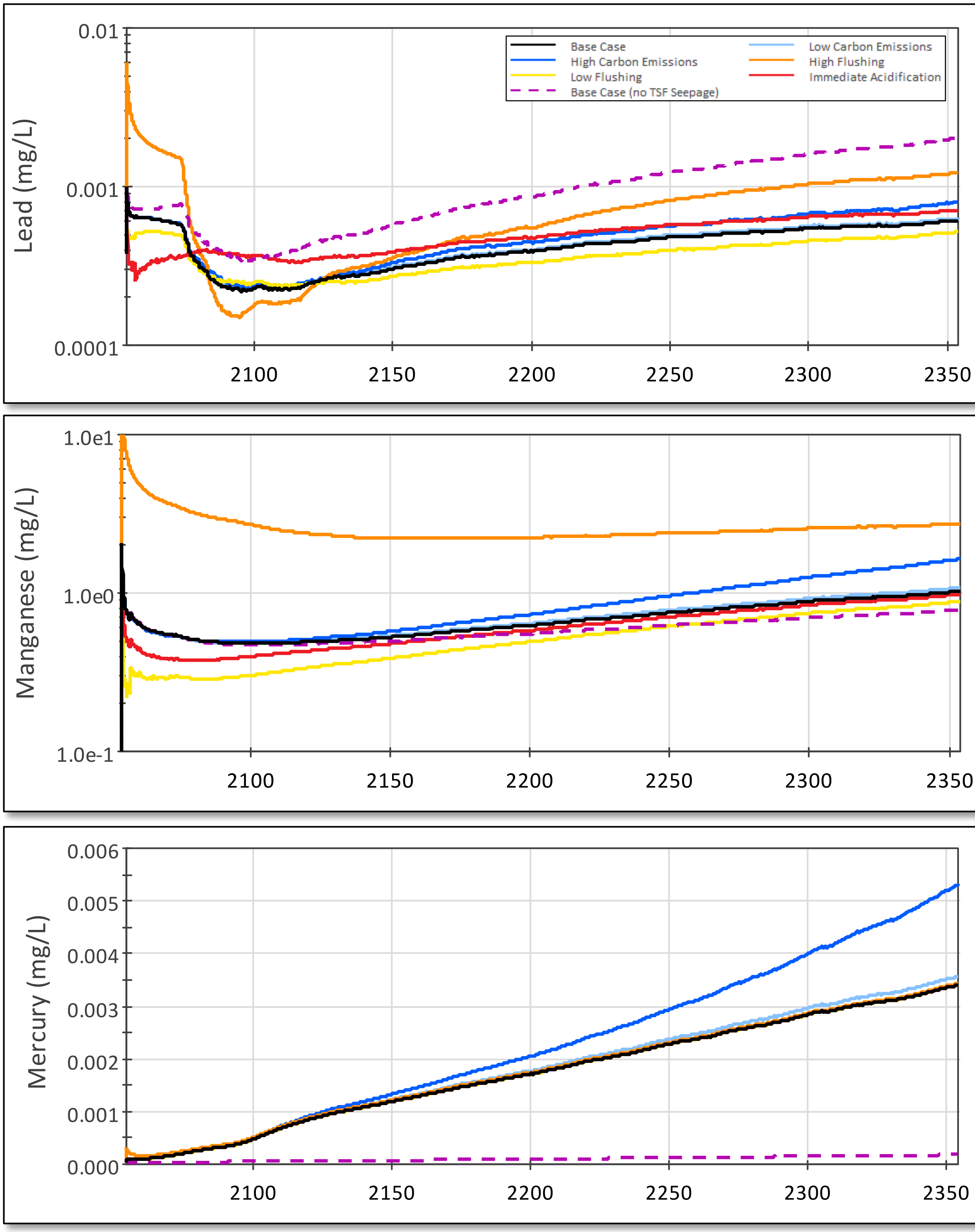

Figure 8-15 Predicted lead, manganese, and mercury concentration in pit lake - all scenarios

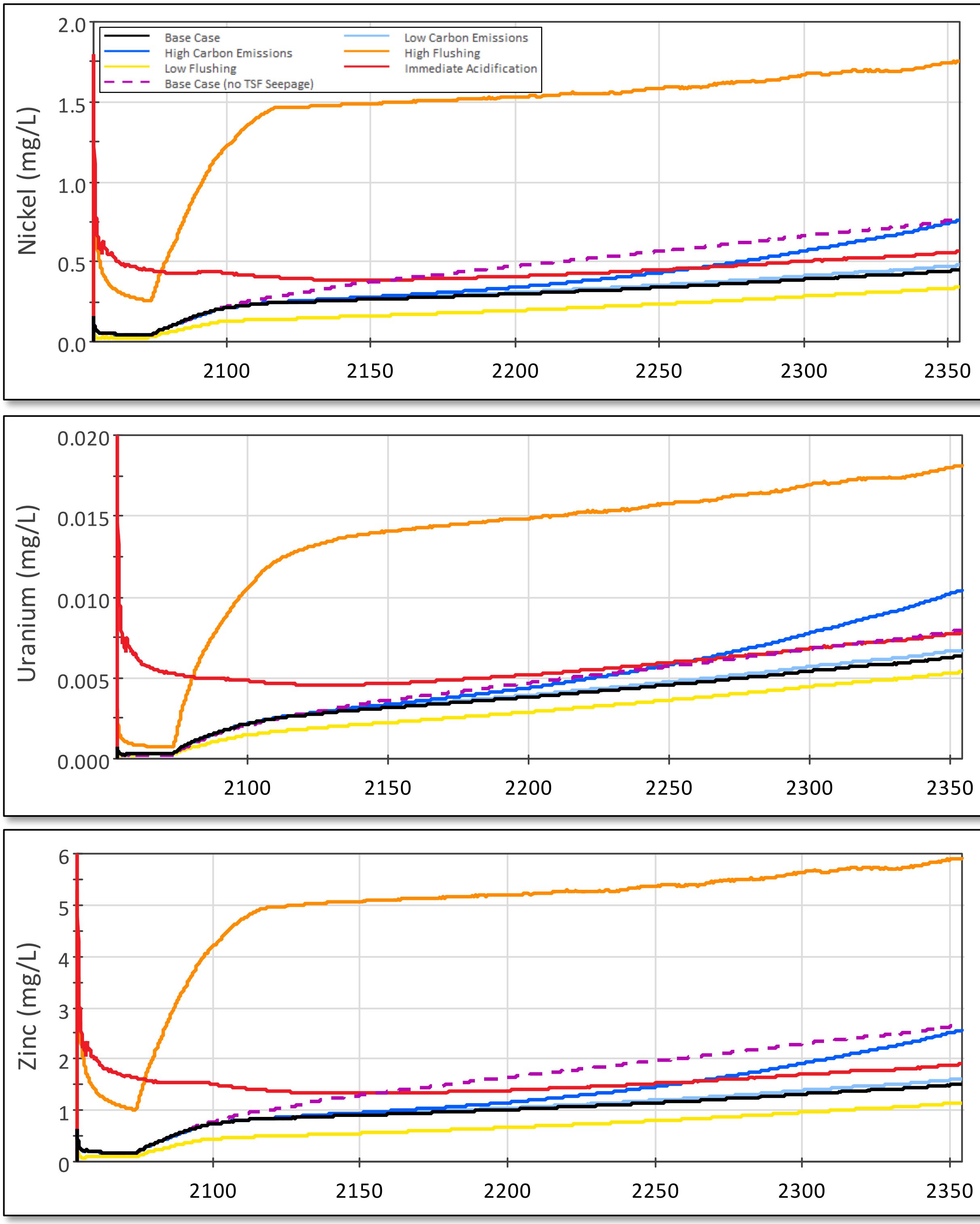

Figure 8-16 Predicted nickel, uranium, and zinc concentration in pit lake - all scenarios

Predicted concentrations for most constituents are elevated in the High Flushing scenario which captures the uncertainty in the solute release mechanisms of inundated talus and damaged rock zone. Aluminum and iron loading rates are higher under this scenario resulting in increased precipitation rates of iron- and aluminum-(oxy)hydroxide minerals (ferrihydrite and gibbsite, respectively) resulting in more efficient sorption and lower concentrations of some metals, specifically arsenic and lead.

Under the assumption that all PAF pit wall lithologies are expected to immediately generate acidic leachate at the start of closure, the Immediate Acidification scenario predicts elevated concentrations of select constituents associated with, and leached during, sulfide oxidation including cobalt, chromium, cadmium, nickel, uranium, and zinc. However, predicted long-term concentrations of these constituents are comparable (within half an order of magnitude) to the Base Case scenario.

The High Carbon Emissions SSP370 climate scenario exemplifies the substantial effects of increased evaporation on an evaporative sink pit lake system. Predicted concentrations during the first 100 years of pit filling are nearly equivalent to the Base Case. Once the steady-state lake elevation is achieved, evapoconcentration rates increase resulting in concentration of nearly all constituents that are not solubility controlled increasing at a more rapid rate through the end of the modeling period. The High Carbon Emissions SSP370 scenario is the only model scenario in which fluoride exhibits solubility controls. After approximately 250 years post closure, fluoride concentrations near 5.7 mg/L at which point fluorite precipitation occurs attenuating fluoride concentrations.

8.3 Density-Driven Outflow

The potential for density-driven outflow was evaluated due to increasing solute concentrations predicted in the lake due to evapoconcentration (Gvirtzman 2006, McCullough et al., 2013). The pre-mining groundwater level in the area surrounding the pit is approximately 190 to 200 m AHD (Advisian, 2022), with a median TDS of approximately 550 mg/L. Long-term steady-state pit lake elevations predicted by the pit lake water balance for select scenarios range from 35 to 85 m AHD and are presented in Table 8-2.

Table 8-2 Long-term pit lake elevations for all water balance scenarios

Scenario	Lake Elevation 300-yrs Post-Closure (m AHD)	TDS at 300-yrs Post-Closure (mg/L)	Density-Corrected Environmental Hydraulic Head *
Base Case (with TSF Seepage)	85.0	3,480	85.4
Low Carbon Emissions (SSP126)	78.0	3,670	78.3
Mod-High Carbon Emissions (SSP370)	35.0	5,560	35.2
Base Case (no TSF Seepage)	50.0	2,440	50.2

** Corrected to density of groundwater. Calculated at the base of the pit, elevation -190 m AHD.*

Figure 8-17 illustrates the concept of hydraulic heads in variable density systems as described by Lusczynski (1961). The concept of density-corrected environmental hydraulic head was originally developed to determined vertical density gradients within aquifers, however, the concept can be applied as a screening level assessment of the risk of density-driven outflow from a terminal sink pit lake that exhibits higher density water (as a result of higher TDS and colder temperature) compared to surrounding groundwater. The density-corrected environmental hydraulic head of the pit lake was calculated at a single point (*i*) with elevation z_i (-190 m AHD) representing the base of the pit (Figure 8-17). The density of the pit lake is represented by ρ_l and the density of groundwater is represented by ρ_g. The gravitational constant is represented by g.

The standard hydraulic head of the pit lake is represented by the following equation, where h_{il} is the observed hydraulic head of the pit lake (e.g., 85 m AHD for the Base Case modeling scenario):

$$h_{il} = z_i + \frac{P}{\rho_l g}$$

This observed hydraulic head of the pit lake is then corrected for the density of groundwater. The concept is visualized in Figure 8-17 where a hypothetical piezometer B (screened at point *i*), is filled with groundwater with density ρ_g. Therefore, the resulting density-corrected environmental head is higher than the observed hydraulic head (piezometer A) due to the lower density of groundwater within the theoretical piezometer B. The density-correct environmental head is calculated using the following equation:

$$h_{ig} = h_{il} + \frac{\rho_l}{\rho_g}$$

The density-correct environmental head of the lake is compared to the observed hydraulic head of the surrounding groundwater calculated at the same point (*i*) (exemplified by piezometer C) to determine if density-driven outflow from the hydraulic sink pit lake would be expected. Calculations assumed a uniform density of the lake water column (i.e., fully mixed), groundwater temperatures of 25°C, and pit lake temperatures of 15°C (representing a conservative estimate).

Density-corrected environmental head of the pit lake scenarios is presented in Table 8-2. Density-driven outflow is not expected under any pit lake scenarios. TDS values in the pit lake are not sufficiently elevated to result in environmental heads in the lake approaching that of the regional groundwater head. Additionally, temperature variations exert little effect on the calculated density-corrected environmental head of the pit. Under the scenario with the highest predicted long-term pit lake elevation (85 m AHD), theoretical TDS values would have to exceed an unrealistic concentration of 2,000,000 mg/L in order to overcome the hydraulic gradient into the pit and induce density-driven outflow.

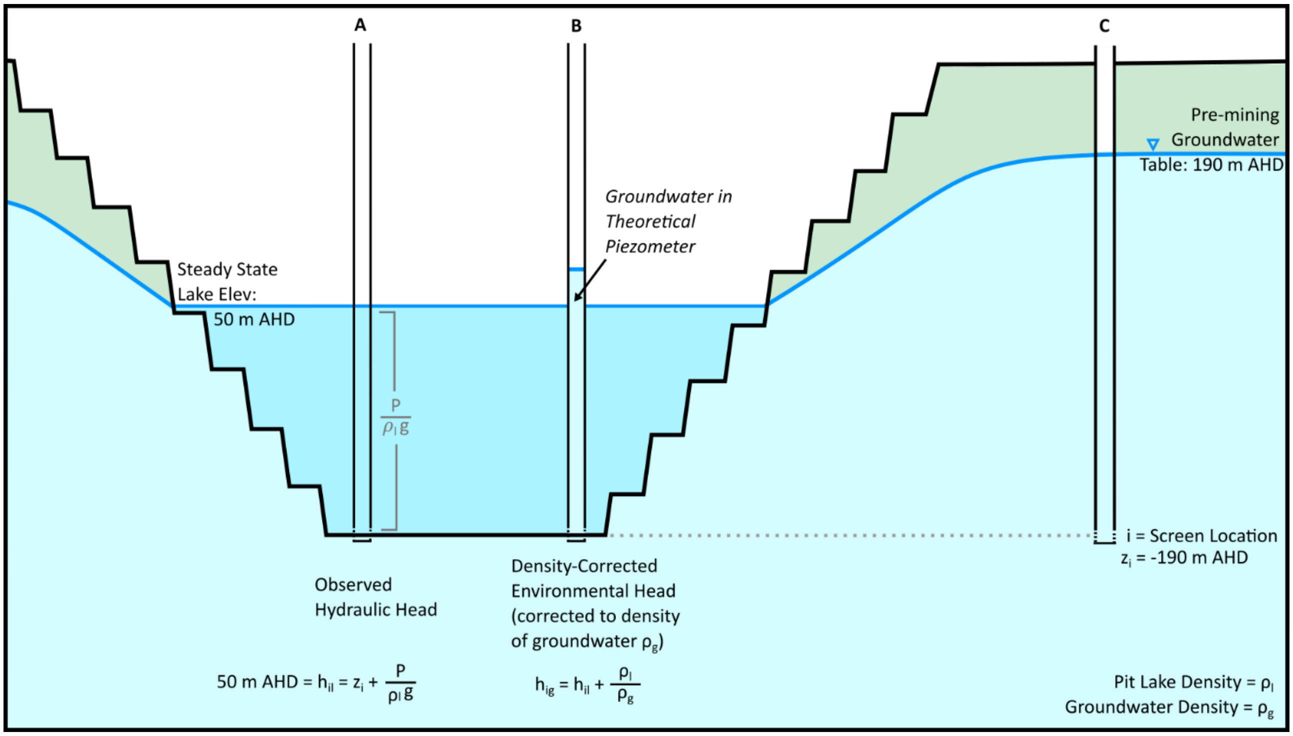

Figure 8-17 Schematic diagram of environmental head of pit lake and groundwater system

8.4 Long-Term Stratification

As in natural lakes, mine pit lakes may permanently or seasonally, vertically stratify. Stratification in pit lakes is caused by density differences in the water column, which are based on temperature and salinity (i.e., TDS) differences. Factors that affect circulation include geometry of the lake (i.e., surface area to depth ratio) and surface wind shear stress. Mixing or seasonal turn-over of lake waters generally results when the kinetic energy of the upper portion of the lake (i.e., water movement from wind shear and other currents) or increasing surface water density due to lower atmospheric temperatures is sufficiently high to displace the deeper, denser water in the lake.

This analysis assessed the possibility for the development of a naturally stratified system based on water quality and mineral reactions expected to occur within the limnological system. Permanent stratification of the Winu lake would affect pit lake water quality differently in each of the stratified zones. A permanently stratified (meromictic) lake would result in a bottom layer that does not mix with the upper water column. The upper, mixed water zones (mixolimnion) would undergo seasonal turnover based on seasonal temperature changes, and would generally reflect a mixture of groundwater, surface/pit wall runoff, rinsing of damaged rock zone and talus on the pit wall, and direct precipitation in equilibrium with atmospheric gas conditions. The bottom layer (monimolimnion) is expected to exhibit low-oxygen to anoxic conditions and higher TDS as a result of the dissolution of settling mineral precipitates under the low redox conditions.

Simple, analytical equations were applied to provide a screening-level assessment for evaluating long-term stratification potential in the pit lake (Orlob, 1983, Tchobanoglous and Schroeder, 1985; Jewell, 2009).

The ratio of maximum depth as a percentage of the mean diameter of the lake (relative depth) can provide a simple estimate of the likelihood of stratification (Lyons et al., 1994; Castendyk and Jewell, 2002). A relative depth greater than 20% indicates the lake is likely to be permanently stratified (Castendyk and Jewell, 2002) on the assumption that large depth/area ratios result in less wind mixing. The relative depth for the Winu pit lake at Base Case steady state conditions (83 m AHD) is 25%, and ranges from 24 to 26% for all water balance scenarios, suggesting the likelihood for the development of permanent stratification at Winu.

A simplified estimate of the thickness of the thermocline can be calculated as a function of the lake length (Jewell, 2009). At a steady state lake elevation of approximately 85 m AHD as predicted by the Base Case model, the thermocline thickness is estimated to be approximately 6 m thick, although this method is considered a simplified estimate as wind strength and duration are also recognized as controlling factors in thermocline development.

In the monimolimnion, TDS values are expected to be higher than the mixolimnion as a result of the settling and redissolution of precipitation products occurring in the overlying oxygenated mixolimnion. Anoxic conditions expected in the monimolimnion were simulated in the pit lake model as well as allowing for redissolution of these precipitation products (gibbsite, ferrihydrite, calcite, and malachite). The densimetric Froude number (Orlob, 1983, Tchobanoglous and Schroeder, 1985) was calculated using the temperature- and TDS-corrected density of the mixolimnion (assuming 25°C) and monimolimnion (assuming 15°C). The densimetric Froude number provides a screening level assessment of densimetric stability of a lake by comparing inertial forces represented by average flow through velocity with gravitational buoyancy forces. Values below approximately 1/pi are expected to be well stratified systems, weakly stratified systems range from 0.1 and 1, and fully mixed systems are expected to have a Froude number well above 1.0. Froude number calculations notably do not account for surface wind shear velocity, nor does it approximate depth of the chemocline interface between the mixolimnion and monimolimnion. The calculations are also strongly influenced by lake geometry, for which Winu displays a high relative depth.

The densimetric Froude number was calculated on a range of elevations for the interface between the mixolimnion and monimolimnion and is displayed in Figure 8-18. On average, the TDS content of the monimolimnion at 300-years post closure was approximately 330 mg/L higher than expected in the oxygenated mixolimnion (2,440 mg/L) for the Base Case model (assuming no TSF Seepage). Froude numbers calculated at 300 years post-closure ranged from approximately 3×10^{-5} to 1×10^{-7}, well below the 1/pi reference value, therefore supporting the potential for a well stratified lake.

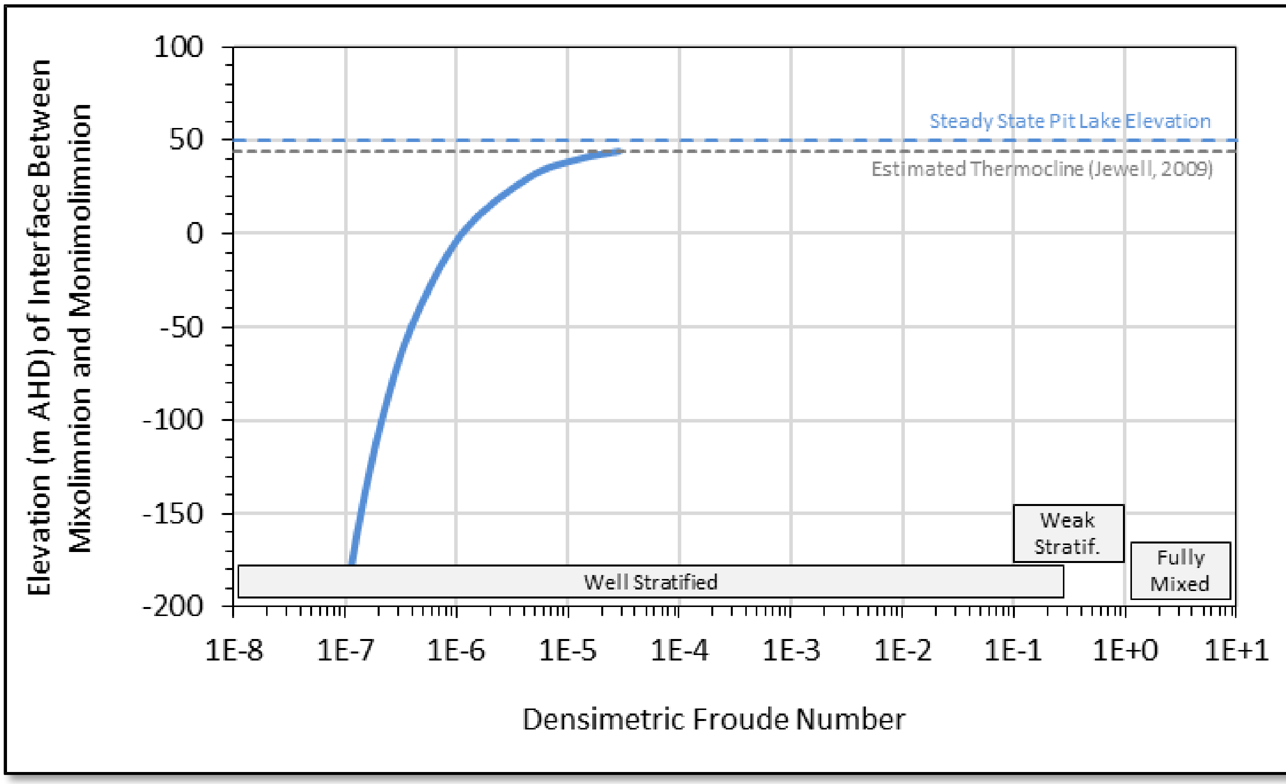

Figure 8-18 Densimetric Froude number calculated for various interface depths between mixolimnion and monimolimnion

The screening level stratification calculations suggest there is a potential for permanent stratification in the pit lake during the post-closure period due to the pit geometry, specifically the relatively small pit lake surface area to depth ratio. Estimates of the likelihood of the development of permanent stratification by the commonly applied Froude number indicate the likelihood of density-induced stratification, however, these calculations are heavily influenced by the lake geometry and high relative depth of the lake. In a system in which the density gradients between the shallow mixolimnion and the deeper anoxic monimolimnion are minor, as predicted by the Winu pit lake model, the cooling of surface water in the pit lake during the fall may be sufficiently dense to cause turnover to some depth. The likelihood and the depth of this seasonal turnover is uncertain. Any permanent stratification that occurs would serve to isolate a portion of the higher-TDS water at depth and slightly improve water quality in the upper portions of the pit lake, including any water that would be exposed to wildlife. In order to induce density driven outflow from the bottom of the pit, TDS concentrations would have to reach unrealistic concentrations (exceeding 2,000,000 mg/L) in the monimolimnion (Section 8.3). These concentrations are not expected to occur at Winu. Additionally, these concentrations are likely unattainable in any natural system due to expected solubility controls.

9 Key Findings and Implications for Mining and Closure

Key findings from pit lake modeling include:

- The open pit is predicted to act as a long-term, evaporative hydraulic sink with no expected discharge to the environment. All sensitivity analyses indicate a similar or lower pit lake elevation than the base case providing confidence that the hydraulic sink conclusion is reliable.
- Groundwater that enters the pit post closure will have excess alkalinity. Groundwater is the major source of water to the pit and dominates the chemistry of the pit lake during filling and post closure.
- Kinetic testing results for the PAF waste rock and ore (that also represent some of the materials remaining in the ultimate pit wall) indicate slow reactivity with very long (i.e., decades) lag times to acidification.
- It has been conservative assumed that seepage from the TSF is expected to represent a significant source of mass loading to the pit lake system, resulting in carbonate mineral precipitation and buffering of the lake pH and alkalinity concentration. Additional TSF modeling of draindown and desaturation timelines in the TSF, may help refine TSF seepage water quality source terms and predictions.
- Due to the long acidification lag time and the chemical nature of the groundwater, the resulting pit lake chemistry is predicted to be circumneutral with abundant buffering capacity to maintain circumneutral conditions over the long term (i.e., centuries to millennia).
- Long-term (i.e., centuries) pit lake chemistry will be driven by evapoconcentration, resulting in gradual increases in constituent concentrations through time. Concentrations of some constituents will ultimately be limited by mineral saturation and mineral precipitation. Alkalinity loading from groundwater and TSF seepage is expected to provide sufficient alkalinity to the pit lake to preclude any chance of late-time acidification. Long-term evapoconcentration is unlikely to create conditions suitable for density-driven groundwater discharge from the pit lake because of the strong hydraulic gradient toward the lake that is predicted for the entire post-closure period.
- Trends in metal concentrations are driven by the mechanisms by which mass loading and solute release calculations are performed in the numerical model (Section 5.2), timing of acidification of PAF wall rock lithologies, and the resulting mineral saturation and associated metals sorption. Metals controlled by mineral saturation display largely stable concentration trends during the modeling period. These metals include aluminum, copper, and iron (controlled by the precipitation of gibbsite, Cu-carbonate minerals, and ferrihydrite saturation

indices, respectively). Most remaining metals and metalloids exhibit increasing concentration trends throughout the modelled period due to evapoconcentration, except for those strongly controlled by adsorption (e.g., arsenic).

- A number of sensitivity analyses were performed to evaluate the potential effects of alternative parameter values for uncertain parameter values or potential for significant variability. The sensitivity analyses indicate that results, and therefore model conclusions, are largely insensitive to variations in these inputs.
- Predicted TDS concentrations for all scenarios are not expected to be sufficiently elevated to overcome the hydraulic gradient into the terminal sink. Therefore, density-driven outflow to the surrounding groundwater system is not predicted to occur.

Implications for mining and closure include:

- No extraordinary measures, such as selective mining out of sulfide-rich material or avoiding the mining of particular zones which may lead to an increase in sulfide rich material in the pit wall, are recommended or required.
- Assuming there will be minimal treatment or engineering controls to the surface of the WRL during operations (i.e., no seasonal cover), no seepage from the base of the WRL is expected.
- Seepage from the TSF will report to the pit lake, however, the timing of the arrival of seepage requires further work. Any TSF seepage that travels through the vadose zone to the water table will be captured by the cone of depression caused by the strong, pit lake hydraulic sink. TSF seepage migration was simulated conservatively in the model (zero travel time from the base of the TSF to the pit lake) and is predicted to contribute chemical mass to the pit lake, although it is not expected to substantially affect the acid-base balance of the pit lake at any time. Seepage from the TSF to the pit lake increases the steady-state elevation of the lake, however a strong hydraulic gradient is still expected to remain at all times.
- Standard post-closure monitoring is recommended; however, no extraordinary measures are recommended for management of the pit lake chemistry.

10 References

AMIRA, 2002. AMIRA P387A Project ARD Test Handbook. Ian Wark Research Institute Environmental Geochemistry International Pty Ltd. May 2002.

Advisian, 2022. Winu Dewatering Strategy and Groundwater Supply Updated 2022 (311012-01475-5.1.1-TM-001-Rev0). Advisian (Worley Group). 14 October 2022.

Bentley, 2024. Leapfrog Modeling Software. Seequent Ltd. The Bentley Subsurface Company. 2024.

DIR, 1997. Safety Bund Walls Around Abandoned Open Pit Mines; Version 1. Department of Industry and Resources. December 1997.

Castendyk, D., and Jewell, P., 2002. Turnover in Pit Lakes I. Observations of Three Pit Lakes in Utah, USA, Tailings and Mine Waste Conference Proceedings, 2002.

DMIRS, 2020. Mine Closure Plan Guidance. Version 4.0. Government of Western Australia. Department of Mines, Industry Regulation and Safety. March 3, 2020 (updated in January 2023).

DRDMW, 2022a. Guideline for construction or modification of Category 2 and 3 levees; Version 2.01. Department of Regional Development, Manufacturing and Water. Queensland Government. February 2022.

DRDMW, 2022b. Guideline for construction of new levees for the modification of existing levees; Version 2.1. Department of Regional Development, Manufacturing and Water. Queensland Government. November 2022.

Dzombak, D.A., and Morel, F.M.M., 1990, Surface Complexation Modeling--Hydrous ferric oxide: New York, John Wiley, 393 p.

Eary, L.E., 1999. Geochemical and Equilibrium Trends in Mine Pit Lakes. Applied Geochemistry vol. 14, 1999 pp. 963-987.

Garrels, R.M. and C.L. Christ, 1965. Solutions, Minerals and Equilibria. Harper and Row, New York.

Golder, 2021. Pit Lake Assessment: Updated Screening-Level Geochemical Model. Winu Final Study. Prepared by Golder Associates Pty Ltd. July 2021.

GoldSim Technology Group (2021), GoldSim User's Guide (Version 14.0), https://www.goldsim.com/Web/Customers/Education/Documentation/, October 2021.

Gvirtzman H., 2006. Groundwater hydrology and paleohydrology at the Dead Sea rift valley. In: Enzel Y, Agnon A, Stein M (eds). New frontiers in Dead Sea paleoenvironmental research. GSA Book, Washington, DC, pp 95–111.

HydroGeoLogica (HGL), 2021a. Review and Comments on Winu Waste Rock Geochemical Testing. Prepared by HydroGeoLogica Inc. May 12, 2021.

HydroGeoLogica (HGL), 2021b. Review of Winu Tailings Geochemistry. Prepared by HydroGeoLogica Inc. May 13, 2021.

Hydrogeologica (HGL), 2024. Winu Project – Evaluation of Waste Rock Landform (WRL) Seepage Potential. Prepared by HydroGeoLogica, Inc. June 12, 2024.

Jewell, P.W., 2009. Technical Papers: Stratification Controls of Pit Mine Lakes. Mining Engineering, February 2009.

Langevin, C.D., Hughes, J.D., Banta, E.R., Provost, A.M., Niswonger, R.G., and Panday, Sorab, 2017, MODFLOW 6 Modular Hydrologic Model: U.S. Geological Survey Software, https://doi.org/10.5066/F76Q1VQV

Lund, M.A., Blanchette, M.L., Harkin, C., 2018. Seasonal river flowthrough as a pit lake closure strategy: is it a sustainable option in a drying climate? In: Wolkersdorfer C, Sartz L, Weber A, Burgess J, Tremblay G (eds), Proc, 11th ICARD & IMWA annual conf: mine water—risk to opportunity, vol I. Tshwane Univ of Technology, Pretoria, pp 34–41.

Lund, M., van Etten, E., Polifka, J. et al., 2020. The Importance of Catchments to Mine-pit Lakes: Implications for Closure. Mine Water Environ 39, 572–588. https://doi.org/10.1007/s10230-020-00704-8

Lusczynski, N.J., 1961. Head and flow of ground water of variable density. Journal of Geophysical Research, volume 66, issue 12, pages 4247–4256.

Lyons, B.W., Doyle, G.A., Petersen, R.C., and Swanson, E.E., 1994. "The limnology of future pit lakes in Nevada: the importance of shape,". Tailings and Mine Waste '94, Balkema Press, pp. 245-248.

McCullough, C. D., Marchand, G., & Unseld, J., 2013. Mine closure of pit lakes as terminal sinks: best available practice when options are limited? Mine Water and the Environment, 32(4), 302-313.

Nordstrom D.K and C.N. Alpers. 1999. Geochemistry of Acid Mine Waters. In The Environmental Geochemistry of Mineral Deposits, Part A: Processes, Techniques, and Health Issues. G.S. Plumlee and M.J. Logsdon, editors. Reviews in Economic Geology Volume 6A, Society of Economic Geologists, Inc.

Okane, 2020. Winu Copper Project – Conceptual Cover System Modeling Report. November, 2020. Prepared for: Rio Tinto. Prepared by: Okane Consultants Pty Ltd. November 2020.

Okane, 2024. Winu Updated Tailings Storage Facility Cover System Numerical Modeling. Rev0. Prepared by O'Kane Consultants Pty Ltd. April 2024.

Orlob, G., 1983. Mathematical modeling of water quality: streams, lakes, and reservoirs. Wiley-Interscience Publication. International Institute for Applied Systems Analysis.

Parkhurst, D.L., and Appelo, C.A.J., 2013, Description of input and examples for PHREEQC version 3—A computer program for speciation, batch-reaction, one-dimensional transport, and inverse geochemical calculations: U.S. Geological Survey Techniques and Methods, book 6, chap. A43, 497 p., https://doi.org/10.3133/tm6A43

Queensland Department of Environment and Science. (Queensland Department of Environment and Science, 2018). SILO – Australian climate data from 1920 to 2018. Retrieved from https://www.longpaddock.qld.gov.au/silo/

Richardson, C. W., and D. A. Wright. 1984. WGEN: A Model for Generating Daily Weather Variables. U. S. Department of Agriculture, Agricultural Research Service, ARS-8, 83 p.

Rio Tinto, 2021, Winu Waste Rock Characterisation – Primary Sulfide (Hypogene) Zone; Version 4. Prepared by Rio Tinto. 14 May 2021.

Rio Tinto, 2022, Winu Tailings Characterisation; Version 2.1. Prepared by Rio Tinto Safety Technical Projects/Rio Tinto Copper and Diamonds. 28 February 2022.

Rio Tinto, 2023. Winu Project Environmental Protection Act 1986 (WA) Section 38 Referral Supporting Document (Doc. No. C0007-0750-U-REP-00001). November 2023.

Rio Tinto, 2024a. Climate Project Summary: Winu. Rio Tinto. February 5, 2024.

Rio Tinto, 2024b. Winu Waste Characterisation – Upper (Oxidised and Overburden) Zone; Version 9. Prepared by Rio Tinto. 4 March 2024.

Rio Tinto, 2024c. Winu Waste Characterisation – Secondary Sulfide (Enriched) Zone; Version 6. Prepared by Rio Tinto. 29 February 2024.

Rio Tinto, 2024d. Winu Operations Closure Plan: Draft version for Consultation. Prepared by Rio Tinto Winu Pty Ltd. [In Progress]

Rio Tinto, 2024e. Winu Acid and Metalliferous Drainage (AMD) Management Plan. Prepared by Rio Tinto Winu Pty Ltd. [In Progress]

Šimůnek, J., M. Šejna, H. Saito, M. Sakai, and M. Th. van Genuchten, The Hydrus-1D Software Package for Simulating the Movement of Water, Heat, and Multiple Solutes in Variably Saturated Media, Version 4.17, HYDRUS Software Series 3, Department of Environmental Sciences, University of California Riverside, Riverside, California, USA, pp. 342, 2013.

SRK, 2023. Winu Copper-Gold Project: Static Geochemical Test Results for Final Tailings Following Carbon In Leach Processing and Cyanide Decomposition – DRAFT. Prepared by SRK Consulting. 1 February 2023.

SRK, 2024. Tailings Geochemistry Following Carbon In Leach Processing and Cyanide Decomposition Winu Copper-Gold Project, Western Australia. Prepared by SRK Consulting. March 2024.

Snyder, Richard & Eching, S. Penman-Monteith daily (24-hour) and Hargreaves-Samani Equations for Estimating Reference Evapotranspiration from Monthly Data. 2002. Regents of the University of California. Created January 2002. Revised November 2006. https://www.researchgate.net/publication/238006282_Penman-Monteith_daily_24-hour_and_Hargreaves-Samani_Equations_for_Estimating_Reference_Evapotranspiration_from_Monthly_Data

Tchobanoglous, G. and Schroeder, E. D., 1985. Water Quality Characteristics, Modeling, Modification, Addison-Wesley Publishing Company, January 11, 1985.

Yihdego, Yohannes and Webb, John (2018). Comparison of evaporation rate on open water bodies: energy balance estimate versus measured pan. Journal of Water and Climate Change. 2018.

Water, Waste and Land Australia Pty Ltd (WWL), 2023. Winu HDTSF Seepage Modeling (127-008-5). November 2023.

Water, Waste and Land Australia Pty Ltd (WWL), 2024. Winu HDTSF 5H Pre-Feasibility Design Report (127-032-1). May 2024.

Williams, 2012. Some Mining Applications of Unsaturated Soil Mechanics. Geotechnical Engineering Journal of the SEAGS & AGSSEA Vol. 43 No.1. March 2012.

Appendix A Pit Wall Geochemical Source Terms

Source Term for Inundated Talus and Damaged Rock Zone (One-Time Saturated Flushing) - Pre-Acidification

Source Term Category		Cover/ Overburden	Mafic Primary Sulfide	Leached Cap (Metasediment & Mafic)	Cu-Ox (Metasediment & Mafic)	Metasediment Secondary Sulfide	Metasediment Primary Sulfide
Temperature	°C	25	25	25	25	25	25
pH	s.u.	7.15	6.46	7.63	7.37	4.01	6.01
Total Alkalinity	mg/L as $CaCO_3$	12	1	13	9	0	3
Ca	mg/L	3	124	1	1	39	29
Na	mg/L	79	13	213	4	32	5
K	mg/L	3	8	5	2	4	4
Mg	mg/L	2	87	1	1	20	25
SO4	mg/L	161	673	437	2	420	183
Cl	mg/L	8	4	5	4	2	5
F	mg/L	0.1	0.2	0.3	0.2	0.2	0.1
Nitrate	mg/L as N	0.077	0.154	0.167	0.068	0.105	0.138
Nitrite	mg/L as N	0.008	0.008	0.005	0.008	0.032	0.008
Ammonia	mg/L as N	0.038	0.055	0.019	0.009	0.382	0.08
P	mg/L	0.015	0.013	0.035	0.008	0.005	0.01
Al	mg/L	0.147	0.012	0.128	0.092	8.331	0.015
Sb	mg/L	0.0005	0.0005	0.0005	0.0005	0.0005	0.0005
As	mg/L	0.0008	0.0005	0.0005	0.0006	0.0016	0.0005
Ba	mg/L	0.0117	0.0104	0.0083	0.0045	0.0092	0.009
B	mg/L	0.028	0.027	0.025	0.025	0.245	0.04
Cd	mg/L	0.00006	0.00065	0.00005	0.00005	0.31657	0.00503
Co	mg/L	0.005	0.421	0.001	0.001	5.099	0.334
Cr	mg/L	0.0008	0.0005	0.0006	0.0005	0.0536	0.0005
Cu	mg/L	0.023	0.138	0.004	0.051	58.266	0.445
Fe	mg/L	0.062	0.031	0.069	0.054	7.699	0.043
Pb	mg/L	0.0006	0.0005	0.001	0.0005	0.001	0.0015
Mn	mg/L	0.005	0.583	0.003	0.002	2.694	3.65
Mo	mg/L	0.0028	0.0007	0.0054	0.001	0.0005	0.0011
Hg	mg/L	0.00005	0.00005	0.00005	0.00005	0.00005	0.00005
Ni	mg/L	0.002	0.198	0.001	0.001	3.272	0.256
Se	mg/L	0.005	0.008	0.007	0.005	0.013	0.006
Si	mg/L	7.1	1.7	4.8	5.9	2.7	2.2
Sr	mg/L	0.1	0.168	-	-	0.232	0.083
Ag	mg/L	0.0006	0.0005	0.0005	0.0005	0.0005	0.0005
U	mg/L	0.0005	0.0005	0.0005	0.0005	0.0402	0.0005
V	mg/L	0.005	0.006	0.005	0.005	0.005	0.005
Zn	mg/L	0.006	0.066	0.008	0.004	12.758	1.034

- not measured (Sr not measured in MEP analyses, source term set to 0 mg/L)

Highlighted values indicate all MEP or column results were below limit-of-detection. One-half limit-of-detection shown.

Source terms are charge balanced on sodium.

Source Term for Inundated Talus and Damaged Rock Zone (One-Time Saturated Flushing) - Post-Acidification

Source Term Category		Cover/ Overburden	Mafic Primary Sulfide	Leached Cap (Metasediment & Mafic)	Cu-Ox (Metasediment & Mafic)	Metasediment Secondary Sulfide	Metasediment Primary Sulfide
Temperature	°C	25	25	25	25	25	25
pH	s.u.	7.15	2.8	7.63	7.37	4.01	3.63
Total Alkalinity	mg/L as $CaCO_3$	12	0	13	9	0	0
Ca	mg/L	3	102	1	1	39	35
Na	mg/L	79	631	213	4	32	30
K	mg/L	3	7	5	2	4	4
Mg	mg/L	2	229	1	1	20	19
SO4	mg/L	161	4199	437	2	420	381
Cl	mg/L	8	7	5	4	2	2
F	mg/L	0.1	0.1	0.3	0.2	0.2	0.2
Nitrate	mg/L as N	0.077	0.299	0.167	0.068	0.105	0.106
Nitrite	mg/L as N	0.008	0.131	0.005	0.008	0.032	0.03
Ammonia	mg/L as N	0.038	0.14	0.019	0.009	0.382	0.35
P	mg/L	0.015	0.049	0.035	0.008	0.005	0.007
Al	mg/L	0.147	85.225	0.128	0.092	8.331	7.609
Sb	mg/L	0.0005	0.0005	0.0005	0.0005	0.0005	0.0005
As	mg/L	0.0008	0.0128	0.0005	0.0006	0.0016	0.0015
Ba	mg/L	0.0117	0.0008	0.0083	0.0045	0.0092	0.0087
B	mg/L	0.028	0.025	0.025	0.025	0.245	0.234
Cd	mg/L	0.00006	0.19138	0.00005	0.00005	0.31657	0.28804
Co	mg/L	0.005	41.05	0.001	0.001	5.099	4.515
Cr	mg/L	0.0008	0.128	0.0006	0.0005	0.0536	0.0491
Cu	mg/L	0.023	453.063	0.004	0.051	58.266	48.922
Fe	mg/L	0.062	199.788	0.069	0.054	7.699	6.962
Pb	mg/L	0.0006	0.0005	0.001	0.0005	0.001	0.0009
Mn	mg/L	0.005	8.104	0.003	0.002	2.694	2.375
Mo	mg/L	0.0028	0.0005	0.0054	0.001	0.0005	0.0009
Hg	mg/L	0.00005	0.00005	0.00005	0.00005	0.00005	0.00005
Ni	mg/L	0.002	31.238	0.001	0.001	3.272	2.916
Se	mg/L	0.005	0.05	0.007	0.005	0.013	0.011
Si	mg/L	7.1	7.5	4.8	5.9	2.7	2.3
Sr	mg/L	0.1	0.082	-	-	0.232	0.201
Ag	mg/L	0.0006	0.0005	0.0005	0.0005	0.0005	0.0005
U	mg/L	0.0005	0.026	0.0005	0.0005	0.0402	0.0366
V	mg/L	0.005	0.351	0.005	0.005	0.005	0.005
Zn	mg/L	0.006	87.773	0.008	0.004	12.758	11.63

- not measured (Sr not measured in MEP analyses, source term set to 0 mg/L)

Highlighted values indicate all MEP or column results were below limit-of-detection. One-half limit-of-detection shown.

Source terms are charge balanced on sodium.

Source Term for Pit Wall Runoff (Ongoing Unsaturated Rinsing) - Pre-Acidification

Source Term Category		Cover/ Overburden	Mafic Primary Sulfide	Leached Cap (Metasediment & Mafic)	Cu-Ox (Metasediment & Mafic)	Metasediment Secondary Sulfide	Metasediment Primary Sulfide
Temperature	°C	25	25	25	25	25	25
pH	s.u.	7.15	6.46	7.63	7.37	4.01	6.01
Total Alkalinity	mg/L as $CaCO_3$	12	1	13	9	0	3
Ca	mg/L	3	124	1	1	39	29
Na	mg/L	79	13	213	4	32	5
K	mg/L	3	8	5	2	4	4
Mg	mg/L	2	87	1	1	20	25
SO4	mg/L	161	673	437	2	420	183
Cl	mg/L	8	4	5	4	2	5
F	mg/L	0.1	0.2	0.3	0.2	0.2	0.1
Nitrate	mg/L as N	0.077	0.154	0.167	0.068	0.105	0.138
Nitrite	mg/L as N	0.008	0.008	0.005	0.008	0.032	0.008
Ammonia	mg/L as N	0.038	0.055	0.019	0.009	0.382	0.08
P	mg/L	0.015	0.013	0.035	0.008	0.005	0.01
Al	mg/L	0.147	0.012	0.128	0.092	8.331	0.015
Sb	mg/L	0.0005	0.0005	0.0005	0.0005	0.0005	0.0005
As	mg/L	0.0008	0.0005	0.0005	0.0006	0.0016	0.0005
Ba	mg/L	0.0117	0.0104	0.0083	0.0045	0.0092	0.009
B	mg/L	0.028	0.027	0.025	0.025	0.245	0.04
Cd	mg/L	0.00006	0.00065	0.00005	0.00005	0.31657	0.00503
Co	mg/L	0.005	0.421	0.001	0.001	5.099	0.334
Cr	mg/L	0.0008	0.0005	0.0006	0.0005	0.0536	0.0005
Cu	mg/L	0.023	0.138	0.004	0.051	58.266	0.445
Fe	mg/L	0.062	0.031	0.069	0.054	7.699	0.043
Pb	mg/L	0.0006	0.0005	0.001	0.0005	0.001	0.0015
Mn	mg/L	0.005	0.583	0.003	0.002	2.694	3.65
Mo	mg/L	0.0028	0.0007	0.0054	0.001	0.0005	0.0011
Hg	mg/L	0.00005	0.00005	0.00005	0.00005	0.00005	0.00005
Ni	mg/L	0.002	0.198	0.001	0.001	3.272	0.256
Se	mg/L	0.005	0.008	0.007	0.005	0.013	0.006
Si	mg/L	7.1	1.7	4.8	5.9	2.7	2.2
Sr	mg/L	0.1	0.168	-	-	0.232	0.083
Ag	mg/L	0.0006	0.0005	0.0005	0.0005	0.0005	0.0005
U	mg/L	0.0005	0.0005	0.0005	0.0005	0.0402	0.0005
V	mg/L	0.005	0.006	0.005	0.005	0.005	0.005
Zn	mg/L	0.006	0.066	0.008	0.004	12.758	1.034

- not measured (Sr not measured in MEP analyses, source term set to 0 mg/L)

Highlighted values indicate all MEP or column results were below limit-of-detection. One-half limit-of-detection shown.

Source terms are charge balanced on sodium.

Source Term for Pit Wall Runoff (Ongoing Unsaturated Rinsing) - Post-Acidification

Source Term Category		Cover/ Overburden	Mafic Primary Sulfide	Leached Cap (Metasediment & Mafic)	Cu-Ox (Metasediment & Mafic)	Metasediment Secondary Sulfide	Metasediment Primary Sulfide
Temperature	°C	25	25	25	25	25	25
pH	s.u.	7.15	2.8	7.63	7.37	4.01	3.63
Total Alkalinity	mg/L as $CaCO_3$	12	0	13	9	0	0
Ca	mg/L	3	102	1	1	39	35
Na	mg/L	79	631	213	4	32	30
K	mg/L	3	7	5	2	4	4
Mg	mg/L	2	229	1	1	20	19
SO4	mg/L	161	4199	437	2	420	381
Cl	mg/L	8	7	5	4	2	2
F	mg/L	0.1	0.1	0.3	0.2	0.2	0.2
Nitrate	mg/L as N	0.077	0.299	0.167	0.068	0.105	0.106
Nitrite	mg/L as N	0.008	0.131	0.005	0.008	0.032	0.03
Ammonia	mg/L as N	0.038	0.14	0.019	0.009	0.382	0.35
P	mg/L	0.015	0.049	0.035	0.008	0.005	0.007
Al	mg/L	0.147	85.225	0.128	0.092	8.331	7.609
Sb	mg/L	0.0005	0.0005	0.0005	0.0005	0.0005	0.0005
As	mg/L	0.0008	0.0128	0.0005	0.0006	0.0016	0.0015
Ba	mg/L	0.0117	0.0008	0.0083	0.0045	0.0092	0.0087
B	mg/L	0.028	0.025	0.025	0.025	0.245	0.234
Cd	mg/L	0.00006	0.19138	0.00005	0.00005	0.31657	0.28804
Co	mg/L	0.005	41.05	0.001	0.001	5.099	4.515
Cr	mg/L	0.0008	0.128	0.0006	0.0005	0.0536	0.0491
Cu	mg/L	0.023	453.063	0.004	0.051	58.266	48.922
Fe	mg/L	0.062	199.788	0.069	0.054	7.699	6.962
Pb	mg/L	0.0006	0.0005	0.001	0.0005	0.001	0.0009
Mn	mg/L	0.005	8.104	0.003	0.002	2.694	2.375
Mo	mg/L	0.0028	0.0005	0.0054	0.001	0.0005	0.0009
Hg	mg/L	0.00005	0.00005	0.00005	0.00005	0.00005	0.00005
Ni	mg/L	0.002	31.238	0.001	0.001	3.272	2.916
Se	mg/L	0.005	0.05	0.007	0.005	0.013	0.011
Si	mg/L	7.1	7.5	4.8	5.9	2.7	2.3
Sr	mg/L	0.1	0.082	-	-	0.232	0.201
Ag	mg/L	0.0006	0.0005	0.0005	0.0005	0.0005	0.0005
U	mg/L	0.0005	0.026	0.0005	0.0005	0.0402	0.0366
V	mg/L	0.005	0.351	0.005	0.005	0.005	0.005
Zn	mg/L	0.006	87.773	0.008	0.004	12.758	11.63

- not measured (Sr not measured in MEP analyses, source term set to 0 mg/L)

Highlighted values indicate all MEP or column results wer below limit-of-detection. One-half limit-of-detection shown.

Source terms are charge balanced on sodium.

Appendix B Tabulated Pit Lake Chemistry Predictions

Base Case Scenario

Years Post Closure		Median Groundater	10	20	50	100	150	200	300
Year			2064	2074	2104	2154	2204	2254	2354
Temperature	°C	25	25	25	25	25	25	25	25
pH	s.u.	7.61	8.09	8.09	8.03	7.95	7.92	7.91	7.90
Total Alkalinity	mg/L as $CaCO_3$	98	110	110	98	84	83	82	84
TDS	mg/L	-	550	627	926	1387	1845	2392	3477
Ca	mg/L	17	21	23	35	60	75	88	109
Na	mg/L	133	146	167	239	341	458	599	889
K	mg/L	8	11	13	19	30	41	54	79
Mg	mg/L	8	14	15	21	30	39	51	75
SO_4	mg/L	35	112	145	304	570	787	1036	1509
Cl	mg/L	140	155	170	212	259	337	437	653
F	mg/L	0.4	0.5	0.6	1.0	1.5	2.1	2.8	4.1
Nitrate	mg/L as N	3.05	3.362	3.687	4.555	5.485	7.103	9.209	13.720
Nitrite	mg/L as N	0.005	0.008	0.010	0.015	0.023	0.031	0.041	0.060
Ammonia	mg/L as N	0.02	0.289	0.528	1.629	3.641	5.152	6.850	9.956
P	mg/L	0.07	0.08	0.09	0.10	0.12	0.15	0.20	0.30
Al	mg/L	0.005	0.015	0.015	0.013	0.011	0.011	0.011	0.011
Sb	mg/L	0.0001	0.0004	0.0005	0.0010	0.0018	0.0026	0.0034	0.0050
As	mg/L	0.0005	0.00021	0.00015	0.00002	0.00004	0.00006	0.00009	0.00015
Ba	mg/L	-	0.0066	0.0109	0.0150	0.0099	0.0084	0.0074	0.0064
B	mg/L	-	0.031	0.050	0.147	0.312	0.438	0.580	0.843
Cd	mg/L	0.00005	0.00126	0.00130	0.01434	0.01783	0.02005	0.02277	0.02974
Co	mg/L	-	0.060	0.059	0.327	0.402	0.456	0.523	0.684
Cr	mg/L	0.0005	0.0006	0.0006	0.0011	0.0011	0.0011	0.0012	0.0015
Cu	mg/L	0.0005	0.0260	0.0261	0.0268	0.0281	0.0292	0.0304	0.0331
Fe	mg/L	0.025	0.00005	0.00005	0.00005	0.00006	0.00006	0.00006	0.00006
Pb	mg/L	0.0005	0.0006	0.0006	0.0002	0.0003	0.0004	0.0005	0.0006
Mn	mg/L	0.012	0.577	0.540	0.484	0.535	0.634	0.764	1.025
Mo	mg/L	0.002	0.004	0.005	0.010	0.019	0.026	0.035	0.051
Hg	mg/L	0.00002	0.00012	0.00020	0.00057	0.00124	0.00176	0.00234	0.00341
Ni	mg/L	0.0005	0.0450	0.0438	0.2195	0.2666	0.3006	0.3436	0.4481
Se	mg/L	0.005	0.008	0.008	0.011	0.015	0.020	0.026	0.039
Si	mg/L	18.3	20.8	22.6	27.0	31.3	40.3	52.1	78.1
Sr	mg/L	0.336	0.391	0.433	0.560	0.713	0.933	1.212	1.803
Ag	mg/L	0.000005	0.000367	0.000564	0.001441	0.003079	0.004347	0.005774	0.008436
U	mg/L	0.000025	0.000291	0.000360	0.002287	0.003199	0.003862	0.004641	0.006360
V	mg/L	-	0.00072	0.00064	0.00013	0.00025	0.00041	0.00058	0.00089
Zn	mg/L	0.0025	0.1770	0.1695	0.7628	0.9115	1.0220	1.1610	1.5100

Low Carbon Emissions Scenario

Years Post Closure		Median Groundater	10	20	50	100	150	200	300
Year			2064	2074	2104	2154	2204	2254	2354
Temperature	°C	25	25	25	25	25	25	25	25
pH	s.u.	7.61	8.09	8.09	8.03	7.95	7.92	7.91	7.90
Total Alkalinity	mg/L as $CaCO_3$	98	110	111	99	85	83	83	85
TDS	mg/L	-	555	634	944	1429	1914	2498	3669
Ca	mg/L	17	21	22	35	61	75	90	111
Na	mg/L	133	147	169	244	353	476	628	942
K	mg/L	8	11	13	20	31	43	56	84
Mg	mg/L	8	14	15	21	31	41	53	79
SO_4	mg/L	35	112	146	310	587	815	1079	1585
Cl	mg/L	140	157	174	218	268	353	462	698
F	mg/L	0.4	0.5	0.6	1.0	1.6	2.2	2.9	4.3
Nitrate	mg/L as N	3.05	3.414	3.756	4.670	5.685	7.440	9.735	14.690
Nitrite	mg/L as N	0.005	0.008	0.010	0.015	0.024	0.032	0.043	0.063
Ammonia	mg/L as N	0.02	0.293	0.537	1.666	3.755	5.339	7.130	10.430
P	mg/L	0.07	0.08	0.09	0.11	0.12	0.16	0.21	0.32
Al	mg/L	0.005	0.015	0.015	0.013	0.011	0.011	0.011	0.011
Sb	mg/L	0.0001	0.0004	0.0005	0.0010	0.0019	0.0026	0.0035	0.0052
As	mg/L	0.0005	0.00021	0.00015	0.00002	0.00004	0.00006	0.00010	0.00016
Ba	mg/L	-	0.0066	0.0110	0.0148	0.0098	0.0083	0.0073	0.0063
B	mg/L	-	0.031	0.051	0.150	0.322	0.454	0.603	0.884
Cd	mg/L	0.00005	0.00123	0.00127	0.01441	0.01820	0.02075	0.02382	0.03192
Co	mg/L	-	0.059	0.058	0.328	0.411	0.471	0.545	0.731
Cr	mg/L	0.0005	0.0006	0.0006	0.0011	0.0011	0.0012	0.0012	0.0016
Cu	mg/L	0.0005	0.0260	0.0261	0.0268	0.0282	0.0293	0.0306	0.0336
Fe	mg/L	0.025	0.00005	0.00005	0.00005	0.00006	0.00006	0.00006	0.00006
Pb	mg/L	0.0005	0.0006	0.0006	0.0002	0.0003	0.0004	0.0005	0.0006
Mn	mg/L	0.012	0.569	0.535	0.485	0.546	0.652	0.792	1.078
Mo	mg/L	0.002	0.004	0.005	0.010	0.019	0.027	0.036	0.053
Hg	mg/L	0.00002	0.00012	0.00021	0.00058	0.00128	0.00182	0.00243	0.00357
Ni	mg/L	0.0005	0.0443	0.0432	0.2202	0.2719	0.3104	0.3583	0.4785
Se	mg/L	0.005	0.008	0.009	0.011	0.015	0.021	0.027	0.041
Si	mg/L	18.3	21.0	23.0	27.7	32.4	42.1	55.1	83.6
Sr	mg/L	0.336	0.397	0.440	0.573	0.739	0.975	1.277	1.922
Ag	mg/L	0.000005	0.000366	0.000566	0.001468	0.003169	0.004498	0.006002	0.008829
U	mg/L	0.000025	0.000285	0.000356	0.002303	0.003266	0.003988	0.004828	0.006739
V	mg/L	-	0.00070	0.00062	0.00013	0.00026	0.00041	0.00059	0.00089
Zn	mg/L	0.0025	0.1740	0.1673	0.7653	0.9290	1.0540	1.2100	1.6120

High Carbon Emissions Scenario

Years Post Closure		Median Groundater	10	20	50	100	150	200	300
Year			2064	2074	2104	2154	2204	2254	2354
Temperature	°C	25	25	25	25	25	25	25	25
pH	s.u.	7.61	8.09	8.09	8.03	7.95	7.92	7.91	7.89
Total Alkalinity	mg/L as $CaCO_3$	98	111	111	100	85	84	85	90
TDS	mg/L	-	558	640	972	1550	2225	3135	5559
Ca	mg/L	17	21	22	35	63	80	100	137
Na	mg/L	133	148	171	252	386	560	799	1452
K	mg/L	8	11	13	20	34	50	71	129
Mg	mg/L	8	14	15	22	33	48	68	121
SO_4	mg/L	35	112	147	318	637	945	1344	2370
Cl	mg/L	140	158	175	226	295	419	599	1106
F	mg/L	0.4	0.5	0.6	1.0	1.7	2.6	3.7	5.8
Nitrate	mg/L as N	3.05	3.434	3.797	4.838	6.246	8.850	12.610	23.250
Nitrite	mg/L as N	0.005	0.008	0.010	0.016	0.026	0.038	0.054	0.096
Ammonia	mg/L as N	0.02	0.294	0.543	1.722	4.090	6.204	8.879	15.540
P	mg/L	0.07	0.08	0.09	0.11	0.14	0.19	0.27	0.51
Al	mg/L	0.005	0.015	0.015	0.013	0.011	0.011	0.011	0.011
Sb	mg/L	0.0001	0.0004	0.0005	0.0010	0.0020	0.0031	0.0044	0.0077
As	mg/L	0.0005	0.00021	0.00015	0.00002	0.00005	0.00008	0.00012	0.00021
Ba	mg/L	-	0.0067	0.0111	0.0146	0.0094	0.0078	0.0067	0.0057
B	mg/L	-	0.031	0.051	0.154	0.349	0.525	0.750	1.316
Cd	mg/L	0.00005	0.00123	0.00128	0.01432	0.01885	0.02296	0.02935	0.05131
Co	mg/L	-	0.059	0.059	0.326	0.428	0.524	0.671	1.159
Cr	mg/L	0.0005	0.0006	0.0006	0.0011	0.0011	0.0013	0.0015	0.0025
Cu	mg/L	0.0005	0.0260	0.0261	0.0268	0.0284	0.0299	0.0322	0.0397
Fe	mg/L	0.025	0.00005	0.00005	0.00005	0.00006	0.00006	0.00006	0.00006
Pb	mg/L	0.0005	0.0006	0.0006	0.0002	0.0004	0.0005	0.0006	0.0008
Mn	mg/L	0.012	0.570	0.537	0.494	0.584	0.747	0.984	1.644
Mo	mg/L	0.002	0.004	0.005	0.010	0.021	0.032	0.045	0.080
Hg	mg/L	0.00002	0.00012	0.00021	0.00060	0.00139	0.00211	0.00303	0.00532
Ni	mg/L	0.0005	0.0443	0.0434	0.2189	0.2832	0.3453	0.4413	0.7586
Se	mg/L	0.005	0.008	0.009	0.011	0.017	0.024	0.034	0.062
Si	mg/L	18.3	21.2	23.2	28.7	35.6	50.1	71.4	132.7
Sr	mg/L	0.336	0.399	0.445	0.593	0.810	1.154	1.643	3.017
Ag	mg/L	0.000005	0.000367	0.000571	0.001513	0.003442	0.005204	0.007442	0.013080
U	mg/L	0.000025	0.000286	0.000359	0.002303	0.003426	0.004474	0.005946	0.010450
V	mg/L	-	0.00070	0.00062	0.00014	0.00029	0.00047	0.00067	0.00109
Zn	mg/L	0.0025	0.1743	0.1679	0.7615	0.9664	1.1710	1.4910	2.5670

High Flushing Scenario

Years Post Closure		Median Groundater	10	20	50	100	150	200	300
Year			2064	2074	2104	2154	2204	2254	2354
Temperature	°C	25	25	25	25	25	25	25	25
pH	s.u.	7.61	7.98	8.00	7.91	7.86	7.85	7.84	7.84
Total Alkalinity	mg/L as $CaCO_3$	98	89	92	77	71	71	72	75
TDS	mg/L	-	791	823	1203	1670	2126	2679	3780
Ca	mg/L	17	41	39	68	99	113	128	151
Na	mg/L	133	152	172	255	360	476	618	908
K	mg/L	8	15	16	22	33	43	56	82
Mg	mg/L	8	39	36	38	44	53	65	89
SO_4	mg/L	35	295	295	512	775	990	1242	1726
Cl	mg/L	140	161	175	216	262	339	440	655
F	mg/L	0.4	0.6	0.7	1.1	1.6	2.2	2.8	4.2
Nitrate	mg/L as N	3.05	3.498	3.800	4.648	5.563	7.178	9.285	13.800
Nitrite	mg/L as N	0.005	0.018	0.018	0.023	0.030	0.038	0.048	0.067
Ammonia	mg/L as N	0.02	0.367	0.593	1.682	3.685	5.196	6.894	10.000
P	mg/L	0.07	0.09	0.09	0.11	0.13	0.16	0.21	0.30
Al	mg/L	0.005	0.012	0.012	0.010	0.009	0.009	0.009	0.009
Sb	mg/L	0.0001	0.0009	0.0009	0.0013	0.0021	0.0028	0.0037	0.0053
As	mg/L	0.0005	0.00040	0.00026	0.00000	0.00001	0.00002	0.00004	0.00008
Ba	mg/L	-	0.0134	0.0155	0.0107	0.0084	0.0075	0.0068	0.0061
B	mg/L	-	0.071	0.083	0.218	0.390	0.516	0.659	0.926
Cd	mg/L	0.00005	0.00629	0.00542	0.08459	0.10310	0.10620	0.11050	0.12150
Co	mg/L	-	0.394	0.333	1.921	2.247	2.307	2.406	2.654
Cr	mg/L	0.0005	0.0011	0.0010	0.0046	0.0054	0.0054	0.0054	0.0056
Cu	mg/L	0.0005	0.0268	0.0268	0.0283	0.0298	0.0309	0.0323	0.0353
Fe	mg/L	0.025	0.00005	0.00005	0.00006	0.00006	0.00006	0.00007	0.00007
Pb	mg/L	0.0005	0.0018	0.0015	0.0002	0.0004	0.0006	0.0008	0.0012
Mn	mg/L	0.012	4.226	3.531	2.625	2.222	2.248	2.406	2.744
Mo	mg/L	0.002	0.005	0.006	0.011	0.019	0.026	0.035	0.051
Hg	mg/L	0.00002	0.00017	0.00024	0.00060	0.00127	0.00178	0.00236	0.00344
Ni	mg/L	0.0005	0.3003	0.2528	1.2910	1.4950	1.5300	1.5940	1.7560
Se	mg/L	0.005	0.014	0.013	0.005	0.008	0.013	0.018	0.031
Si	mg/L	18.3	23.1	24.5	28.6	32.7	41.6	53.5	79.6
Sr	mg/L	0.336	0.477	0.503	0.643	0.794	1.012	1.293	1.885
Ag	mg/L	0.000005	0.000870	0.000975	0.001770	0.003354	0.004617	0.006049	0.008725
U	mg/L	0.000025	0.000793	0.000772	0.011270	0.014140	0.014930	0.015910	0.018150
V	mg/L	-	0.00333	0.00221	0.00001	0.00003	0.00011	0.00026	0.00052
Zn	mg/L	0.0025	1.2030	1.0070	4.4250	5.0930	5.2000	5.4010	5.9200

Low Flushing Scenario

Years Post Closure		Median Groundater	10	20	50	100	150	200	300
Year			2064	2074	2104	2154	2204	2254	2354
Temperature	°C	25	25	25	25	25	25	25	25
pH	s.u.	7.61	8.10	8.10	8.04	7.95	7.93	7.92	7.90
Total Alkalinity	mg/L as $CaCO_3$	98	112	112	101	86	84	83	85
TDS	mg/L	-	531	611	904	1363	1822	2367	3451
Ca	mg/L	17	20	22	33	58	72	85	106
Na	mg/L	133	145	166	237	340	456	598	887
K	mg/L	8	10	12	19	30	41	54	79
Mg	mg/L	8	12	13	19	28	38	50	73
SO_4	mg/L	35	97	132	287	553	771	1019	1490
Cl	mg/L	140	154	170	212	259	337	437	652
F	mg/L	0.4	0.5	0.6	1.0	1.5	2.1	2.8	4.1
Nitrate	mg/L as N	3.05	3.350	3.678	4.548	5.479	7.097	9.202	13.720
Nitrite	mg/L as N	0.005	0.008	0.009	0.014	0.023	0.031	0.040	0.059
Ammonia	mg/L as N	0.02	0.282	0.523	1.625	3.637	5.149	6.846	9.952
P	mg/L	0.07	0.08	0.09	0.10	0.12	0.15	0.20	0.30
Al	mg/L	0.005	0.015	0.015	0.014	0.011	0.011	0.011	0.011
Sb	mg/L	0.0001	0.0003	0.0004	0.0009	0.0018	0.0025	0.0034	0.0049
As	mg/L	0.0005	0.00020	0.00015	0.00003	0.00006	0.00008	0.00011	0.00017
Ba	mg/L	-	0.0059	0.0103	0.0156	0.0101	0.0085	0.0075	0.0065
B	mg/L	-	0.028	0.047	0.141	0.306	0.432	0.574	0.837
Cd	mg/L	0.00005	0.00086	0.00096	0.00846	0.01069	0.01285	0.01545	0.02210
Co	mg/L	-	0.033	0.037	0.194	0.248	0.301	0.365	0.519
Cr	mg/L	0.0005	0.0005	0.0005	0.0008	0.0007	0.0007	0.0008	0.0012
Cu	mg/L	0.0005	0.0260	0.0261	0.0267	0.0280	0.0290	0.0303	0.0329
Fe	mg/L	0.025	0.00005	0.00005	0.00005	0.00006	0.00006	0.00006	0.00006
Pb	mg/L	0.0005	0.0005	0.0005	0.0003	0.0003	0.0003	0.0004	0.0005
Mn	mg/L	0.012	0.283	0.298	0.309	0.396	0.500	0.629	0.885
Mo	mg/L	0.002	0.004	0.005	0.010	0.019	0.026	0.034	0.051
Hg	mg/L	0.00002	0.00012	0.00020	0.00057	0.00124	0.00175	0.00233	0.00340
Ni	mg/L	0.0005	0.0245	0.0269	0.1298	0.1635	0.1977	0.2390	0.3392
Se	mg/L	0.005	0.007	0.008	0.011	0.015	0.020	0.026	0.039
Si	mg/L	18.3	20.6	22.4	26.9	31.2	40.1	52.0	78.0
Sr	mg/L	0.336	0.384	0.427	0.553	0.707	0.926	1.205	1.796
Ag	mg/L	0.000005	0.000327	0.000530	0.001414	0.003056	0.004326	0.005753	0.008414
U	mg/L	0.000025	0.000251	0.000327	0.001536	0.002280	0.002937	0.003698	0.005375
V	mg/L	-	0.00059	0.00057	0.00021	0.00034	0.00050	0.00066	0.00097
Zn	mg/L	0.0025	0.0952	0.1026	0.4535	0.5598	0.6725	0.8098	1.1490

Immediate Acidification Scenario

Years Post Closure		Median Groundater	10	20	50	100	150	200	300
Year			2064	2074	2104	2154	2204	2254	2354
Temperature	°C	25	25	25	25	25	25	25	25
pH	s.u.	7.61	8.04	8.04	8.01	7.94	7.92	7.90	7.89
Total Alkalinity	mg/L as $CaCO_3$	98	99	100	95	83	82	81	83
TDS	mg/L	-	592	666	947	1400	1857	2404	3490
Ca	mg/L	17	28	29	38	63	77	91	112
Na	mg/L	133	150	171	241	343	459	601	890
K	mg/L	8	11	12	19	30	41	54	79
Mg	mg/L	8	13	14	20	29	39	51	74
SO_4	mg/L	35	147	178	321	580	797	1045	1519
Cl	mg/L	140	155	170	212	259	337	437	652
F	mg/L	0.4	0.5	0.6	1.0	1.5	2.1	2.8	4.1
Nitrate	mg/L as N	3.05	3.360	3.685	4.555	5.485	7.102	9.208	13.720
Nitrite	mg/L as N	0.005	0.010	0.011	0.016	0.024	0.032	0.041	0.060
Ammonia	mg/L as N	0.02	0.305	0.545	1.638	3.646	5.157	6.854	9.961
P	mg/L	0.07	0.08	0.09	0.10	0.12	0.15	0.20	0.30
Al	mg/L	0.005	0.013	0.013	0.013	0.011	0.011	0.011	0.011
Sb	mg/L	0.0001	0.0004	0.0005	0.0010	0.0018	0.0026	0.0034	0.0050
As	mg/L	0.0005	0.00001	0.00001	0.00001	0.00003	0.00005	0.00008	0.00014
Ba	mg/L	-	0.0066	0.0108	0.0144	0.0098	0.0083	0.0074	0.0064
B	mg/L	-	0.060	0.076	0.160	0.320	0.446	0.587	0.851
Cd	mg/L	0.00005	0.04345	0.03942	0.03338	0.02928	0.03048	0.03335	0.04080
Co	mg/L	-	0.745	0.693	0.644	0.593	0.630	0.700	0.869
Cr	mg/L	0.0005	0.0041	0.0036	0.0025	0.0017	0.0016	0.0016	0.0019
Cu	mg/L	0.0005	0.0262	0.0263	0.0269	0.0282	0.0293	0.0305	0.0333
Fe	mg/L	0.025	0.00005	0.00005	0.00005	0.00006	0.00006	0.00006	0.00006
Pb	mg/L	0.0005	0.0003	0.0004	0.0004	0.0004	0.0005	0.0006	0.0007
Mn	mg/L	0.012	0.399	0.383	0.404	0.487	0.589	0.719	0.979
Mo	mg/L	0.002	0.004	0.005	0.010	0.019	0.026	0.035	0.051
Hg	mg/L	0.00002	0.00012	0.00020	0.00057	0.00124	0.00176	0.00234	0.00341
Ni	mg/L	0.0005	0.4825	0.4496	0.4211	0.3871	0.4101	0.4544	0.5636
Se	mg/L	0.005	0.006	0.007	0.010	0.014	0.019	0.025	0.038
Si	mg/L	18.3	20.8	22.6	27.0	31.3	40.3	52.1	78.1
Sr	mg/L	0.336	0.409	0.448	0.568	0.718	0.937	1.217	1.807
Ag	mg/L	0.000005	0.000367	0.000564	0.001441	0.003079	0.004347	0.005774	0.008436
U	mg/L	0.000025	0.005723	0.005274	0.004757	0.004688	0.005224	0.006023	0.007802
V	mg/L	-	0.00002	0.00004	0.00009	0.00021	0.00035	0.00051	0.00081
Zn	mg/L	0.0025	1.7820	1.6400	1.4750	1.3290	1.3980	1.5400	1.9000

No TSF Seepage Scenario

Years Post Closure		Median Groundater	10	20	50	100	150	200	300
Year			2064	2074	2104	2154	2204	2254	2354
Temperature	°C	25	25	25	25	25	25	25	25
pH	s.u.	7.61	8.12	8.14	8.19	8.26	8.34	8.42	8.53
Total Alkalinity	mg/L as $CaCO_3$	98	116	123	141	174	213	266	369
TDS	mg/L	-	518	567	763	1056	1356	1721	2432
Ca	mg/L	17	18	17	15	11	9	7	4
Na	mg/L	133	141	158	220	313	408	522	745
K	mg/L	8	10	11	15	21	27	34	49
Mg	mg/L	8	13	14	18	24	31	38	54
SO_4	mg/L	35	82	88	126	180	231	288	404
Cl	mg/L	140	158	176	244	344	447	573	816
F	mg/L	0.4	0.5	0.5	0.7	1.0	1.3	1.7	2.5
Nitrate	mg/L as N	3.05	3.431	3.838	5.302	7.464	9.674	12.400	17.600
Nitrite	mg/L as N	0.005	0.008	0.008	0.012	0.017	0.022	0.028	0.039
Ammonia	mg/L as N	0.02	0.037	0.040	0.058	0.084	0.109	0.138	0.194
P	mg/L	0.07	0.08	0.09	0.13	0.18	0.23	0.29	0.42
Al	mg/L	0.005	0.016	0.017	0.019	0.023	0.027	0.033	0.044
Sb	mg/L	0.0001	0.0003	0.0003	0.0004	0.0005	0.0007	0.0009	0.0012
As	mg/L	0.0005	0.00033	0.00036	0.00002	0.00003	0.00003	0.00004	0.00004
Ba	mg/L	-	0.0022	0.0022	0.0024	0.0033	0.0042	0.0052	0.0073
B	mg/L	-	0.011	0.011	0.022	0.034	0.044	0.054	0.075
Cd	mg/L	0.00005	0.00125	0.00128	0.01610	0.02679	0.03455	0.04170	0.05690
Co	mg/L	-	0.059	0.056	0.347	0.566	0.721	0.860	1.152
Cr	mg/L	0.0005	0.0007	0.0007	0.0018	0.0029	0.0038	0.0048	0.0069
Cu	mg/L	0.0005	0.0259	0.0260	0.0263	0.0270	0.0281	0.0300	0.0349
Fe	mg/L	0.025	0.00005	0.00005	0.00004	0.00004	0.00004	0.00004	0.00004
Pb	mg/L	0.0005	0.0007	0.0008	0.0004	0.0006	0.0009	0.0013	0.0020
Mn	mg/L	0.012	0.578	0.540	0.472	0.503	0.559	0.631	0.783
Mo	mg/L	0.002	0.003	0.003	0.004	0.006	0.007	0.009	0.013
Hg	mg/L	0.00002	0.00004	0.00004	0.00005	0.00008	0.00010	0.00013	0.00018
Ni	mg/L	0.0005	0.0444	0.0424	0.2344	0.3785	0.4802	0.5722	0.7647
Se	mg/L	0.005	0.007	0.008	0.010	0.014	0.018	0.024	0.033
Si	mg/L	18.3	21.4	23.9	32.9	46.6	60.5	77.5	110.4
Sr	mg/L	0.336	0.393	0.438	0.607	0.855	1.109	1.420	2.017
Ag	mg/L	0.000005	0.000170	0.000180	0.000210	0.000300	0.000397	0.000497	0.000719
U	mg/L	0.000025	0.000240	0.000261	0.002210	0.003679	0.004771	0.005791	0.007955
V	mg/L	-	0.00094	0.00099	0.00006	0.00007	0.00008	0.00008	0.00008
Zn	mg/L	0.0025	0.1768	0.1685	0.8312	1.3190	1.6670	1.9880	2.6640